Measuring and Modelling Autophagic Flux

by

André du Toit

Thesis presented in partial fulfilment of the requirements for the degree of Master of Science (Biochemistry) in the Faculty of Science at Stellenbosch University

Supervisor: Dr. B. Loos

Co-supervisor: Prof. J.-H. S. Hofmeyr

March 2016

Declaration

By submitting this thesis electronically, I declare that the entirety of the work contained therein is my own, original work, that I am the sole author thereof (save to the extent explicitly otherwise stated), that reproduction and publication thereof by Stellenbosch University will not infringe any third party rights and that I have not previously in its entirety or in part submitted it for obtaining any qualification.

Date: March 2016 .....

Acknowledgements

I would like to express my sincere gratitude to my supervisors, Dr Ben Loos and Prof Jannie Hofmeyr, for their excellent mentorship, constant guidance and patience, especially since I am dyslexic, for their acceptance and note-worthy dedication in time and effort. I wish to thank the Departments of Physiological Sciences and Biochemistry, particularly the Disease Signalling Group (DSG), for fellowship and support. Further thanks to Dr Lydia Lacerda, Dr Annadie Krygsman, Lize Engelbrecht and Rozanne Adams for technical support as well as Nolan Muller for generating the transmission electron microscopy images at the Diagnostic Electron Microscopy Unit in Tygerberg Hospital. I wish to acknowledge Prof Noboru Mizushima for kindly providing GFP-LC3 MEF cells and Dr Robea Ballo for kindly providing wild type MEF cells. This work was supported by grants from National Research Foundation. I wish to thank my parents and friends for their support. Finally, and most importantly, I would like to acknowledge the role of faith in God that provided strength throughout the duration of this project, as well as Aneeta Anne Sindhu for her love and support during the good and the bad.

This thesis is dedicated to God and Aneeta Anne Sindhu

Contents

List of Figures

List of Tables

Nomenclature

Abbreviations

MEF: Mouse embryonic fibroblast

MEF GFP-LC: Mouse embryonic fibroblast stably expressing GFP-LC3

GFP: Green fluorescence protein

PVDF: Poly-vinylidene fluoride

PMSF: Phenylmethylsulfonylfluoride

RIPA: Radio-immunoprecipitation

CO_2: Carbon dioxide

dH_2O: Distilled water

BSA: Bovine serum albumine

DMSO: Dimethylsulfoxide

DMEM Dulbecco's modified Eagle's medium

EDTA: Ethylenediaminetetraacetic acid

SDS: Sodium dodecyl sulphate

FBS: Foetal bovine serum

ECL: Enhanced chemiluminescence

PAGE: Polyacrylamide gel electrophoresis

TBS-T: Tris-buffered saline and Tween 20

ER: Endoplasmic recticulum

LC3: Microtubule-associated protein 1 light chain 3

LC3-PE: Microtubule-associated light chain 3-phosphatidylethanolamine (LC3 II)

mTOR: Mechanistic target of rapamycin

pmTOR: Phosphorylated mechanistic target of rapamycin

LAMP-2A: Lysosomal-sssociated membrane protein-2A

p62: Nucleoporin p62 (SQSTM1)

GAPDH: Glyceraldehyde-3-phosphate dehydrogenase

Beclin 1: BCL2 interacting protein 1

SQSTM1: Sequestosome 1 (P62)

UVRAG: UV-radiation resistance-associated gene

PE: Phosphatidylethanolamine

3D: Three-dimensional

TEM: Transmission electron microscopy

ROI: Region of interest

PySCeS: Python Simulator for Cellular Systems

Units Of Measurements

s: seconds

hr: hour

°C: degrees Celcius

kDa: kilodalton

μm: micrometer

nm: nanometer

g: gram

mg: milligram

μg: microgram

L: litre

mL: milliliter

μL: microliter

fL: femtoliter

M: molar

μM: micromolar

nM: nanomolar

Model Abbreviations

J: Flux

P: Phagophores

A: Autophagosomes

AL: Autophagolysosomes

AA: Amino acids

L: Lysosomes

$mTOR$: Mechanistic target of rapamycin

$pmTOR$: Phosphorylated mechanistic target of rapamycin

Coeffients

C_v^J: Flux-control coefficient

C_v^n: Concentration-control coefficient

ε_n^v: Species elasticity coefficient

Model Variables

J_{basal}: Basal flux (n_{A}/hr/cell)

J_{induced}: Rapamycin-induced flux (n_{A}/hr/cell)

τ: Transition time (hr)

n_{species}: Species concentration (number/cell)

A: Autophagosomes (n_{A}/cell)

AL: Autophagolysosomes (n_{AL}/cell)

L: Lysosomes (n_{L}/cell)

Summary

Introduction. Autophagy is a dynamic process that is responsible for cellular protein degradation, which involves sequestering of bulk cytoplasm and its delivery to lysosomes where degradation and recycling occurs. Autophagy is vital for cellular function and can be induced during periods of nutrient deprivation for the recycling of proteins and for removing potentially harmful proteins and organelles. A reduction in the autophagic degradative capacity has been linked to several diseases such as those associated with neurodegeneration. These attributes make autophagy an attractive therapeutic target; clinical trials using autophagy inducers have already shown promising results. In order to successfully exploit autophagy, it is crucial to determine whether the autophagic flux is too high or too low, and adjust it accordingly. However, the accurate measurement of autophagic flux still remains a challenge.

Aims. The aim of this project was therefore, first, to develop a novel method to accurately measure autophagic flux. Second, to assess autophagy using conventional techniques and compare it with the new approach. Our third aim was to construct a kinetic model of the autophagic system that could simulate our experimentally generated data and thereby help us understand the contribution of the different processes involved in autophagy and its dynamic behaviour.

Methods. We made use of fluorescent-based imaging to acquire z-stack images of mouse embryonic fibroblasts that stably express GFP-LC3. Images were processed and the total autophagic vesicles pool size was measured using ImageJ with the WatershedCounting3D plugin. Cells were cultured in the presence of

an acidotrophic fluorescent dye that allows (in-combination with GFP-LC3) the visualisation of autophagosomes, autophagolysosomes and lysosomes. Cells were encased in a humidified atmosphere in the presence of 5% CO_2 at 37°C in a microscope slide of the IX81 Olympus microscope. First we determined the concentration of bafilomycin A_1 required for the complete inhibition of the autophagosome and lysosome fusion process. We calculated the autophagic flux as the initial rate of increase in the number of autophagosomes after inhibition of fusion. Second, we increased autophagosomal synthesis through induction with 25 nM rapamycin and again calculated the autophagic flux from the initial rate of increase in autophagosomes after fusion inhibition. In parallel, we assessed changes in the autophagic markers LC3-II and p62 with Western blot analysis and in the morphology of autophagic vesicles with electron microscopy at time points suggested by the fluorescent experimental data. A kinetic model of the autophagic system was constructed and parameterised so as to fit the experimental data. Computational modelling was done with the Python Simulator for Cellular Systems (PySCeS).

Results. Although we found that 100 nM bafilomycin A_1 was sufficient to inhibit the fusion of autophagosomes and lysosomes, we chose to use 400 nM bafilomycin A_1 in order to be absolutely sure the inhibition was complete. Induction of autophagosomal synthesis with 25 nM rapamycin increased the autophagic flux in MEF cells from its basal value of 25.4 autophagosomes/cell/hr to 105.4 autophagosomes/cell/hr. The transition time, i.e., the time required to clear the autophagosomal pool, decreased from its basal value of 0.53 hr to 0.16 hr after induction. Similarly the transition times for the basal and induced autophagolysosomal pools were 6.7 hr and 2.4 hr. Whereas with our fluorescence microscopy method we measured a four-fold increase in autophagic flux from the basal to the induced state, traditional approaches such as Western blot analysis measure only a two-fold increase; electron microscopy proved to be inadequate for assessing autophagic vesicles. Autophagosomes constituted a small percentage of the total GFP-LC3-positive vacuoles. Upon induction with rapamycin the number of autophagosomes/cell increased slightly from 13 to 17, whereas the number of

autophagolysosomes/cell increased considerably from 165 to 251. Autophagosomal size was about four times smaller than autophagolysosomal size. Simulating the autophagic system with our kinetic model provided an excellent fit to the experimental data.

Conclusion. Our novel approach quantifies autophagic variables such as the flux and the number of the different types of autophagic vesices accurately at single cell level, and, used in combination with kinetic modelling of the dynamics of autophagy, hold promise for future therapeutic application.

Opsomming

Inleiding. Autofagie is 'n dinamiese proses wat verantwoordelik is vir sellulêre proteïen degradasie, 'n proses waarin sitoplasma in vesikels gesekwestreer word en na lisosome afgelewer word waar degradasie en herwinning plaasvind. Autofagie is noodsaaklik vir sellulêre funksie en kan geïnduseer word tydens periodes van voedingstoftekorte vir die herwinning van proteïene vir energiedoeleindes en as 'n meganisme vir die verwydering van potensieel skadelike proteïene en organelle. 'n Afname in die autofagiese degradasiekapasiteit is al geassosieer met verskeie siektes soos neurodegenerasie. Hierdie eienskappe maak autofagie 'n aantreklike terapeutiese teiken. Studies met induseerders van autofagie het reeds belowende resultate in kliniese proewe getoon. Om autofagie suksesvol te benut is dit noodsaaklik om te bepaal of die autofagiese fluksie te hoog of te laag is, en om dit dan dienooreenkomstig aan te pas. Die akkurate meting van autofagiese fluksie was egter tot nou toe 'n uitdaging.

Doel. Die doel van hierdie projek was om, eerstens,'n nuwe metode te ontwikkel om autofagiese fluksie akkuraat te meet. 'n Tweede doel was om autofagie met konvensionele tegnieke te assesseer en dan met die nuwe benadering te vergelyk. Die derde doel was om 'n kinetiese model van die autofagie sisteem te bou wat die eksperimentele data kan simuleer en ons sodoende help om die bydrae van die verskillende prosesse betrokke by autofagie tot die dinamiese gedrag van autofagie te verstaan.

Metodes. Fluoressensie-gebaseerde afbeelding is gebruik om z-stapel beelde van muis embrioniese fibroblaste wat stabiele GFP-LC3 uitdruk te verkry. Hierdie

beelde is verwerk en die totale autofagiese vesikelpoelgrootte is bepaal met ImageJ en die WatershedCounting_3D sisteem. Selle is gekweek in die teenwoordigheid van 'n asidotrofiese fluoresserende kleurstof wat, in kombinasie met GFP-LC3, die visualisering van autofagosome, autofagolisosome en lisosome moontlik maak. Selle is omhul in 'n gehumidifiseerde atmosfeer in die teenwoordigheid van 5% CO_2 by 37°C in 'n mikroskoopskyfie van die Olympus IX81 mikroskoop. Ons het eers die konsentrasie van bafilomisien A_1 nodig om die fusie van autofagosome en lisosome volkome te inhibeer bepaal. Die autofagiese fluksie is toe bereken as die aanvanklike snelheid waarmee autofagosome toeneem na inhibisie van fusie. Daarna het ons autofagosomale sintese verhoog deur induksie met 25 nM rapamisien en weer die fluksie gemeet as die aanvanklike snelheid waarmee autofagosome toeneem na inhibisie van fusie. Parallel aan hierdie eksperimente het ons die veranderings in die autofagiese merkers LC3-II en p62 met Westernklad analise en die veranderings in die morfologie van autofagiese vesikels met elektronmikroskopie bepaal by tydspunte afgelei uit die fluoressensie eksperimentele data. Rekenaarmatige modellering is gedoen met die Python Simulator for Cellular Systems (PySCeS).

Resultate. Alhoewel ons gevind het dat 100 nM bafilomisien A_1 voldoende was om die fusie van autofagosome en lisosome te inhibeer, het ons 400 nM bafilomisien gebruik om absoluut seker te maak dat die inhibisie volledig was. Induksie van autofagosomale sintese met 25 nM rapamisien het die autofagiese fluksie in MEF selle van die basale waarde van 25.4 autofagosome/sel/uur na 105.4 autofagosome/sel/uur verhoog. Die transisietyd, nl. die tyd nodig om die autofagosomale poel te vervang, het verminder van die basale waarde van 0.53 uur na die geïnduseerde waarde van 0.16 uur. Soortgelyk het die transisietyd vir die autofagolisosomale poel afgeneem van 6.7 uur voor induksie and 2.4 uur na induksie. Waar ons met die fluoressensie mikroskopie metode 'n viervoudige toename in autofagiese fluksie gemeet het van basale na geïnduseerde vlakke, het tradisionele metodes soos Westernklad analise slegs 'n tweevoudige verhoging gemeet; elektronmikroskopie was nie bevoeg om autofagiese vesikels te assesseer nie. Autofagosome het maar 'n klein persentasie van die totale GFP-LC3-positiewe vakuole uitgemaak.

Na induksie met rapamisien het die aantal autofagosome/sel effens verhoog van 13 na 17, terwyl die aantal autofagolisosome/sel aansienlik verhoog het van 165 na 251. Die grootte van autofagosome was ongeveer vier maal kleiner as die van autofagolisosome. Simulering van die autofagiese sisteem met ons kinetiese model het uitstekend op die eksperimentele data gepas.

Gevolgtrekking. Ons nuwe benadering kwantifiseer autofagiese veranderlikes soos fluksie en die aantal van die verskillende tipes autofagiese vesikels akkuraat op enkelselvlak, en hou, in kombinasie met kinetiese modellering van die dinamika van autofagie, belofte in vir toekomstige terapeutiese toepassings.

Chapter 1

Introduction

Autophagy was first observed in the 1950's by Clark [34] and Novikoff [187], and later in the 1960's the term autophagy was coined by de Duve [39]. Initially the role of autophagy was perplexing, but as time progressed it became clear that autophagy serves as a cellular degradation system. With the advent of the second millennium, new molecular tools made it possible to identify the molecular machinery as well as the regulatory mechanisms of autophagy. Soon it became apparent that autophagy maintains cellular integrity by providing a means of removing potentially harmful proteins and organelles. During periods of starvation autophagy supplies amino acids for energy production by increasing protein degradation. Impaired autophagy has been implicated in the progression of several diseases, most notably neurodegeneration, since it leads to the build-up of harmful proteins and organelles that would otherwise be degraded via autophagy. These attributes of autophagy make it an attractive therapeutic target.

Chapter 2 is an extensive literature review of autophagy that includes its history, its biological roles, its molecular machinery, and its regulation. To exploit autophagy for therapeutic purposes, it is crucial to determine whether or not autophagic flux is too high or too low, and adjust it accordingly.

Conventionally, autophagy is assessed with Western blot analysis and electron and fluorescence microscopy, which still remain the gold standards in autophagy research. These techniques are discussed in depth in Chapter 2. Although they do

generate invaluable information about the internal workings of the autophagic machinery and its regulatory components, they are not really suitable for measuring the autophagic flux, which we have defined as the rate of flow through the pathway at steady state [142]. The main aim of this project was therefore to develop a novel method that accurately measures the autophagic flux. In Chapter 3 we describe the fluorescence microscopy technique with which we quantitatively could measure the changes with time in the number of autophagosomes, autophagolysosomes and lysosomes in a single cell during basal and rapamycin-induced autophagy. Inhibiting the fusion of autophagosomes and lysosomes with bafilomycin and measuring the initial rate of accumulation of autophagosomes allowed us to calculate the steady-state autophagic flux. These results are described in Chapter 4. An additional aim of this project was to compare our novel technique with the traditional techniques under the same conditions. We assessed changes in the autophagic markers LC3-II and p62 with Western blot analysis and in the morphology of autophagic vesicles with electron microscopy at time points suggested by the fluorescence microscopy experimental data.

Cytoplasmic proteins serve as substrates for the autophagic system; amino acids are the end products of the degradation of proteins through autophagy. We therefore also assessed total amino acid and total cellular protein levels during basal and rapamycin-induced autophagy to supplement our autophagic flux data. The results of these investigations are also described in Chapter 4. One of the important conclusions was that the traditional techniques do not measure the autophagic flux accurately.

A great deal is known about the individual processes involved in autophagy, but the degree of control that each of these processes exerts over the autophagic system is not known. In order to successfully exploit the autophagic system for therapeutic purposes, it is not only necessary to be able to numerically quantify autophagic flux, but also to be able to determine the degree of control each step exerts over the autophagic system. One of the ways of gaining this type of insight is to construct a mathematical model of the autophagic system with which the dynamic and steady-state behaviour of the system can be studied. In Chapter 5

we describe the initial development of such a kinetic model, similar to the type of model used to study metabolism, that simulates the time-course of the autophagic vesicles during the process of autophagy.

Chapter 6 is a general discussion that places our results in the context of related published work and maps out future studies that will build on the foundation laid by our study.

Chapter 2

Literature review

2.1 Introduction

Autophagy is a highly dynamic metabolic process whereby a cell digests parts of itself, hence the origin of its name *autophagy*, from the Greek *auto* meaning 'self' and *phagen* meaning to 'eat'. This 'self-eating' process is an evolutionary conserved process in eukaryotes by which cytoplasm is sequestered in a double membraned vesicle that subsequently fuses with a lysosome resulting in the degradation of the cytoplasmic cargo. More than 50 years ago, when autophagy was initially discovered, the question as to why the cell would self-digest its own components was perplexing. The leading explanation was that autophagy serves as a cellular degradation system. However, since then we have learnt that autophagy is more than that, not only degrading long-lived proteins, misfolded/damaged proteins as well as organelles and invading micro-organisms, but also acting as an adaptive response to provide energy and nutrients to the cell during periods of stress. As our knowledge about autophagy expands it has been shown to be implicated in far-reaching fields such as cancer, immune response, neurodegeneration, atherosclerosis, cardiomyopathy, human development and ageing. Recent developments in molecular techniques and microscopy allowed the elucidation of invaluable information about the molecular workings of autophagy. Currently much is known about the regulatory mechanism, but little is known about the degree of control

these regulatory mechanism have over the autophagic system. In this literature review, we will therefore highlight key advances that lead to our current understanding of the autophagy process, as well as the molecular machinery involved. Furthermore we will consider the current methodologies used in autophagic research, focussing on their advantages and pitfalls, as well as a systems biological approach that accurately measures autophagy activity thereby allowing a better understanding of the dynamic nature of the autophagic process.

2.1.1 History of autophagy

2.1.1.1 The early years of the autophagy concept

In the late 1950s both Clark and Novikoff, using electron microscopy, observed membrane-bound compartments which they termed 'dense bodies' that encased mitochondria in mouse kidney cells. Little was however known about their function [34, 187, 188]. It was only later shown that these 'dense bodies' include lysosomal enzymes, and therefore play a part in a degradation system. A few years later Ashford and Porter described membrane-bound vesicles in rat hepatocytes containing semi digested mitochondria and endoplasmic reticulum after being exposed to glucagon [6]. In the same year Novikoff and Essner also observed that these 'dense bodies' contained semi-digested mitochondria and a lysosomal hydrolase [188]. One year later at a symposium on lysosomes in 1963, de Duve coined the term 'autophagy' for a process that produces single or double membrane vesicles in various states of disintegration that contain parts of the cytoplasm and organelles [39]. He suggested that the sequestering vesicles that contain cytoplasm or mitochondria be called 'autophagosomes', that they were related to lysosomes and that they were part of a naturally occurring process. However, the origin of the membranes of these sequestering vesicles was controversial, and it was suggested by de Duve that these membranes were derived from smooth endoplasmic reticulum [39].

In the early 1960s it was known that autophagy occurs in normal rat liver cells and that, if these rats were starved, the numbers of autophagosomes present in the

hepatocyte cytoplasm would increase [184]. In 1967 de Duve and his colleagues demonstrated that glucagon can induce autophagy [41]. In the late 1970s Pfeifer reported the converse, that insulin receptor signalling inhibits autophagy [198]. Ground-breaking work by Mortimore and Schworer in 1977 further demonstrated that amino acids that are the end product of autophagic degradation have an inhibitory effect on autophagy in rat liver cells [175]. Early studies on autophagy from the 1950s to the late 1980s were mainly based on morphological analyses derived from electron microscopy. Novikoff and the early pioneers in the field all examined the matured stage of these vesicles just prior to fusion with the lysosome, as well as the subsequent phase just after fusion that resulted in the degradation of the cytoplasmic cargo. However, it was Gordon and Seglen that in 1988 started using electro-injected radioactive probes to further examine the autophagic process; this study ultimately lead to the identification of the phagophore (the initial sequestering vesicle that matures into an autophagosome), as well as the amphisome (the result of the fusion between an autophagosome and an endosome) [64].

In the early 1960s de Duve proposed the existence of a mechanism for non-specific bulk degradation of cytoplasm as a means to maintain cellular homoeostasis, as well as the need for a more selective proteolytic mechanism to degrade cellular organelles and proteins that would otherwise not be degraded by the bulk acquisition of cytoplasm [39]. The first evidence of organelle specific degradation by autophagy was provided in 1973 when Bolender and Weibel found evidence that the smooth endoplasmic reticulum can be engulfed [17]. In the following years more evidence arose with regards to organelle specific degradation, for example mitochondria that are selectively cleared during insect metamorphosis [12], and peroxisomes that are selectively cleared by autophagy in yeast cells [250]. In the late 90's Lemasters and colleagues demonstrated that changes in mitochondrial membrane potential stimulated autophagy [135]. In the following years more evidence was provided on the selectivity of the autophagic system particularly in yeast and later in higher eukaryotes.

2.1.1.2 The era of molecular biology

Our understanding of the molecular control of autophagy vastly improved in the late 90's with the tools of the molecular biological era. These tools revolutionized our ability to genetically manipulate the autophagic process in order to elucidate the regulatory mechanisms that underlie the system, so uncovering the significance of autophagy in human health and disease. Although autophagy was initially discovered in rats, major breakthroughs in our understanding of autophagy regulation came from analysis of a genetically altered yeast system. Ground breaking work preformed by the Ohsumi laboratory demonstrated that the morphology of autophagic vacuoles in yeast was similar to that reported in mammalian cells [236]. They were the first to genetically screen autophagy-defective yeast mutants and showed that protein turnover was affected in non-specific macro-autophagy [248]. They later followed up with similar screens for mutants that affected selective protein degradation through peroxisomes (pexophagy)[244] and vacuolar hydrolases (cytoplasm to vacuole targeting (Cvt) pathway) [79]. Two years later the Ohsumi laboratory identified a novel protein kinase, Atg1, that was required for the autophagic process; this was the first autophagy-related gene-product published [156]. To this day novel proteins are being identified through genomic screening of yeast mutants defective in selective degradation of mitochondria via selective autophagy (mitophagy) [103, 190].

In 2000 distinct types of autophagy were discovered in the yeast system that function as mechanisms for maintaining cellular integrity by controlled degradation. Although similar in terms of the formation of the autophagic vacuoles, these types of autophagy show distinct differences. The Cvt pathway, pexophagy and mitophagy show high selectivity in contrast to macroautophagy, which is generally considered to be non-selective. Macroautophagy, pexophagy and mitophagy are degradative in contrast to the Cvt pathway, which is biosynthetic by providing peptidase enzymes for the degradative vacuoles [114]. Interestingly, all these various types of autophagy share a subset of the Atg proteins that are essential for autophagosome formation. These Atg proteins are referred to as the "core machinery" and have been grouped into several functional classes: the Atg1–Atg13–Atg17

kinase complex, the class III phosphatidylinositol 3-kinase (PtdIns3K) complex consisting of Vps34, Vps15, Atg6 and Atg14, the ubiquitin-like Atg12 and Atg8 protein conjugation system and Atg9 with its cycling system. Furthermore it has been shown that this core machinery is localized at the phagophore assembly site [233]. An additional core set of components is required in the autophagy process when the autophagic cargo is degraded and released into the cytosol through the use of permeases for recycling [50]. Furthermore, these two subsets of core components play a crucial part in negative feedback regulation of amino acids on the autophagic system.

The identification of the Atg genes in yeast started the search for the Atg homologues in the mammalian system. Mizushima described a novel protein conjugation system in humans in which the first mammalian autophagy genes, Atg5 and Atg12, were identified, and furthermore showed that the Atg12–Atg5 conjugation system is conserved in higher eukaryotes [164]. Two years later Yoshimori and colleagues made a crucial finding in higher eukaryotes with the identification of the mammalian Atg8 homologue, LC3 (also known as MAP1LC3) [98]. They subsequently developed an LC3-based assay for monitoring autophagy capacity in mammals. However, it already became clear that the increased synthesis or lipidation of LC3 does not necessarily indicate the autophagy activity. It is crucial to follow flux through the entire pathway and to assess the autophagic degradative capacity [142].

Besides the conjugation systems, several other mammalian Atg homologues have been identified. Of these, two Atg1 homologues, Unc-51-like kinase 1 (ULK1) and ULK2 have been shown to be essential for autophagy induction. They form part of a large complex that includes mAtg13 (mammalian homologue of Atg13) and FIP200, which is a scaffold protein (an orthologue of yeast Atg17). These will be discussed later in more detail. Mizushima and his colleagues followed autophagosome formation using green fluorescent protein (GFP) linked to Atg5, elucidating in a step-wise manner the sequestration of cytoplasm in a vesicle [165]. The complexity of autophagy regulation is becoming more apparent from recent studies in higher eukaryotes. Recently, numerous additional components involved

in autophagy have been identified in large scale screens with human cells, indicating their interaction with either the autophagy-related proteins or their participation in signal transduction [13]. The origin of the autophagosomal membrane still remains unclear and under debate. Studies have suggested that the autophagosomal membrane may originate from the endoplasmic reticulum [9, 272], the plasma membrane [207] and the mitochondrial outer membrane [67]. This suggests that various organelles can provide the required membrane components for autophagosomal formation [245].

2.2 The molecular machinery of autophagy

In all living organisms, cells are in a constant state of dynamic shifting, which ranges from organism development, metabolic perturbations and regeneration of damaged cells/tissues. It ranges from changes in nuclear architecture (nuclear remodelling) to the removing and replenishing of intracellular components to promote healthy growth and development as well as to adapt to both the micro- and macro-environment. Autophagy is a generic term that is used for all pathways that result in the degradation of intracellular components through lysosomal digestion (Fig. 2.1). Autophagy has far-reaching implications; it degrades damaged and old cellular components so that they can be replaced with new ones, or even with alternative types that would change the characteristics of the cell, such as its adaptive response to stress or a developmental cue during maturation of the organism. Furthermore autophagy acts as a survival strategy by degrading intracellular components for fuel to synthesize ATP; the digested autophagic cargo can serve as substrate for further anabolic reactions. Autophagy can be categorised into three main groups: micro-autophagy, macro-autophagy and chaperone-mediated autophagy (CMA) (see Fig. 2.1). Furthermore, macro-autophagy, although most notably responsible for the degradation of long-lived proteins, is also involved in selective degradation of organelles. We will be focussing on macro-autophagy (generally referred to as autophagy), and highlight some of the selective forms of autophagy throughout this literature review. In this section we will discuss the

autophagy "core machinery" proteins and other autophagy-related proteins and their involvement in the induction of the autophagic system, cargo recognition, autophagosome formation and fusion between autophagosomes and lysosomes.

2.2.1 Autophagy-related (Atg) proteins: the core machinery

Macro-autophagy, hereafter referred to as autophagy, is a dynamic process that can be viewed as consisting of several distinct steps. It starts by the induction of the autophagic system, which promotes the elongation of the double membrane called the phagophore; this process is facilitated by the autophagic core machinery. Subsequent completion of the vesicle forms the autophagosome, which fuses with a lysosome resulting in the degradation of the autophagic cargo and consequently the recycling of the digested goods (Fig. 2.1). Several key proteins are involved in the regulation and formation of autophagosomes and the subsequent events (see Fig. 2.2). The "core machinery" proteins that are intimately involved in autophagy can be grouped into several functional units that are responsible for the different steps that form part of the autophagy process. In this section we will consider the mechanisms of the distinct steps involved in autophagy.

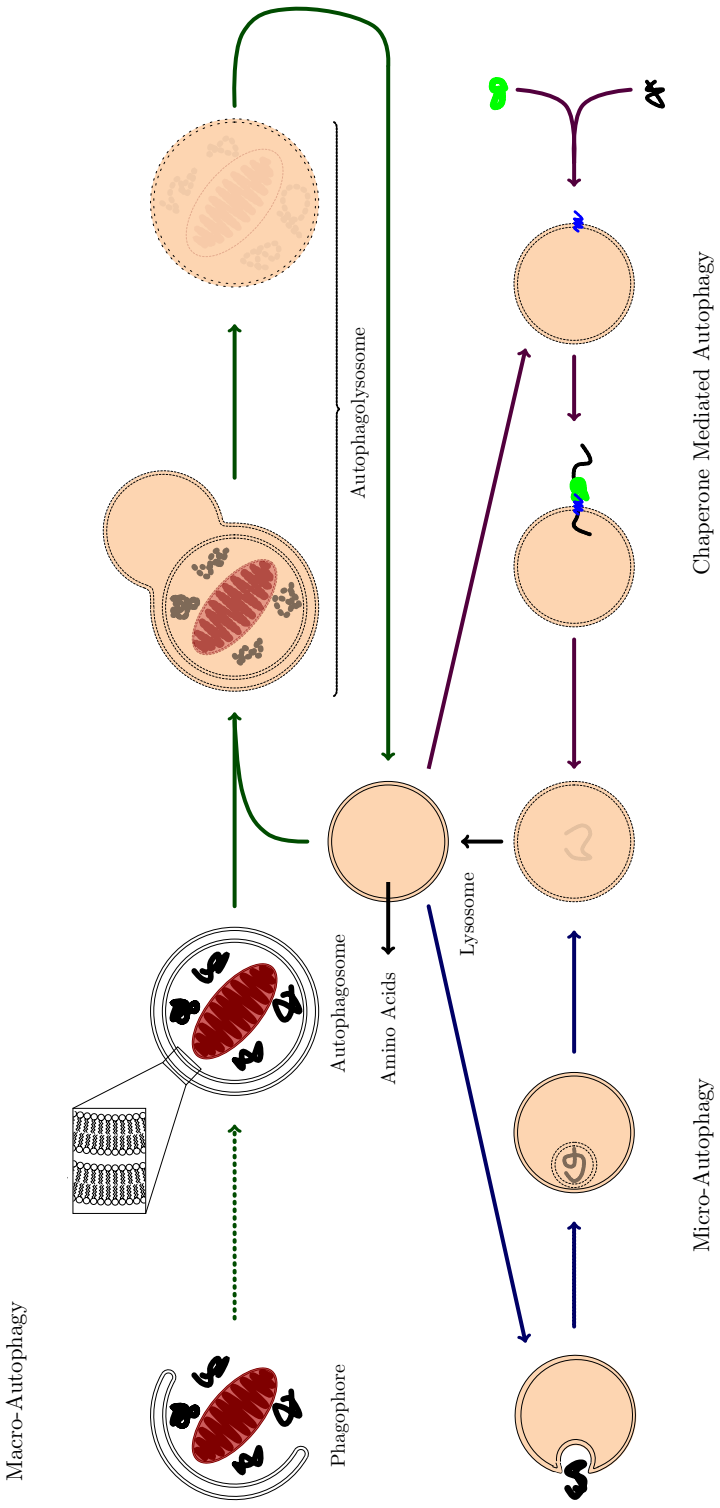

Figure 2.1: The various types of autophagy found in eukaryotes. Macro-autophagy (—) plays a role in the bulk degradation of long-lived proteins. Micro-autophagy (—) is selective for lysosomal degradation while chaperone-mediated autophagy (CMA) (—) is a highly selective for proteolytic degradation.

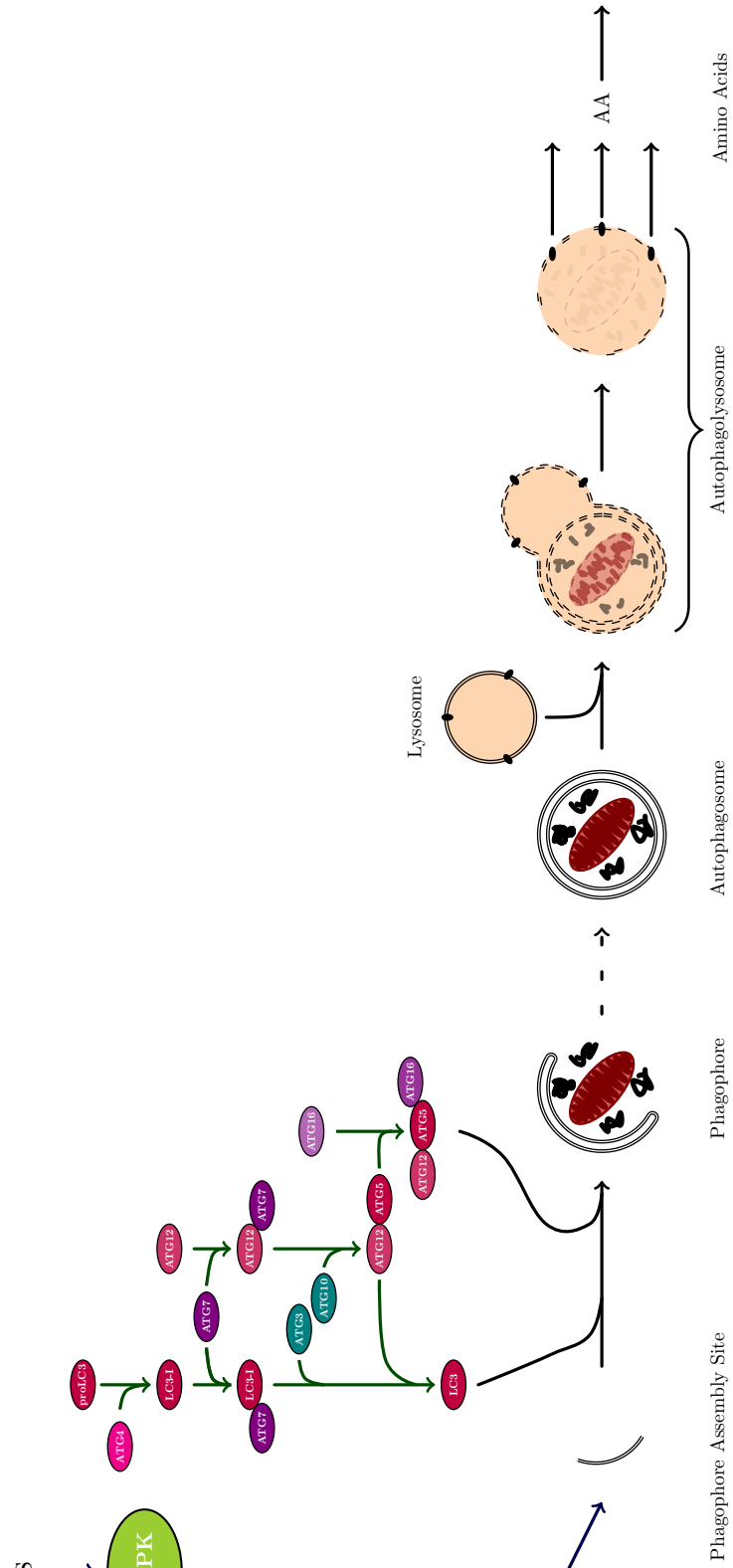

Figure 2.2: Schematic view of the macro-autophagy pathway in eukaryotes. Ubiquitin-like (Ubl) conjugation systems of LC3 (—), Autophagy upstream induction pathway (—).

2.2.1.1 Induction

The organism requires an efficient system to induce autophagy in order to adapt to both intracellular and extracellular stress. mTOR, a central regulator of autophagy is the mammalian target of rapamycin. In *Drosophila* and yeast, dTOR and Tor respectively integrate a broad intracellular network of signal transduction pathways (see section 2.3) that negatively regulate a serine/threonine kinase, Atg1 [24]. For instance, in yeast the inhibition of Tor by rapamycin intervention or nutrient deprivation leads to the activation of Atg1, which increases the binding affinity of Atg1 to Atg13 and Atg17 [101]. Furthermore, the activation of Atg1 stimulates the formation of Atg1-Atg13-Atg17 scaffold proteins and the subsequent recruitment of other various autophagy related proteins to the phagophore assembly site (PAS) to initiate autophagosome formation [29, 106]. Therefore, Atg1 plays a crucial role in the induction of autophagy. Additionally, Atg1 can inhibit the activation of a downstream dTor effector, ribosomal protein S6 kinase (S6K) by preventing the phosphorylation and subsequent activation of S6K during nutrient deprivation in *Drosophila* [134]. However, how autophagy proteins or their activities are regulated by S6K still remains unclear. In the mammalian system two homologues of Atg1 exist, namely Unc-51-like kinase (ULK1 and ULK2), and one homologue of Atg17, namely focal adhesion kinase family-interacting protein of 200 kD (FIP200). FIP200 forms a complex with mammalian Atg13 (mAtg13) and the ULKs, which localizes to the phagophore site upon starvation [76, 98]. Upon induction of autophagy, by either chemical intervention or starvation, ULKs undergo autophosphorylation that is facilitated by conformational change (see Fig. 2.3) [23], which subsequently phosphorylates mammalian Atg13 and FIP200 (see Fig. 2.3) [97]. Unlike in yeast, it appears that ULKs-Atg13-FIP200 forms a stable complex despite the nutritional condition in mammalian cells. During periods of abundant nutrients, mTOR associates with the ULKs-Atg13-FIP200 complex [87] and thereby phosphorylates the conserved C-terminal domain (CTD) of ULKs and Atg13, which subsequently inhibits autophagy. Once mTOR is inhibited, ULK1 and ULK2 are activated and subsequently phosphorylate and activate Atg13 and FIP200, which is essential for the induction of autophagy [87, 97]. The phospho-

rylation by either mTOR or ULKs of Atg13 exerts opposite effects on autophagy, which is modulated by the nutrient status, likely as a result of the phosphorylation on different Atg13 residues. Interestingly, in yeast the dephosphorylation of Atg13 during starvation induces autophagy [101], whereas in *Drosophila* phosphorylation of Atg13 is amplified to induce autophagy [24]. It is therefore conceivable that the phosphorylation of Atg13 in yeast requires TOR, whereas in *Drosophila* it requires Atg1. Additionally, Atg101 is the most recent protein to be identified to form part of the autophagic core machinery that binds to the ULKs-Atg13-FIP200 complex and stabilizes Atg13, which is required for the autophagy response in mammals [160].

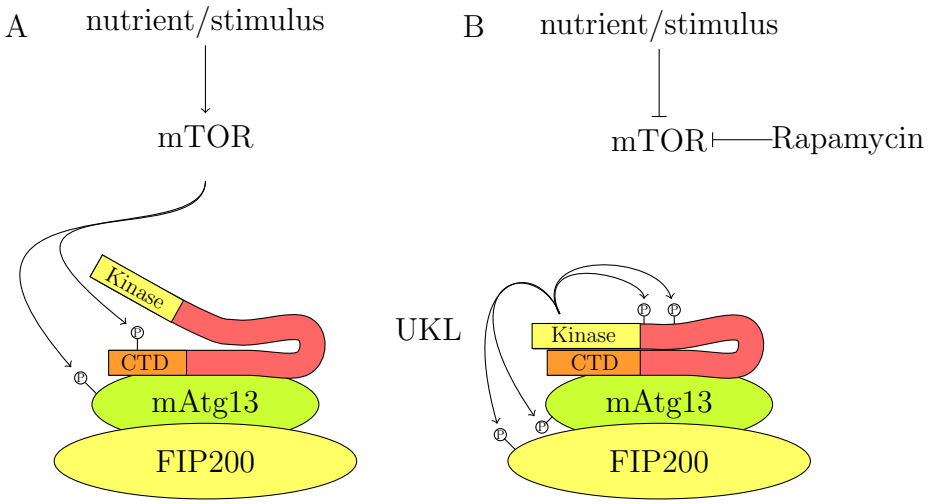

Figure 2.3: Conformational change in ULKs facilitates autophagy induction. **A**. ULK in open configuration as a result of the phosphorylation of ULK by mTOR, therefore inhibiting autophagy induction. **B**. Dephosphorylation of CTD domain of ULK results in the conformational change that promotes autophosphorylation of ULK and subsequent phosphorylation of mAtg13 and FIP200, which in turn stimulates autophagy.

2.2.1.2 Cargo recognition and selectivity

Although autophagy is generally responsible for the bulk degradation of cytoplasmic proteins, and so is the foremost means of degradation of long-lived proteins, it can also selectively target specific organelles. Selective autophagy is mediated

through specific receptor proteins that allow the autophagic machinery to recognize specific cargo such as mitochondria for degradation. Since the C-terminal motif of mammalian p62 (also known as sequestosome 1, SQSTM1) and yeast Atg19 share structural and functional similarity, it suggests that p62 is an Atg19 analogue that acts as a receptor for ubiquitinated proteins or organelles in higher eukaryotes. Autophagy plays an important role in the selective clearance of ubiquitinated substrates and aggregate-prone proteins, in a process which is facilitated by p62 [16]. p62 allows for the binding of both mono or poly-ubiquitinated proteins to microtubule-associated protein 1 light chain 3 (LC3) which results in the subsequent engulfment and degradation of the ubiquitinated cargo.

2.2.1.3 Autophagosome formation

Most vesicle formation in endomembrane trafficking systems is facilitated by either budding from pre-existing organelles or by the formation of a continuous membrane forming a single membrane layer vesicle. In contrast, autophagosomes are formed from a double-membrane vesicle which is to be assembled at the pre-autophagosomal structure site by the addition of new membranes. It is therefore conceivable that formation of the sequestering vesicle is most likely the most complicated step of autophagy. During the formation of autophagosomes, multiple Atg proteins are recruited for the maturation process of autophagosomes in an organized manner. The initiation of nucleation and assembly of the phagophore requires the class III phosphatidylinositol 3-kinase (PtdIns3K) complex, which is composed of PtdIns3K, vacuolar protein sorting-associated protein 34 (Vps34), mAtg14 (also known as Barkor), p150 (also known as PIK3R4), UV radiation resistance-associated protein (UVRAG) and Beclin1 (mammalian homologue of Atg6/Vps30) [92, 108, 139, 232]. Beclin1, which is required for autophagy, is negatively regulated by Bcl-2 (B-cell lymphoma/leukemia-2) and Bcl-X_L (B-cell lymphoma-extra large), an anti-apoptotic protein, that sequesters and binds to Beclin1 during periods of nutrient abundance. Therefore, the dissociation of Beclin1 from Bcl-2 is required for the induction of autophagy in mammals. The PtdIns3K complex is responsible for the production of phosphatidylinositol-3-phosphate (Pt-

dIns3P) as well as for the targeting and the recruitment of various other autophagy proteins that bind to PtdIns3P, such as Atg18, Atg20, Atg21, and Atg24 in yeast [82, 189, 231]. This indicates that in yeast Atg20 and Atg24 interact with the regulatory complex. However, in the mammalian system, the mammalian homologue of Atg20 has not been identified, and the role of mAtg24 is not well defined [82]. Additionally, the PtdIns3K complex further recruits ubiquitin-like (Ubl) conjugation systems, LC3 (also known as mAtg8) and Atg12–Atg5-Atg16 to the phagophore construction site which is vital for elongation of the membrane and subsequent expansion of the developing autophagosome [233, 234]. Similar to ubiquitin, Atg12 is activated by Atg7, which has homology to the ATP-binding and catalytic sites of the E1 ubiquitin activation enzyme, and is transferred to Atg10 (a ubiquitin-like E2 conjugating enzyme) that attaches covalently to a lysine residue of Atg5, the substrate protein [59] (see Fig. 2.2). Unlike ubiquitin, the conjugation of Atg12 to Atg5 is irreversible and does not require substrate-specific E3 ligase. The Atg12–Atg5 conjugate further complexes with Atg16 to form Atg12–Atg5-Atg16 which tetramerises by self-oligomerisation and attaches to the developing autophagosome [82, 163]. LC3 is first cleaved by Atg4, a cysteine protease, to expose a C-terminal glycine residue, which then, similar to Atg12, is activated by Atg7 and transferred to Atg3 (a ubiquitin-like E2 conjugating enzyme). Furthermore, LC3 is conjugated to phosphatidylethanolamine (PE) via the E3-like Atg12–Atg5 conjugate to form LC3-PE (also known as LC3-II) [74]. During basal conditions, when nutrients are available, the majority of LC3 is cytosolic. However, upon induction of autophagy, these endogenous cytoplasmic LC3 reserves are mobilized, lipidated and subsequently localized to both sides of the autophagosome double membrane at the phagophore assembly site [98]. Since LC3 plays an important role in determining membrane curvature it is conceivable that LC3 has some control over the size of the autophagosome [266]. Additionally, LC3-II levels are widely used to assess autophagy since these levels vary linearly with the number of autophagosomes [167]. Recent studies have shown that mAtg9 may facilitate membrane trafficking and/or fusion, since it is the only integral membrane protein identified that is required for autophagy [81]. Therefore the role of mAtg9

may include the supply of the growing phagophore with membrane material and furthermore assisting in the expansion of the phagophore [23, 275].

2.2.1.4 Vesicle fusion and autophagosome breakdown

Upon the completion of the autophagosome maturation process, LC3-PE is cleaved by Atg4 from the outer membrane and released into the cytosol [112]. The fusion of autophagosomes and lysosomes is mediated by the same machinery that is used in homotypic vacuole fusion. The fusion process requires lysosome-associated membrane protein 2 (LAMP2) and the small GTPase Rab7 [94, 238]. Upon completion of the fusion process the inner compartment of the autophagosome is exposed to the lysosomal acid hydrolases that include proteinases A and B as well as cathepsin B and L [239]. The exposure of the autophagic cargo to the hydrolases results in its degradation and the subsequent transportation of digested goods back to the cytoplasm, mostly in the form of amino acids, which can be used for protein synthesis and nutrients during periods of starvation.

2.2.2 Non-Atg components required for autophagy

2.2.2.1 Cytoskeleton

In order for autophagy to proceed optimally, efficient protein trafficking is required during autophagosome formation, a process that is mediated by the cytoskeletal networks. For instance, in yeast the actin cytoskeleton and the actin-related protein 2/3 complex (Arp2/3 complex), which serves as nucleation sites for new actin filaments, is required for the anterograde transport of Atg9 to the pre-autophagosomal assembly site [168, 209]. Similarly, in higher eukaryotes microtubules are involved in autophagy for transport of Atg proteins as well as autophagosomes. The depolymerisation of microtubules by chemical intervention with nocodazole in primary rat hepatocytes has been shown to inhibit autophagosome formation [115]. Additionally, microtubules and tubulin deacetylase HDAC6 have been shown to be essential for autophagic degradation of polyglutamine aggregates [93, 194]. Furthermore, mutation in the dynein motor machinery impairs

the autophagic clearance of aggregate-prone proteins, which leads to premature aggregate formation [205]. In addition, there is an increase in the levels of the autophagosome marker LC3-II, suggesting an impairment in autophagosome and lysosome fusion. In mammalian cell lines it appears that autophagosomes are formed in peripheral regions of the cell, and move bidirectionally along microtubules. Their movement depends on the dynein motor protein that transports them to the centre of the cell, leading to their accumulation at the microtubule centre. This process is similar to other trafficking pathways [95]. The accumulation of autophagosomes and lysosomes at the microtubule-organizing centre allows for the fusion of autophagosomes and lysosomes driven by dynein motors that can either result in the complete fusion, or the so called kiss-and-run event where there is a partial transfer of vesicle content while still remaining as two separate vesicles [95, 115].

2.3 Metabolic regulation of autophagy

Autophagy is a tightly orchestrated intracellular process that plays a key role in the bulk degradation of cytoplasmic proteins and organelles. It serves multiple vital biological roles such as maintaining cellular integrity and utilizing endogenous energy reserves during periods of starvation. It is therefore not surprising that autophagy is regulated by a broad intracellular nutrient and stress-sensing network (Fig. 2.4). In this section we will discuss metabolic triggers and signalling pathways that modulate autophagy activity.

2.3.1 Metabolic triggers of autophagy

Because autophagy plays an integral role in cellular metabolism and in maintaining cellular integrity, it is essential that autophagy can either be up or down regulated in response to a stimulus. Therefore, multiple signalling pathways are required, each of which monitors defined cellular processes to assess the metabolic status of the cell in order to adjust autophagy flux. Key metabolites involved in energy production and protein synthesis, such as ATP or essential nutrients (for example

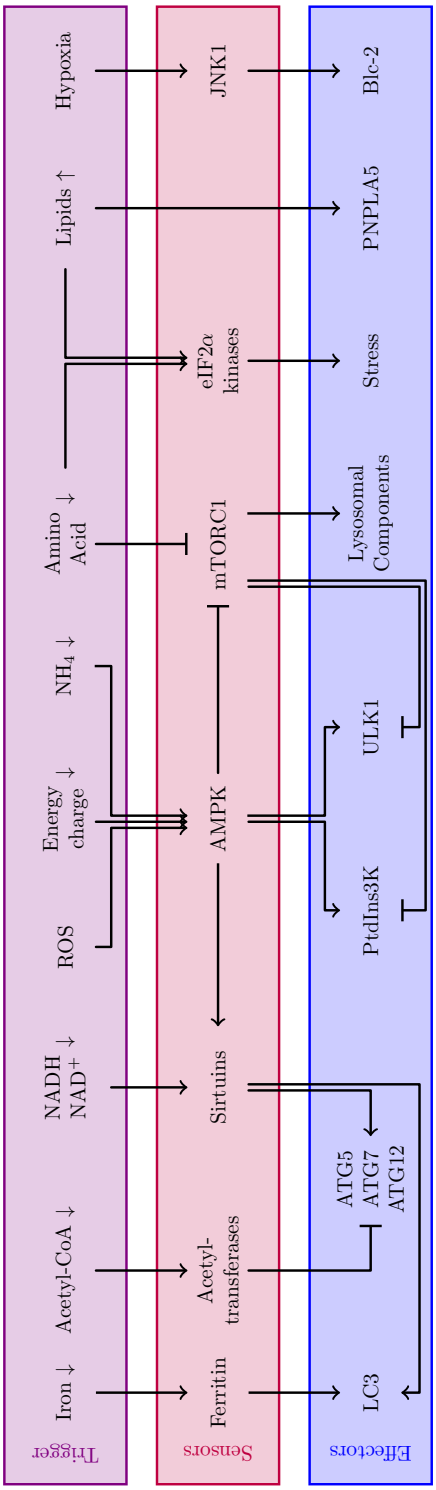

Figure 2.4: Metabolic regulation of autophagy [57].

glucose and amino acids), can induce autophagy. Besides the induction of autophagy through changes in the cell's energetic state, it can also be stimulated by the accumulation of metabolic by-products such as ammonia. In this section we will discuss the main key regulators of autophagy: reduced energy charge, amino acid depletion, depletion of cytosolic acetyl-CoA, ammonia levels, lipids, reactive oxygen species and hypoxia.

2.3.1.1 Reduced energy charge

The term "energy charge" refers to the metabolic status of the cell. It was coined by Atkinson and Walton in the late 60's, when they mathematically derived an equation that describes the adenylate system of a cell as function of intracellular ATP, ADP, and AMP concentrations [7]. The energy charge decreases when ATP is not actively synthesized through oxidative phosphorylation or glycolysis, alongside with the accumulation of AMP. These changes in ATP and AMP levels effectively change the energy charge and stimulate autophagy through AMP-activated protein kinase (AMPK) [78]. AMPK plays an essential role as a cellular energy sensor in multiple signalling cascades that regulate several intracellular metabolic pathways. Once activated, it is responsible for promoting ATP production by increasing the activity and or expression of proteins involved in catabolic processes such as fatty acid oxidation, glucose uptake and ketogenesis (see section 2.3.2). Conversely, AMPK inhibits energy expenditure of anabolic conditions by switching off biosynthetic pathways in order to preserve energy for essential metabolic reactions required for survival. AMPK is highly sensitive to fluctuations in the AMP and ATP ratio and consequently regulates the cellular machinery that is responsible for maintaining energy charge of the cell. It therefore acts as a metabolic master switch. Interestingly, since autophagy also requires ATP in several steps in its pathway, a rapid reduction in ATP levels and energy charge below a critical limit is more likely to trigger cell death rather than an adaptive autophagic response [56]. Cells that mainly depend on glycolysis for fuel are extremely sensitive to glucose fluctuations, and therefore withdrawal from glucose will induce autophagy as a result of a reduction in energy charge [78]. Interestingly, the inhibition of hex-

okinase II, which catalyses the first step of glycolysis by phosphorylating glucose, also promotes autophagy; however, the mode of action differs greatly. This is as a result of hexokinase II directly interacting with mammalian target of rapamycin complex1 (mTORC1) and thus inhibiting its activity, consequently inducing autophagy [210]. It is worth noticing that toxins such as rotenone, that is used as an inhibitor of the electron transport chain, inhibits mitochondrial ATP synthesis and surprisingly also inhibits autophagy [148]. It is therefore possible that toxins may not be considered as appropriate means to discern complex integration linking metabolism and autophagy. In conclusion, glucose deprivation and the consequent change in ATP and AMP affects the cell's energy charge, which is a potent activator of autophagy.

2.3.1.2 NADH/NAD$^+$ ratio

Nicotinamide adenine dinucleotide (NAD) is a coenzyme found in all living cells and exists in both a reduced (NADH) or oxidized (NAD$^+$) state. In either of its forms NAD is an essential substrate that is involved in redox reactions of multiple metabolic pathways, including glycolysis and oxidative phosphorylation. During periods of nutrient-poor conditions there is an accumulation of NAD$^+$ at the expense of NADH. The resulting shift in the NADH/NAD$^+$ ratio stimulates autophagy through the activation of histone deacetylases of the sirtuin family [88]. Upon activation of NAD$^+$-dependent enzymes such as poly-(ADP-ribose)-polymerase-1 (PARP-1), which consumes NAD$^+$, there is a depletion of intracellular levels of both NAD$^+$ and NADH [61]. The inhibition of NAD$^+$-dependent enzymes and metabolic pathways responsible for the supply of NAD precursors are potent inducers of autophagy once sirtuins are activated [88]. Thus, the dependence of sirtuins on NAD-reserves links the energy status of the cell via the intracellular NADH/NAD$^+$ ratio, as well as the total availability of NAD (including precursors) directly to the enzymatic activity of sirtuins and, consequently, autophagy.

2.3.1.3 Depletion of amino acids

Amino acids play a crucial role in biological processes. The induction of autophagy can be brought on by the availability of amino acids through four distinct mechanisms. Firstly, a reduction in the availability of intracellular amino acids results in the accumulation of uncharged tRNA species. This consequently activates eukaryotic translation initiation factor 2a kinase 4 (eIF2aK4) which in turn inhibits protein synthesis and induces autophagy through the activation of transcription factor 4 (ATF4) [271]. Secondly, the absence of various amino acids (especially leucine, glutamate, and glutamine) diminishes intracellular acetyl-CoA stores and therefore induces autophagy, since acetyl-CoA cannot be effectively generated [149]. Thirdly, the dwindling of the presence of amino acids in the lysosomal lumen effectively turns off the "inside-out mechanism" that promotes the association of mTORC1 with the lysosomal surface membrane. Subsequent activation of mTORC1 localised to lysosomes induces autophagy [281]. Fourthly, the reduction in amino acid availability results in the depletion of α-ketoglutarate, which promotes autophagy alongside the inhibition of prolyl hydroxylase [43]. These four mechanisms constitute a broad intracellular amino acid-sensing network that intimately links amino acid levels to autophagy. Additionally, proteasome inhibitors can also reduce intracellular amino acid levels and therefore induce autophagy. However the degree of control that each of these mechanisms has over the autophagy pathway is not known. All these amino acid sensing mechanisms contribute to the orchestration of autophagic responses to shortage of amino acids.

2.3.1.4 Depletion of cytosolic acetyl-CoA

Nutrient deprivation over several hours results in a significant reduction in cytosolic acetyl-CoA levels alongside the induction of autophagy [149]. Similar trends have been found in several pharmacological studies where the inhibition of acetyl-CoA synthesis, either through direct inhibition or substrate limitations, accompanied the induction of autophagy [47]. The dwindling reserve of cytosolic acetyl-CoA is a potent stimulator of autophagy, which is thought to be facilitated by acetyl-CoA acting as donor of acetyl groups for acetyl transferases. Some of the autophagic

machinery components are regulated via acetyl transferases at the transcriptional or the post-translational level by modulation through histone acetylation [133, 149]. In contrast, the replenishment of intracellular acetyl-CoA levels inhibits starvation-induced autophagy in both cell culture and mouse models [149].

2.3.1.5 Ammonia levels

Ammonia is a stress-inducing and toxic byproduct of amino acid catabolism, and acts as a potent activator of autophagy [48]. In contrast to amino acid deprivation-induced autophagy, ammonia-induced autophagy does not rely on either mTORC1 inhibition [77] or ULK1/ULK2 activation [28]. Harder *et al.* [77] suggest that ammonia triggers autophagy through the activation of AMPK and the unfolded protein response (UPR). The role of the UPR in autophagy induction was substantiated by the finding of elevated ER stress markers DDIT3/CHOP and HSPA5 during ammonia treatment [77]. Interestingly, tumours generate high levels of ammonia due to an increase in glutamine catabolism via glutaminolysis, which up-regulates autophagy. This may be observed in established tumours and may contribute to the resistance of tumours to treatments as a result of the protective function of autophagy [65].

2.3.1.6 Reactive oxygen species and hypoxia

Reactive oxygen species (ROS) are reactive molecules containing oxygen and play an important role in cell signalling and homeostasis [42]. It is well documented that ROS is an effective inducer of autophagy [27]. The major contributors to ROS generation are mitochondria, NADPH oxidase complexes (NOX), peroxisomes, and the endoplasmic reticulum [27, 68, 176]. Acute ROS exposure can lead to extensive cellular damage that may induce autophagy mediated cell death [27]. Cells maintain tolerable levels of ROS on a basal level and are able to protect themselves from damage caused by rapid increases in mitochondrial ROS through anti-oxidative strategies [27, 68]. Hypoxia is a condition where cells are exposed to oxygen levels below 1% (hypoxic stress), in contrast to normoxia which is characterised by 2–9% oxygen. However, hypoxic conditions play physiologically significant roles as in, for

example, developing embryos, but are also created in pathological conditions such as brain injuries, cardiovascular ischaemia, and solid tumours. There is an increasing amount of data that shows that hypoxia induces autophagy. Interestingly, the autophagy induction pathways of hypoxia and their cellular consequences appear to be different between cell types. For instance, hypoxia enhances mitochondrial autophagy (mitophagy) as an adaptive response in an attempt to reduce the levels of reactive oxygen species to preserve the cell's integrity. However, in several cancer cell lines prolonged exposure to hypoxic conditions can induce autophagic cell death [10]. Oxygen deprivation induces hypoxia-inducible factor-1 (HIF-1) that promotes transcription of various genes. This response subsequently decreases mitochondrial biogenesis and respiration and promotes erythropoiesis and angiogenesis. Therefore, the induction of HIF-1 is an adaptive response to counteract deleterious effects caused by O_2 deficiency. Interestingly, mouse embryonic fibroblasts (MEFs) promote mitochondrial selective autophagy in response to hypoxic conditions in order to remove damaged mitochondria. This process is dependent on HIF-1 as well as the anti-apoptotic Bcl-2 adenovirus E1a nineteen kDa interacting protein 3 (BNIP3) which is a HIF-1-induced target [280]. BNIP3 induces autophagy by competing with Beclin1 to bind with Bcl-2, which subsequently promotes the dissociation of Bcl-2 and Beclin1 and therefore promotes autophagy. Although BNIP3 is regulated by HIF-1, it is also the target gene of the E2F family transcription factors that are under the control of the retinoblastoma protein (RB) family [246]. Thus hypoxia can induce autophagy by promoting the binding of HIF-1 and or E2F to the BNIP3 promoter with subsequent expression of BNIP3, as well as through the RB-E2F-BNIP3 signalling pathway. Interestingly, the increase in autophagic capacity observed in tumours appears to be independent of the HIF-1pathway. Here, autophagy is alternatively induced through the AMPK-mTOR [196] and protein kinase C δ(PKCδ)-JNK1 pathway [25].

2.3.2 Metabolic sensors that initiate autophagy

2.3.2.1 AMP-activated protein kinase

AMPK is a highly conserved energy sensor in eukaryotes which is activated when there is decrease in intracellular ATP, hence a reduction in the energy status of the cell. It is a heterotrimeric protein that is composed of a catalytic α-subunit, a regulatory γ-subunit and a scaffolding β-subunit. All subunits are expressed as multiple isoforms, namely $\alpha 1$, $\alpha 2$, $\gamma 1$, $\gamma 2$, $\gamma 3$, $\beta 1$ and $\beta 2$. The binding of AMP with another AMP or ADP (AMP with a much higher affinity) to the γ-subunit prevents the dephosphorylation of the α-subunit at T172 and the subsequent inhibition of its catalytic activity [78]. Therefore a decrease in the energy charge, hence a decrease in ATP levels and an increase AMP, will dramatically increase AMPK activity. The phosphorylation of the α-subunit can be catalysed by serine/threonine kinase 11 (STK11, also known as LKB1), calcium/calmodulin-dependent protein kinase kinase 2 (CAMKK2) and by mitogen-activated protein kinase kinase kinase 7 (MAP3K7, also known as TAK1) [78]. MAP3K7 is required for the starvation-induced phosphorylation of AMPK and subsequent activation of autophagy [36] in cancer cells as well as *in vivo* in mouse hepatocytes [90]. It is also worth noting that AMPK can be activated allosterically with pharmacological chemicals such as salicylate (the active compound of aspirin). AMPK can stimulate autophagy via the inhibition of mTORC1, or, more directly, phosphorylate and thereby activate ULK1 [109] as well as the various subunits of the BECN1-VPS34 complex. During glucose deprivation AMPK phosphorylates BECN1 at serine residues 93 and 96, which induces autophagy. Since AMPK plays a major role in the regulation of metabolism, it is not surprising that it can stimulate autophagy by multiple mechanisms.

2.3.2.2 Mammalian target of rapamycin complex 1

The mammalian target of rapamycin complex 1 (mTORC1) is composed of mTOR itself, two mTORC1-specific regulatory proteins and several other mTOR-associated proteins that are shared with the mammalian target of rapamycin complex 2

(mTORC2). These two mTORC1 specific regulatory proteins are regulatory-associated protein of MTOR complex 1 (RPTOR, best known as raptor) and AKT1 substrate 1 (AKT1S1, generally known as PRAS40). In addition, several other shared mTOR-associated proteins include DEP-domain-containing MTOR-interacting protein (DEPTOR) and mammalian LST8 homologue (mLST8, also known as GβL). mTORC1 acts as an energy/nutrient/redox sensor whose activity is regulated by amino acids, growth factors, energy reserves, nutrient availability and oxidative stress. Its role is to control the translation of proteins in response to growth factors in the presence of adequate nutrients. Growth factors can activate mTORC1 by phosphorylation via the receptor tyrosine kinase (RTK)-Akt/PKB signalling pathway, which leads to the phosphorylation of ribosomal protein S6 kinase (RPS6K, also known as p70S6K) and eukaryotic translation initiation factor 4E binding protein 1 (EIF4EBP1). The active forms of RPS6K and EIF4EBP1 consequently promote protein synthesis [227]. Once phosphorylated, mTORC1 can suppress autophagy by phosphorylating and inhibiting of ULK1 [109], transcription elongation factor b (TFEb) [223], Atg14 [277] and Autophagy/Beclin1 Regulator (AMBRA) [179]. AMPK can induce autophagy by indirectly phosphorylating, thereby activating, tuberous sclerosis complex 2 (TS2) which negatively regulates mTORC1 [78]. Additionally AMPK can phosphorylate RPTOR, which suppresses mTORC1 activity, hence promoting autophagy [78]. The availability of amino acids, which are positive regulators of mTORC1, can suppress autophagy through various pathways, many of which have not been fully elucidated. For instance, lysosomes act as temporary stores of amino acids since they are the major site of protein degradation and amino acid recycling. It is therefore not surprising that mTORC1 and its regulators Rheb (Ras homologue enriched in brain), and Rag GTPases (RRAG, a Ras-related GTPase) reside on the lysosomal surface (Fig. 2.5) [44]. The Rag GTPase complexes together with a trimeric p14, p18, and MP1 protein complex form the regulator scaffolding. This implies that an amino acid-sensing system exists on the surface of lysosomes, which assesses amino acid availability within the lysosome lumen, and signals to the Ragulator-Rag complex. However, the exact site of localisation still remains elusive. This

reflects a currently unknown function of lysosomes to connect with intracellular pools of amino acids [218]. Additionally, α-ketoglutarate, which is a glutaminolysis intermediate, has been shown to be a potent activator of autophagy in the absence of amino acids, a process which is thought to be facilitated by the lysosomal RHEB-dependent pathway [44]. Interestingly, a decrease in α-ketoglutarate has been shown to extend life expectancy by inhibiting mTORC1 and by inducing autophagy [30]. However, these attributes of α-ketoglutarate are credited to its ability to inhibit mitochondrial ATP synthesis through the F_1F_0-ATPase. The tuberous sclerosis complexes 1 and 2 (TSC1 and TSC2) regulate Rheb activity by phosphorylation, thereby linking nutrient-sensing networks. Leucine depletion strongly correlates with the activation of autophagy, therefore it is not surprising that it can promote autophagy through multiple pathways. For instance, leucine can allosterically activate glutamate dehydrogenase thereby promoting glutaminolysis. It can also activate RRAG via leucyl-tRNA synthetase [69]. Not only do Rag GTPases signal amino-acid concentrations to mTORC1, but also glucose levels [45, 66]. This suggests that AMPK may not be the only glucose sensor. Importantly, mTORC1 not only regulates lysosomal biogenesis and represses autophagy, but also functions as a general regulator of anabolic reactions [227]. Since both mTORC1 and AMPK control broad intracellular metabolic networks, the use of chemical inhibitors of mTORC1 such as rapamycin have wide-ranging metabolic consequences other than inducing autophagy. In addition, when downstream autophagy signalling pathways are affected, mTORC1 inhibitors lose their capacity to induce autophagy.

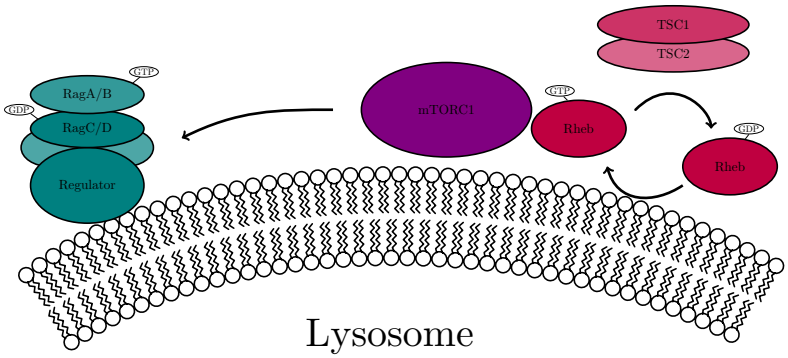

Figure 2.5: mTOR localisation to the lysosome.

2.3.2.3 eIF2a kinases

The activation of initiation factor 2a (eIF2A) forms part of the integrated stress response that allows cells to limit protein synthesis alongside the activation of autophagy in response to the accumulation of unfolded proteins. This is an attempt to restore homeostasis [124]. There are four kinase variants that are expressed by mammals that can phosphorylate eIF2a, which are eIF2ak1 (also known as HRI), eIF2ak2 (also known as PKR), eIF2ak3 (also known as PERK) and eIF2ak4 (also known as GCN2) [229]. Various stimuli, such as heme availability, can activate these kinases. In summary, the regulation of autophagy is closely linked to the integrated stress response network.

2.3.2.4 Sirtuins

Sirtuins are class III histone deacetylases, belonging to a protein family that consists of several mammalian variants (SIRT1-7). Sirtuins catalyse the deacetylation of protein substrates. Unlike other deacetylases that hydrolyse acetyl-lysine residues, sirtuin-mediated deacetylation requires NAD^+ hydrolysis for lysine deacetylation. The subsequent hydrolysis of NAD yields O-acetyl-ADP-ribose and nicotinamide, which are inhibitors of sirtuins [88]. Of all the known sirtuin deacetylases, sirtuin 1 (SIRT1) is the best studied. It is mainly localized within the nucleus where it is responsible for the deacetylation of histones such as H1

and H2, as well as various other proteins. These include transcription factors such as forkhead box O1 (FOXO1) and NF-kB [88]. Resveratrol, a plant-derived polyphenolic compound with wide-ranging health benefits, can activate SIRT1 and promote autophagy [128]. Interestingly, the expression of the cytoplasm-restricted mutant of SIRT1 could induce autophagy, which suggests that SIRT1 could induce autophagy without assistance of its transcriptional cascade [170]. Although Atg5, Atg7, Atg12 and LC3 have been implicated in the SIRT1-induced autophagy cascade, the precise mechanism through which autophagy is induced via SIRT1 activation still remains elusive [130]. Since sirtuins form part of broad intracellular networks, similar to that of mitochondrial biogenesis and inflammation [201], it is not surprising that SIRT1 can be activated by other factors than NAD^+ [22]. For instance, a low caloric diet can stimulate SIRT1 activity, whereas a high-fat diet can reduce SIRT1 activity [22]. To conclude, SIRT1 can promote autophagy under defined circumstances and contributes to the pro-autophagic activity of AMPK.

2.3.2.5 Acetyltransferases

Transfer of acetyl groups plays a major role in signalling cascades, post-translational modification of proteins as well as histone modification. Histone modification leads to nuclear remodelling of chromatin architecture that can either result in chromatin condensation or expansion. Reductions in the intracellular pool of acetyl-CoA results in overall reduction of protein acetylation in the cytoplasm, as well as in the nucleus [47, 149]. Accordingly, the availability of acetyl-CoA, which is the sole donor of acetyl groups, determines the catalytic activity of several acetyltransferases. Reduction in the availability of acetyl-CoA has been linked to autophagy activity and the E1A-binding protein p300 (EP300) has been found to play a critical role in the regulation of autophagy [149]. The physiological role of EP300 is to monitor intracellular acetyl-CoA availability and to respond to the transition between a fed and unfed state and the accompanying shifting between intracellular endogenous energy reserves. Furthermore, the inhibition of EP300 stimulates autophagy even during conditions of high abundance of acetyl-CoA [149]. EP300 inhibits several proteins involved in autophagy induction by acetylating proteins

of the core autophagic machinery such as Atg5, Atg7, Atg12, and LC3 [131]. Although EP300 is implicated in autophagy regulation, it is likely that other acetyltransferases, such as the inhibitor of growth (ING) family, may play a part in regulating autophagy [149]. Interestingly, several histone acetyltransferases have been connected to autophagy regulation in yeast, which lacks an EP300 orthologue [46]. Furthermore, in yeast models, mutated histone-coding genes can cause an increase in autophagy as a result of over-expression of components of the core autophagic machinery [47]. Acetyltransferases form part of a broad intracellular acetylation network where activation of one can inhibit another. For instance, tubulin acetyltransferase 1 (ATAT1, best known as MEC17) is negatively regulated by EP300. ATAT1 can be activated by AMPK, and conversely AMPK can inhibit EP300 activity by phosphorylation on the serine residue 89 [269]. Therefore the activation of AMPK causes the inhibition of EP300 as well as the activation of MEC17, which subsequently results in the hyperacetylation of α-tubulin. This scenario seems to bring about pro-autophagy effects [147]. To conclude, both hyperacetylation and deacetylation have inhibiting or inducing effects on autophagy, linking energy sensing networks to the control of autophagy.

2.3.2.6 Cell-surface nutrient receptors

Cell-surface nutrient receptors have import biological roles, acting as a means for the cell to respond to extracellular metabolite changes as well as to physiological cues from the brain and pivotal organs. Autophagy, an adaptive response to stress, is therefore associated with a cell-surface receptor signalling cascade. Several cell-surface receptors have been linked to autophagy, but the precise signalling cascade involved still remains unclear. It is thought that increases in intracellular levels of inositol-1,4,5,-triphosphate, diacylglycerol and cyclic AMP play a role in autophagy regulation as a result of cell-surface receptor signal transduction [258]. Several G protein-coupled receptors (GPCRs) found on the cell surface assess nutrient availability in the extracellular microenvironment and communicate with the autophagic machinery. Several identified cell-surface receptors include, but are not limited too, amino acid sensing receptors, γ-aminobutyric acid B recep-

tor 1 (GABBR1), the G protein-coupled receptor GPRC6A, heterodimeric taste receptors, metabotropic glutamate receptors (mGluRs), calcium-sensing receptors (CASR), as well as free fatty acid receptors. In conclusion, several nutrient-sensing networks detect extracellular and/or intracellular nutrient fluctuations and initiate an autophagic response. However, it must still be investigated whether systemic nutrient limitation preferentially stimulates autophagy compared to limitation of a single molecule. Furthermore, it is not known what degree of control each sensor exerts over autophagy, systemically as well as tissue specific. This chapter has shown that different isoforms of key proteins involved in the autophagy induction cascade, such a AMPK, the mTORC1 complex, and acetyltransferases, all contribute to the fine regulation of autophagy.

2.4 The biological role of autophagy

Autophagy, an evolutionary conserved process found in all eukaryotes, is presumed to be the primary means of maintaining cellular homeostasis during conditions of diminishing nutrient reserves as well as metabolic perturbations. This is achieved through targeting endogenous reserves, such as cytoplasmic proteins, for degradation to supply the building blocks for essential anabolic reactions as well as ATP synthesis [230]. Cells with defective autophagic machinery are more susceptible to nutrient perturbation than their wild type counterparts [124]. For instance, genetically altered mice that express defective components of the autophagic machinery die shortly after birth, which is thought to be as a result of the inability to mobilize energy reserves through autophagy. These mice do not survive the period of starvation between placental metabolism and suckling [126]. A reduction in autophagic capacity has been associated with numerous diseases such as neurodegeneration, cardiovascular disorders, cancer and ageing-associated pathologies [31]. In contrast, the autophagic system is exploited by tumours as a means to cope with adverse conditions [65]. On a systemic level, the induction of autophagy extends the lifespan of mice and various other animal models [215]. Here, we will discuss autophagy at the single cell and whole body level and ask how the regula-

tion of autophagy influences the health of an organism as well as susceptibility to disease.

2.4.1 Basal autophagy in intracellular quality control

2.4.1.1 Protein quality control

Basal autophagy plays an essential role in maintaining cellular homeostasis. Intracellular proteins can be categorized into short-lived and long-lived proteins [89, 105]. Short-lived proteins constitute less than 1% of protein content in hepatocytes, but they represent nearly one-third of protein degradation as a result of their rapid turn-over [105, 173]. It is widely accepted that the majority of short-lived proteins are degraded by the ubiquitin-proteasome system, while long-lived proteins are degraded via autophagy. In contrast, long-lived proteins are not selectively degraded, but rather randomly sequestrated by autophagosomes and degraded. Long-lived proteins constitute 99% of intracellular proteins [105]. Short-lived proteins can also be degraded via the autophagic machinery [2]. Only recently, the importance of basal autophagy has come to light, implicating its role as a quality-control system, particularly in neuronal cells and hepatocytes.

Liver-specific Atg7 knock-out mice. The importance of basal autophagy was first revealed in liver-specific Atg7 knock-out mice. Not only did the mice exhibit defective starvation-induced autophagy, but they also developed various abnormalities such as hepatomegaly, even when they were maintained in nutrient rich conditions [119]. Intriguingly, a considerable amount of ubiquitin-positive aggregates was observed in these hepatocytes [119], and both serum alanine aminotransferase and aspartate aminotransferase levels were considerably elevated.

Atg5 and Atg7 mice knock-out embryos. Neonates from Atg5 and Atg7 knockout mice showed minimal defects at birth. However, they had a reduced body size in comparison to their wild type counterparts, and exhibited suckling defects [119, 126]. Systematic analysis of $Atg5^{-/-}$ neonates showed accumulation of ubiquitin-positive aggregates in hepatocytes and some parts of the brain [75], which reflects the significance of basal autophagy that varies among cell and tissue types.

The dorsal root ganglion exhibited the largest amount of protein aggregates, in contrast to other cell/tissue types, such as skeletal muscle and kidney, that showed very few aggregates.

Neuronal cell specific Atg5 and Atg7 knock-outs. The role of basal autophagy in the central nervous system was further investigated in Atg5 and Atg7 knock-out mice. Although these mice were born normally, they showed growth retardation and developed progressive motor and behavioural defects after three weeks [75, 117]. Closer examination of the brain revealed partial loss of cerebellar Purkinje cells, pyramidal cells, as well as axonal swelling in various regions of the brain. Intriguingly, there was a difference between the survival rates of Atg5 and Atg7 knock-out mice. Atg5 knock-out mice exhibited sporadic death, whereas most Atg7 knock-out mice died within three weeks. This suggests that Atg7 may serve functions in neuronal cells other than autophagy, especially since it is implicated in the activation of Atg8 homologues such as GATE-16 [216] and γ-aminobutyric acid $(GABA)_A$-receptor-associated protein (GABARAP) [254]. The mechanism responsible for the observed ubiquitin-positive aggregates is still unclear. However, these aggregates are not found in glial cells. Autophagy arrest leads to the accumulation of ubiquitinated proteins and subsequent protein aggregate formation in the cytoplasm [75]. Therefore, it seems that protein aggregation formation results from impaired protein turnover. Accordingly, basal autophagy facilitates continuous clearance of diffuse cytosolic proteins, and not of aggregate itself, thereby preventing the accumulation of abnormal proteins as well as protein aggregation.

It is essential for cell growth and whole organism development to maintain a fine balance between protein and organelle synthesis and degradation in order to maintain vital cellular functions. By preventing further damage to cellular components by rapidly degrading proteins with potentially deleterious effects, basal autophagy acts as a protein quality control system. Cell-specific differences in autophagy could possibly be attributed to the importance of quality control in non-dividing and post-mitotic cells, in comparison to rapidly dividing cells where abnormal constituents can be rapidly diluted out if they are not degraded.

2.4.2 Adaptive responses to stress

2.4.2.1 Starvation response

Autophagy is characteristically induced upon starvation. In mammals, autophagy can be induced by the absence of nutrients, most notably through caloric and amino acid deprivation. Metabolic perturbations induce autophagy via energy-sensors (see Section 2.3.2) [124]. Therefore decreases in intracellular ATP, amino acids, NADH/NAD^+ ratio, AMPK, sirtuins, and inhibition of mTORC1 result in the induction of autophagy via energy-sensing networks. Furthermore autophagy can be induced in a biphasic manner, a rapid response that occurs in a matter of minutes to hours [170, 241], and a protracted response that relies on the transcriptional programs [223, 257]. The rapid response does not require *de novo* synthesis of macromolecules, but rather relies on the mobilization of endogenous reserves upon autophagy activation through post-translational regulatory mechanisms such as phosphorylation and acetylation. The protracted autophagic response modulates autophagy by regulating multiple kinases that form part of the autophagic "core machinery" such as Atg1 as well as key kinases, such as mTORC1 and Vps34, involved in signalling pathways [13].

2.4.2.2 Systemic autophagy response

Although the majority of studies focus on autophagy in the liver and neuronal cells, autophagy does occur throughout the whole body [161]. In GFP-LC3 transgenic mice it was observed that autophagy is activated after 24 hr food withdrawal in liver, heart, skeletal muscle, exocrine glands, podocytes in kidney and seminal gland cells [161]. Furthermore, autophagy is differentially induced by nutrient deprivation in a tissue-dependent manner. The maximal rate is reached after 24 hr, followed by a decrease in most tissues. In contrast, in some tissues, such as the heart and slow-twitching muscle, the rate of autophagy continues to accelerate after 24 hr. Interestingly, thymic epithelial cells are constitutively active in autophagy even under nutrient-rich conditions. Therefore the regulation of autophagy is organ dependent and also not only limited to an adaptive response to starvation.

Minimal autophagy activity was reported in brain in starvation, because presumably the brain is nutritionally protected under physiological stress conditions. For instance, depending on the nutritional state, the brain can utilize either glucose or ketone bodies, which are supplied by the liver. However, it is crucial to note that assessing autophagic capacity solely on GFP-LC3 vesicles can be misleading (see Section 2.6). For instance, as revealed through this thesis, high flux may obtain at low levels of intermediates such as autophagosomes, which may be true for cells where autophagy plays a major role in cytoprotection and protein degradation. Basal autophagy has been shown to play a vital role in maintaining cellular integrity, and aberrations in autophagy are intimately linked to several neurodegenerative diseases. Therefore, it is possible that a low vesicle count in neuronal cells does not reflect low autophagic flux, but is rather suggestive of high flux; this still needs to be investigated. Thus, a robust and accurate method needs to be developed to assess autophagic flux. Furthermore, the liver characteristically has an abundance of autophagosomes, especially during nutrient deprivation, which may indicate relatively low autophagic flux. It is not unreasonable to expect different rates of autophagic flux in different tissue/cell types, since they differ in protein turnover and amino acid demand.

2.4.3 Autophagy and human disease

2.4.3.1 Neurodegeneration

There is an increasing number of papers in the literature that supports the notion that aberration in autophagy is intimately linked to several human diseases. The basal autophagic flux varies among cell types, and may be particularly heightened in cells, such as neurons, that do not divide after differentiation [75, 117, 119, 120]. Neuronal-specific Atg5 and Beclin1 knock-out mice that survive the postnatal starvation period develop cumulative motor deficits and exhibit abnormal reflexes as well as present excessive ubiquitin-positive inclusion bodies in their neurons [75, 117]. Although the autophagosomal pool size seems remarkably lower than that of other tissue types [161], this may provide indirect evidence of high au-

tophagic flux in these tissues and may reflect the indispensable role of autophagy in maintaining protein quality control. The importance of autophagy becomes more apparent under disease conditions. Recent studies indicate the importance of autophagy, in addition to the ubiquitin/proteasome degradation system, in the clearance of disease-related mutant proteins. For instance, the accumulation of extended polyglutamine-containing proteins is the root of various neurodegeneration diseases such as Huntington's disease and spinocerebellar ataxia, as well as mutated forms of α-synuclein contributing to the origin of familial Parkinson's disease [151, 212, 214]. Chaperone-mediated autophagy is also involved in the degradation of α-synuclein, but the mutant α-synuclein blocks the lysosomal receptor which subsequently inhibits CMA [38]. Affected cells up-regulate macroautophagy in an attempt to compensate for the CMA congestion, which ensures cell survival. However this renders them more susceptible to stress [152].

Alzheimer's disease (AD) is a chronic neurodegenerative disease that is commonly associated with memory loss. It is characterized by the presence of senile plaques in the extracellular space in especially the cerebral cortex, as a result of extensive amyloid beta (Aβ) deposits [91]. These plaques result from dysfunctional proteolytic cleavage of the amyloid precursor protein (APP) that is localized in endocytic and secretory compartments. Autophagosomes are actively formed in synapses and along neuritic processes and require retrograde transport towards the neuronal cell body for degradation. Lysosomes are highly concentrated in these locations for efficient clearance of autophagosomes and its cargo. In Alzheimer's disease, both the maturation process of autophagosomes and their retrograde transport is impaired and leads to extensive accumulation of autophagic vacuoles along dystrophic and degenerating neurites [185]. Furthermore, since both APP and its processing enzymes are found in these impaired autophagosomes, it increases substrate and enzyme interaction time and may lead to further generation of Aβ plaques [276]. Recently, the expression levels of Beclin1 have been shown to be reduced in the brain of patients with late stage Alzheimer's disease [199]. Moreover, the heterozygous deletion of Beclin1 in transgenic mice has been shown to increase intracellular Aβ accumulation and extracellular Aβ deposits in old mice

with subsequent promotion of neurodegeneration [132, 199]. Increased expression of Beclin1 in mice seems to have the reverse effect. In summary, Aβ levels are influenced by both autophagosome production and clearance [222]. Thus, an impediment in the autophagosome maturation process increases Aβ which promotes neurodegeneration.

Parkinson's disease (PD), also known as paralysis agitans, is a neurodegenerative disorder of the central nervous system. It is characterized by the continued loss of dopamine-generating neurons in the substantia nigra. The most notable symptoms of PD, such as tremors and rigidity, are movement-related. PD is an idiopathic disease with no known cause, but several factors have been shown to be involved in the progression of the disease, such as the accumulation in the neurons of α-synuclein (α-syn) into inclusion bodies termed Lewy bodies. Healthy neurons degrade α-syn via chaperone-mediate autophagy (CMA), but in PD mutant variants (A53T and A30P) of α-syn bind to the lysosomal membrane receptor and prevent their own degradation as well as that of other substrates [38]. Therefore pathogenic mutant variants of α-syn are found in cytosolic inclusion bodies. Moreover, α-syn aggregates can only be degraded through the autophagic pathway [259]. Intriguingly, a fraction of α-syn present in Lewy bodies is mono-ubiquitinated, which promotes the transition of aggregation of α-syn to amorphous aggregates as well as stimulates the formation of α-syn aggregate inclusion bodies within dopaminergic cells [49]. It is worth noting that ubiquitination and the majority of other post-translational modifications of α-syn seems to impede its degradation by CMA. Moreover, dopamine-modified α-syn is poorly degraded by CMA and prevents the degradation of other CMA substrates, all of which renders the cells more susceptible to stress.

Huntington's disease (HD) is a neurodegenerative genetic disorder caused by a polyglutamine expansion mutation in the huntingtin protein. Affected individuals have impaired muscle coordination and cognitive as well as behavioural symptoms. Mutated huntingtin proteins have cytotoxic qualities and are also more aggregate-prone, leading to the formation of neuronal intra-nuclear inclusion bodies and neuronal death. Several factors have been implicated in the progression of

HD, including excitotoxicity, metabolic impairment, autophagy, dopamine toxicity and oxidative stress [62]. Several studies have implicated autophagy in the progression of the disease. HD patients' brains are characterised by an increased endosomal and/or lysosomal content, accompanied by lipofuscin accumulation which is suggestive of autophagy [242]. In addition, endosomal and/or lysosomal activity is increased by the expression of mutant huntingtin [107]. The wild type huntingtin protein naturally associates with the ER, and is released from the ER membrane during periods of stress, after which it translocates to the nucleus. Once the stress dissipates, huntingtin translocates back and re-associates with the ER. Cells affected by mutated huntingtin show a disrupted ER as well as an increase in autophagic vesicles [8]. Interestingly, both polyglutamine and polyalanine expansions of proteins make them aggregate-prone and therefore targets for degradation by autophagy [206]. Inhibition of autophagy by either chemical or physiological intervention leads to the accumulation of mutant huntingtin protein aggregate and increased cell susceptibility to stress, whereas the induction of autophagy promotes huntingtin degradation and increases cell viability [202]. In addition, mTOR activity is inhibited as a result of being embroiled within mutant huntingtin protein aggregates, which induces autophagy [208]. This may directly promote huntingtin protein aggregate degradation via autophagy [202, 206, 208]. The accumulation of mutant huntingtin can also induce autophagy through mTOR-independent pathways, which include the insulin signalling pathway that requires Beclin1 and Vps34 [267]. The increase in insulin receptor substrate 2 (IRS2) activity stimulates the clearance of huntingtin regardless of Akt and mTOR activation. The entanglement of Beclin1 in affected neuronal intra-nuclear inclusion bodies seems to reduce the autophagic clearance capacity [226]. Furthermore, in human brains the expression of Beclin1 decreases in an age-dependent manner, which leads to a reduction in the autophagy capacity during ageing and in turn promotes the accumulation of mutant huntingtin and the progression of the disease.

There is no doubt that autophagy has protective effects against neurodegeneration. However, the mechanisms by which autophagy protects against neurodegeneration are still poorly understood. The leading hypothesis indicates that au-

tophagy either directly eliminates inclusion bodies or protein aggregates, or indirectly suppresses aggregate formation by rapidly degrading aggregate prone proteins [16, 93]. Furthermore, p62/sequestosome-1 (SQSTM1) plays a crucial role in preventing spontaneous protein aggregate formation [118]. It has both LC3-binding and ubiquitin-binding domains that mediate recognition and binding of aggregate prone proteins to LC3, a key membrane component of the autophagic sequestering vesicle, thereby facilitating degradation [16, 195]. A recent hypothesis has been proposed that contradicts the degradation of aggregates by autophagy; it rather suggests that the creation of protein aggregates is a cytoprotective mechanism [5, 237]. Therefore, it could be that the role of autophagy is rather to maintain cytosolic protein quality, implying that protein aggregate and inclusion body formation result from impaired protein turnover in autophagy-compromised cells [75]. These data suggest that an exact measurement of autophagic flux is instrumental to understanding the role of autophagy and elucidating its role in the pathogenesis of neurodegeneration.

2.4.3.2 Cancer

Autophagy has long been known to be associated with cancers [18]. It is likely that the role of autophagy varies in the different stages of cancer development. For instance, during normal cell development autophagy acts as a preventive strategy against cancer, in contrast to established tumours that exploit autophagy for their own cytoprotection [96, 153, 260]. Additionally, cancer is one of the first diseases to be genetically linked to autophagy impairment [153]. An example is the mono allelic deletion of BECN1, which encodes the Beclin1 protein. The deletion of BECN1 is present in 40–75% of cases of human breast, ovarian, and prostate cancer [3, 58, 139, 217]. Additionally, unusual expression levels of Beclin1 in various tumours have been linked to poor prognosis [60, 123, 225, 253, 264]. It therefore seems that Beclin1 is mechanistically important in tumorigenesis, a possibility which is supported by the heterozygous disruption of Beclin1 in mice that show decreased autophagy and are more susceptible to spontaneous tumour development [203, 278]. Beclin1 is the mammalian orthologue of yeast Atg6/Vps30

protein, which plays a vital role in the regulation of autophagy. Beclin1 forms part of the class III phosphatidylinositol 3-kinase (PtdIns3K) complex, which consists of PtdIns3K Vps34, mAtg14 and p150 [92, 108, 139, 232]. Beclin1 is the regulator of the PtdIns3K complex, which is required for initiation of the nucleation and assembly of the phagophore. In addition to its regulatory role in autophagy induction, it also has biological roles in anti-apoptosis [33] and endocytic trafficking [243].

Several other proteins involved in the autophagic cascade that exhibit altered expression levels, such as Atg5 [110, 141] and the protein encoded by the ultraviolet irradiation resistance-associated gene (UVRAG), [138] have been reported to be linked with cancers. In fact, several other autophagy-related proteins, such as Atg4c, exhibit tumour suppressor properties, which suggests that this may be an inherent property of autophagy proteins involved in vital signalling cascades [150]. Moreover, the regulation of autophagy signalling is closely associated with oncogenic signalling. Several generally activated oncogenes such as PKB, mTOR and Bcl-2 inhibit autophagy, whereas frequently mutated or epigenetically silenced tumour suppressor genes involved in the mTOR signalling network, such as p53, PTEN and TSC2, stimulate autophagy [18, 162]. These genetic links between molecular dis-regulation and cancer suggest that autophagy may operate as a tumour suppressor pathway, but the exact mechanisms are unclear. Furthermore, studies in autophagy-deficient yeast show an increase in the frequency of mitochondrial DNA mutations, which implies that basal autophagy plays a role in preventing genotoxic stress and DNA damage [137, 153]. A recent study that used immortalized epithelial cells with either Beclin1 or atg5 knockdown mice showed increased DNA damage as well as increased tumorigenicity, indicating that both Atg5 and Beclin1 preserve genomic integrity [153]. Hence, while the primary role of autophagy is to promote cell survival, it can also function as a tumour suppressor. Autophagy can promote tumour survival when exposed to metabolic stress, thereby preventing tumour necrosis. However, the activation of autophagy during metabolic stress conditions has also been shown to prevent cell growth [137]. Therefore it is likely that the pro-survival effects of autophagy are counterbalanced

by its tumour suppressor effects. The pro-survival effects are of great interest in anti-cancer treatment, because of their potential contribution to chemotherapy resistance in tumours. Recent studies have shown that inhibition of autophagy increases cytotoxicity of cancer chemotherapeutic agents [1, 21]. Consequently, the disruption of autophagy could maximize the effects of cancer cytotoxic drugs. A sensitive and quantifiable tool would be required to assess and standardize autophagy flux, and could be used to develop effective autophagy inhibition interventions.

2.4.3.3 Ageing

A hallmark of ageing cells is a build-up of damaged proteins and organelles in parallel with an increase in cellular susceptibility, even in the absence of diseases. Accumulation of damaged proteins and organelles and the resulting inclusion of deposits have particularly deleterious effects in non-dividing, differentiated cells such as neurons and cardiomyocytes. It is evident that non-dividing cells are characterized by an earlier functional decline with age than other cell types. The activity of both macro-autophagy and chaperone-mediated autophagy decreases with ageing [37, 40]. Taking into consideration the recently-obtained data from genetic mouse models with impaired autophagy and which exhibit detrimental phenotypes [75, 117, 119, 177], it could transpire that the progressive loss in autophagic activity with age plays a crucial role in cell and whole organism deterioration. It is interesting that caloric restriction, which is known to induce autophagy, has been shown to delay the effects of ageing [83]. Bergamini [15] suggested the use of anti-lipolytic drugs to simulate caloric restriction in order to induce autophagy and slow the progression of ageing.

2.5 Therapeutic modulation of autophagy in diseases

Autophagy has been identified as a therapeutic target for the treatment of neurodegeneration because of its cytoprotective function in neurons. For instance, the up-regulation of autophagy by targeting the autophagy regulatory protein mTOR with inhibitors such as rapamycin and its analogue CCI-779 protects against neurodegeneration in mouse models [208]. Autophagy inducers improve the clearance of the aggregate-prone mutant huntingtin and α-synuclein, thereby protecting the cellular integrity and promoting health. Furthermore, other small molecules that induce autophagy independent of mTOR have been identified. Since mTOR is an essential protein involved in multiple pathways such as energy sensing pathways, targeting mTOR might lead to unwanted downstream effects. Thus, using mTOR-independent autophagy inducers in combination with rapamycin for therapeutic purposes would allow for the fine manipulation of autophagy without severe side effects.

Autophagy has become an attractive target for therapies that aim to treat various diseases. A practical means of exploiting autophagy in cancer treatment is autophagy-mediated cell death. Induced autophagy-mediated cell death has been reported in tamoxifen-treated MCF-7 cells [220] and soya bean saponin-treated colon cancer [247]. Alternatively, cancer cells can be sensitised by initially up-regulating autophagy followed by its inhibition. Inhibition of autophagy via pharmacological agents can be used to increase the cytotoxicity of cancer chemotherapeutic drugs [4, 21]. Clinical trials are in progress to increase the cytotoxic effect of cancer chemotherapeutic drugs by impairing the autophagic degradative capacity.

The dosages required to induce/inhibit autophagy are based on animal model trials. Too much or too little autophagy can have deleterious effects that can lead to necrosis [82]. It would be wise to differentially target autophagy in a disease-stage and context-specific manner to determine what would be most beneficial. In manipulating autophagy for therapeutic purposes it is important to note the dynamic behaviour of autophagy during the pathogenic course of a disease and

to determine if the autophagic flux is too high or too low and to adjust it accordingly. Furthermore, the numerical quantification of autophagic flux and the kinetic modelling of the mammalian autophagic system are critical for understanding the control of the autophagic process, which would allow for the exploitation of autophagy as adjunct to existing therapies or even as standalone therapeutic treatment.

2.6 Current methodologies for measuring autophagy activity

In the past decade there have been rapid advances in the autophagy research field, with the advent of the discovery of evolutionarily conserved autophagic related genes. The dawn of the molecular era ushered in novel techniques such as genetic manipulation, which uncovered the importance of autophagy in processes ranging from cellular homoeostasis to foetus development. In contrast, accumulating evidence suggests that dysfunctional autophagy contributes to a wide spectrum of human diseases [137, 162]. Therefore, there is a growing demand for accurate assessment of autophagy and an understanding of its role in biological processes. One of the major challenges faced in the autophagy research field is that of monitoring a dynamic process with predominately "static measurements" such as Western blotting and electron microscopy. This is accompanied by inherent shortcomings in conclusions reached from the use of these methods. Furthermore, it remains a challenge not to conflate autophagosomal pool size with autophagic flux. For instance, neurodegeneration was initially thought to be characterized, to some degree, by an increase in autophagy, a conclusion which was based on microscopy techniques that showed an increased presence of autophagosomes. However, an accumulation of autophagosomes may be a result of an obstruction in the later, downstream stages of autophagy [137, 162] (see Section 2.2, Fig. 2.2). These challenges have been only partially overcome by the development of new methods in autophagy research to elucidate autophagy's dynamic nature and to shed light on the functionality of autophagy in cellular processes. In the next sections current

methods used in autophagy research will be discussed with the aim of indicating their shortcomings in the above highlighted challenges.

2.6.1 Methods in monitoring autophagic intermediates

Presently three methods are used to monitor the number of autophagosomes in a cell: electron microscopy, light microscopy and the biochemical detection of LC3-II, which is associated with the autophagosomal membrane.

2.6.1.1 Electron microscopy

Electron microscopy (EM) is the longest-used and most established method for monitoring autophagic vesicles, and is still considered the gold standard in autophagy research. Mammalian autophagy was first discovered in the 1950s whilst studying lysosomes with electron microscopy. Autophagosomes were described as double-membraned structures that contain undigested or partially digested cytoplasmic content, indicating mitochondria or endoplasmic reticulum. Therefore it is rather easy to identify autophagosomes in electron micrographs because their unique morphological characteristics make them distinct from other cellular membranous vesicles. In comparison to autophagosomes, which contain cellular cargo, autophagolysosomes are somewhat more difficult to identify since the cargo is being degraded and there is no other obvious characteristic material to recognize in autophagolysosomes. Electron microscopy allows for ultra-structural characterization and morphometrical analysis of autophagosomes, such as dimensions, autophagosomal count and area occupied. Although electron microscopy is a well-established method in autophagy research and although it provides invaluable data, there are a number of disadvantages which are often overlooked. For instance, EM does not reflect the dynamic nature of the autophagic process, but rather provides a snapshot of the intracellular composition in time on a single z-axis plane. Since EM requires the fixation of cells, the autophagic behaviour cannot be monitored in a time dependent manner on a single cell level. Furthermore, studies that report autophagosomal numbers based on electron micrographs can only reflect the autophagosomal pool size that was visible in a single plane, which provides no

indication of the complete pool size. Hence, EM may lead to the reporting of underestimated pool sizes.

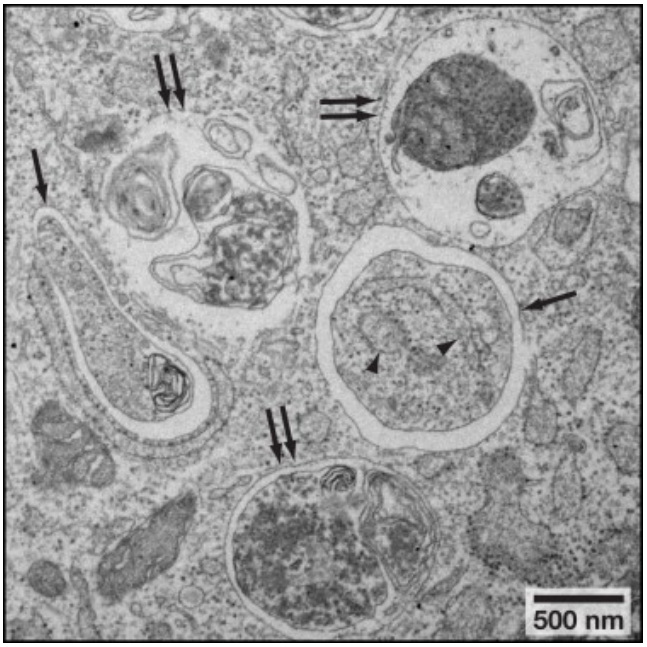

Figure 2.6: Electron microscopy. Typical electron micrograph of mouse embryonic fibroblasts. Single arrows show autophagosomes with a double membrane, double arrows indicate autophagolysosomes, and arrow heads point towards endoplasmic reticulum partially digested inside an autophagosome [167].

2.6.1.2 Fluorescence microscopy

Fluorescence microscopy (FM) makes use of fluorescent proteins or probes that are tagged to the protein of interest. These probes are excited and in turn generate a fluorescence emission signal which is used to produce an image. FM requires considerable less expertise than EM to identify autophagy related structures and therefore has recently become very popular amongst scientists. In autophagy research the most common probe used is the green fluorescence protein (GFP) tagged to microtubule-associated protein light chain 3 (LC3). The formation of a sequestering vesicle requires LC3 for the elongation of its membrane. This protein continues to associate with the outer and inner autophagosomal membrane after

its formation. Moreover, after fusion with the lysosome, LC3 is cleaved from the autophagosome outer membrane, whereas the inner membranous LC3 is degraded by lysosome hydrolases. Therefore endogenous LC3 or LC3-GFP is visualized either as a diffuse cytoplasmic pool or as fluorescing puncta which represent mainly autophagosomes. In contrast to EM, micrographs based on FM can be taken through the z-plane, which allows for the acquisition of the total autophagosomal pool size of a whole cell (see Fig. 2.7). In addition to the ease of identifying autophagosomal structures, FM allows the live imaging of cells, which enables the monitoring of autophagy in real time, thereby assessing the dynamic behaviour of autophagy. Although the number of GFP-LC3 puncta accurately reflects the autophagosomal pool size when acquired in the z-plane, this technique still has some potential experimental pitfalls. Foremost is subjectivity in the selection of GFP-LC3 puncta. A uniform approach needs to be developed that can detect a punctum and automatically quantify the total number of puncta. There are automated puncta-counting software package available, such as WatershedCounting3D, which is a plug-in for ImageJ. Furthermore, common practice is to report the average number of GFP-LC3 puncta as well as the total area of GFP-LC3 puncta per cell, but it is important to exclude experimental artefacts which arise from the formation of large GFP-LC3 aggregates. In addition, autophagy activity is also often expressed as a percentage change in GFP-LC3 puncta. However, in itself this approach could be misleading, since an increase in autophagosomes can be a result of either the induction of autophagy, or of an impairment in lysosome and autophagosome fusion. This is the most crucial aspect, which is currently not well addressed. Another potential pitfall of GFP-LC3 puncta screenings for assessing autophagic activity lies in the fact that GFP-LC3 and LC3 can easily aggregate when over-expressed or co-expressed with aggregate-prone proteins [127]. These GFP-LC3 aggregates can then be mistaken for autophagosomes. However, precautionary steps can be taken to reduce GFP-LC3 aggregate formation, for example by first using stable GFP-LC3 cell lines [167] and second using a C-terminal glycine mutant GFP-LC3 [240]. Stable GFP-LC3 cell lines are selected based on the expression of appropriate levels of GFP-LC3 without artificial aggregation.

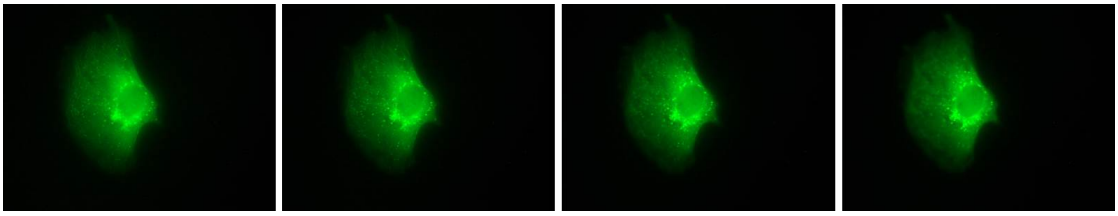

Figure 2.7: Fluorescence microscopy, series of z-stack micro-graphs of a single cell (see Section 3.7.1 for the experimental protocol by which these images were obtained).

2.6.1.3 Biochemical assays

Traditionally, together with EM, biochemical assays are used to assess autophagic activity. The role of LC3 in autophagy (see Section 2.2) has made it a particularly attractive means for assessing autophagic activity. LC3 has several homologues, among which LC3B is most commonly used as a probe in Western blotting. Western blot analysis of endogenous LC3 presents two distinct bands after sodium dodecyl sulphate–polyacrylamide gel electrophoresis (SDS-PAGE) and immunoblotting: one represents LC3-I, which is cytosolic, and the other represents LC3-II that is conjugated with phosphatidylethanolamine (PE). LC3-II is associated with the sequestering vesicle and the autophagosome. Although the true molecular mass of LC3-II is larger than that of LC3-I, conjugation with PE causes it to migrate faster than LC3-II in SDS-PAGE, presumably due to its extreme hydrophobicity. LC3-I and LC3-II are detected on the gel at a molecular mass of approximately 16 kDa and 14 kDa respectively. The amount of LC3-II generally corresponds to the number of autophagosomes, or, more accurately, the overall abundance of the autophagic membrane which is labelled with LC3-II [98]. However, not all LC3-II protein in the cells is localised in autophagosomal membranes, but also seems to be generated independently of autophagy. For instance, in Atg14 and FIP200 deficient mouse embryonic fibroblasts and Beclin1-deficient embryonic stem cells there was a significant amount of LC3-II detectable in Western blots, even though autophagosomal synthesis was completely inhibited [76, 154, 155]. The same was also seen in RNA interference (RNAi)-mediated suppression of various autophagic key proteins [87, 92, 154, 279]. Thus, the suppression of autophagy either genetically or pharmacologically may still result in LC3 being detected by biochemical

assays. Therefore alternative methods should be used in conjunction with LC3 assays to accurately report autophagy activity.

2.6.2 Current methods for monitoring autophagic flux

Electron and fluorescence microscopy as well as biochemical assays are useful to assess autophagic intermediates such as autophagosomes. However, these methods cannot be used to determine autophagic activity, since the accumulation of autophagosomes does not necessarily correlate with high autophagic activity. Similarly, LC3-II levels on their own may not truly reflect the autophagic activity. Culturing cells with lysosomotropic compounds that de-acidify lysosomes, such as bafilomycin A_1, and subsequently impair the lysosomal and autophagosomal fusion process, is required as it will result in the accumulation of autophagosomes and therefore LC3-II. Therefore, hence an enhanced autophagic flux, induced, for example, with rapamycin, will result in a greater increase in the number of autophagosomes after lysosomal and autophagosomal fusion impairment, with a concomitant increase in LC3-II. Currently the assays purporting to measure "autophagic flux" can only distinguish between autophagic induction and inhibition. For example, because electron microscopy is used to quantify the relative numbers of autophagosomes in electron micrographs it cannot reflect the degradation capacity of the autophagic system or the rate of autophagosomal degradation or synthesis.

2.6.2.1 LC3 turnover

The most widely used method to assess autophagic flux is by monitoring LC3 turnover. The method is based on the principle that LC3-II is degraded during the maturation process of autophagolysosomes. Thus, when cells are treated with lysosomotropic agents such bafilomycin A_1 or chloroquine, it results in the accumulation of LC3-II since the de-acidification of lysosomes prevents autophagosome and lysosome fusion [239]. Therefore, currently, the difference in the LC3-II levels between samples in the presence and absence of lysosomal inhibitors reflects the amount of LC3-II that would be delivered to lysosomes for degradation [113, 166, 213]. For instance, under normal conditions there will be an increase in

LC3-II levels when treated with bafilomycin A_1 (Fig. 2.8). However, during the induction of autophagy through rapamycin treatment the difference in LC3-II levels in the presence and absence of bafilomycin A_1 is larger (Fig. 2.8). Therefore, autophagic flux would have increased during rapamycin treatment since more LC3-II is being degraded. Even though the LC3 turnover assay is a relatively simple assay it becomes clear that it only reports on the relative change in flux and not the flux itself.

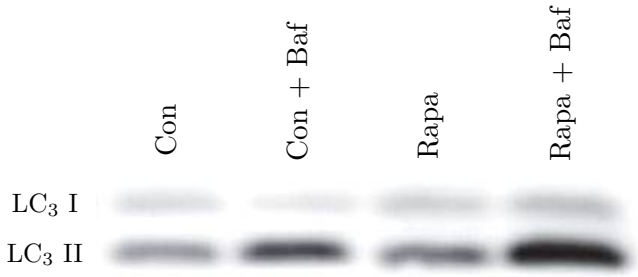

Figure 2.8: Western blot of LC3, lane 1: control condition, lane 2: control condition treated with bafilomycin A_1, lane 3: cells treated with rapamycin, lane 4: cells treated with rapamycin and followed by treating with bafilomycin A_1.

2.6.2.2 Degradation of selective markers

The degradation of LC3 through autophagy results in the reduction of total LC3 levels which could be used to assess autophagic flux, as mentioned above. Whereas induction of autophagy increases the number of GFP-LC3 puncta, the free cytoplasmic and nuclear GFP-LC3 signals are however reduced. The loss in cytoplasmic and nuclear GFP-LC3 signal can sensitively and quantitatively be monitored by flow cytometry [228]. Therefore the total free cellular LC3-GFP, which relates inversely to autophagic activity, can be measured by immunoblot analysis or flow cytometry. In addition, autophagy substrates can be used to assess autophagic flux. Historically autophagy was believed to be the random degradation of cytoplasm, but recent studies showed that several specific substrates are selectively degraded by autophagy. Of these selective substrates, p62 (also known

as SQSTM1/sequestome 1) is the best studied. It is selectively incorporated into the autophagosome by binding directly to LC3 followed by its degradation through autophagy [16]. Therefore the total intracellular p62 levels correlate inversely with autophagic activity. For instance, a reduction in p62 levels compared to control conditions would indicate an increase in autophagic flux. Since the cellular p62 level correlates well with autophagic flux, it provides a promising method to assess it. It is, however, still not clear whether p62 is only degraded through autophagy or partly through the ubiquitin-proteasome pathway. Furthermore, both LC3 and p62 are transcriptionally regulated during autophagy which may result in the inaccurate interpretation of autophagic flux when assessing LC3 and p62 [82, 178].

Besides monitoring LC3 and p62, autophagic flux can also be monitored by measuring the bulk degradation of long lived proteins. One of the now more historical methods, developed in the 1970s, monitors radiolabeled long-lived proteins [167]. This technique involves the culturing of cells with isotope-labelled amino acids (commonly [^{14}C] or [^{3}H]-labelled leucine or valine) for several days. Thereafter cells are cultured with normal media in order to wash out radiolabeled short-lived proteins. The release of the degraded proteins into the cytoplasm is then quantified and gives an indication of autophagic flux. This method provides precise numerical data that reflect the half life of long-lived cellular proteins, and circumvents the pitfalls associated with monitoring a single autophagic substrate. A more recent technique expresses photo-switchable proteins in the cytoplasm; upon activation the change in fluorescence is measured and used to determine the half-life of the fluorescently-labelled protein.

2.6.3 Conclusion

The above sections reviewed the currently available techniques used in autophagy research. Since these methods have potential limitations, it is currently recommended that several of these methods are used in combination to assess autophagic activity. Nevertheless, there is currently no method that can accurately quantify autophagic flux numerically as a rate, which is crucial for determining the dynamic behaviour and the degree of control a given pathway step has over autophagy.

Clearly, better assays are required to accurately assess autophagic flux and its control. Such novel techniques would improve our understanding of the dynamics of autophagy and may allow us to exploit autophagy in new clinical therapies.

2.7 Measuring autophagic flux

Autophagic flux is commonly defined as a measure of autophagic degradation activity. Currently there are a number of proposed methods to assess autophagic flux, many of which reflect whether or not autophagic flux is occurring or changing with a given treatment [113]. However, they remain to a lesser extent able to express autophagic flux and its change in a robust, sensitive and quantifiable manner. We have proposed a novel fluorescent-based microscopy method that fulfils the requirements for quantitative flux analysis as it allows for the measurement of autophagosome flux as a rate at the single cell level in a sensitive and quantifiable manner [142]. The refinement and application of this method is described in this thesis.

2.7.1 Defining autophagic flux

The autophagic pathway is defined as the pathway along which there is a flow of material, and the autophagic flux is the quantitative measurement of the rate of flow through the pathway at a steady state (Fig. 2.9). This definition of autophagic flux is similar to that of flux in metabolic control studies, where metabolic flux refers to the steady-state rate of flow of metabolites along a metabolic pathway [99]. The autophagic system can be regarded as a multi-step pathway with each step characterized by a particular rate, v.

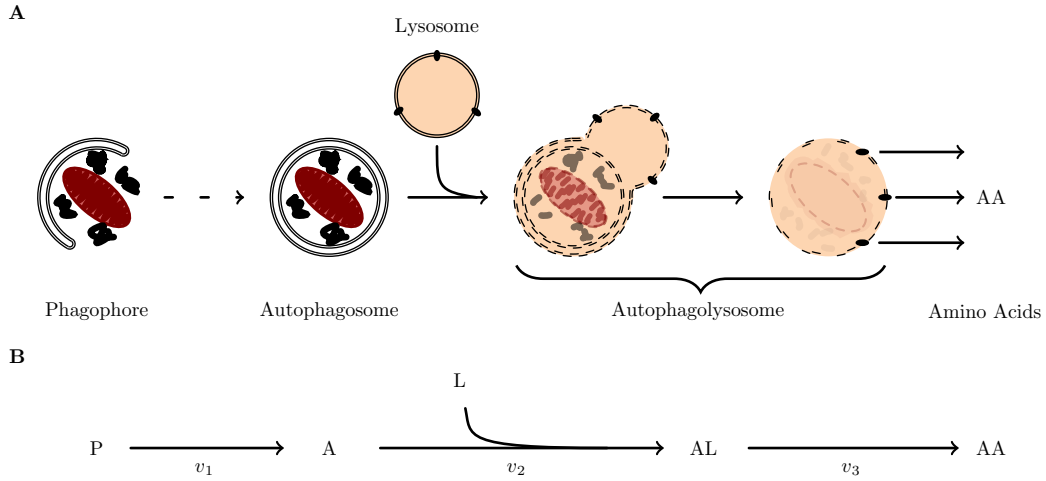

Figure 2.9: (A) Schematic representation of the autophagic process, and (B) reaction network representation of the autophagic process. P, phagophore, A, autophagosome, L, lysosome, AL, autophagolysosome, AA, amino acids.

Each individual step in the pathway proceeds at a particular rate, which is defined by the number of entities processed per time unit per cell. For example, step 2 proceeds at a particular rate, v_2, in which an autophagosome fuses with a lysosome. This rate can be described as either a decrease in the number of autophagosomes per time unit, or, equivalently, as a decrease in the number of lysosomes per time unit (assuming a one-to-one fusion of autophagosome with lysosome), or as an increase in the number of autophagolysosomes produced per time unit:

$$v_2 = \frac{-dn_{\mathrm{A}}}{dt} = \frac{-dn_{\mathrm{L}}}{dt} = \frac{dn_{\mathrm{AL}}}{dt}$$

where n_{A}, n_{L}, and n_{AL} denote the number of entities per cell. As defined here the rate v_2 is a positive quantity.

The following set of ordinary differential equations define the rate at which the number of the different autophagic vesicles change with time:

$$\frac{-dn_{\mathrm{P}}}{dt} = -v_1, \frac{-dn_{\mathrm{A}}}{dt} = v_1 - v_2, \frac{-dn_{\mathrm{AL}}}{dt} = v_2 - v_3, \frac{-dn_{\mathrm{AA}}}{dt} = v_3$$

In order to achieve a steady state, the entities that are only being produced or consumed (P, L and AA) must be regarded as buffered during the experiments,

and are therefore constants. In steady state the rate of change in the numbers of the variable entities A and AL are zero, so that their numbers remain constant in time:

$$\frac{-dn_{\mathrm{A}}}{dt} = \frac{-dn_{\mathrm{AL}}}{dt} = 0$$

which implies that

$$v_1 = v_2 = v_3$$

Therefore the steady-state flux, J, is numerically equal to the steady-state rate of any of the individual reaction steps in the pathway. This allows us to experimentally quantify the autophagic flux by completely blocking one of the reaction steps in the autophagic pathway, such as step 2, and measuring the initial rate of accumulation of the substrate of the inhibited step, in this case autophagosomes. The transition time, τ, of any variable intermediates in the pathway (A and AL) is defined as n/J, which can be interpreted as the turnover time of the intermediate's pool size in steady state, which in turn is equal to the time required to fill the pool size from zero to its steady-state value.

2.7.2 Quantifying autophagic flux

Based on the methods discussed in the current methodologies section, fluorescence microscopy has the enormous potential for determining autophagic flux by measuring the autophagosome pool size per cell and the change thereof over time. Furthermore, monitoring the decay of the fluorescence signal of reporter proteins using photo-switchable proteins has been thus far the most direct way measuring autophagic flux. This technique has been successfully employed in elucidating the kinetic properties of macroautophagy [249], chaperone-mediated autophagy [116], and the proteasome [251]. What sets this method apart from the conventional methods is that it assesses the loss of fluorescence intensity over time, therefore allowing the determination of half-lives of the specific protein within the autophagy context [116, 249].

The proposed method of Loos *et al.* [142] allows for the calculation of autophagosome flux, J. The protocol is based on the time-dependent change in the

total autophagosomal pool size after the complete inhibition of the autophagosomal and lysosomal fusion process. Furthermore, the transition time, τ, can be derived from the ratio of the total autophagosomal pool size and the flux. The transition time differs from the intensity-based half-life as it indicates the time required to turn over the autophagosome pool in the system, which can be used as additional means of quantification, and could be employed to compare systems. Such a protocol requires a reliable means of counting the total number of autophagosomes per cell at several time points under control/treatment conditions and then the complete inhibition of the autophagosomal and lysosomal fusion process (Fig. 2.9). The autophagosomal number (n_{A}) is plotted over time, as well as the change thereof after the complete inhibition of the fusion process (see Fig. 2.10). The initial change in n_{A} per time unit per hour per cell can be considered as the autophagic flux per cell.

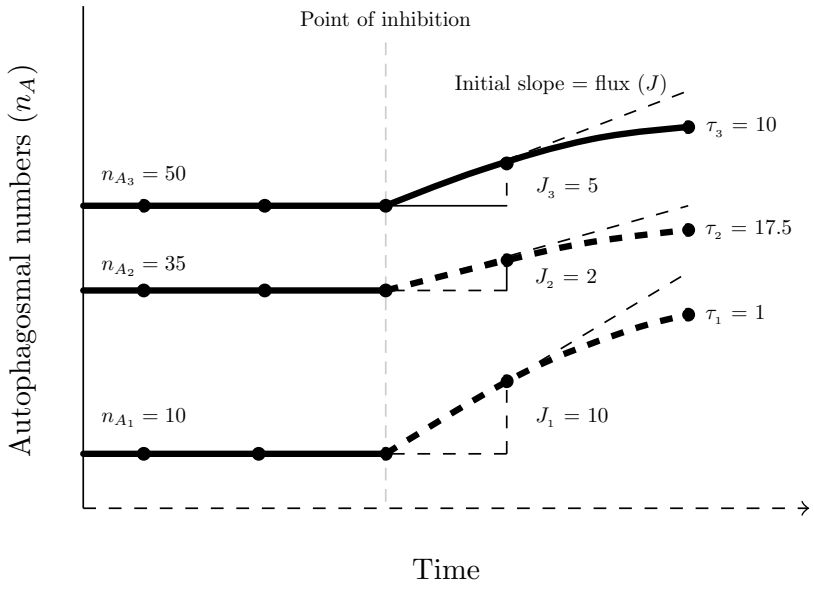

Figure 2.10: Quantifying autophagic flux. The graph depicts three autophagic states. Although the state with $n_{\mathrm{A}} = 50$ has the largest autophagosomal pool size, it does not imply that it also has the highest flux; compare, for example, the state with $n_{\mathrm{A}} = 10$, which has double the flux. Since autophagosomal pool size is monitored over time, the accumulation of autophagosomes after the complete inhibition of the fusion process can be used to calculate autophagic flux: $dn_{\mathrm{A}}/dt = J$. Furthermore, the transition time, $\tau = n_{\mathrm{A}}/J$, quantifies the time taken for the system to turn over its autophagosomal pool.

Chapter 3

Materials and methods

3.1 Consumables and materials

Sterile disposable 5mL (SPL, # 91005), 10mL (SPL, # 91010) and 25mL (SPL, # 91025) serological pipettes, as well as Pipetman P20, P200, and P1000 (Pipetman Starter Kit) were used for cell culturing. Disposable pipette tips, 10μL (Pipetman, # D10), 200μL (Pipetman, # D200) and 1000μL (Pipetman, # D1000), and 2mL Eppendorf tubes (Gilson, #04-230-1150) were used for cell culturing and protein extraction. Chemical solvents and solutions: ethanol, Illovo (#500), methanol, Merck (# 106009) and PBS, Life Technologies (# 10010-023). Cells were maintained in a Shel Lab incubator supplied with 100% carbon dioxide (Afrox, #201-RC). Proteinase inhibitors were purchased from Sigma: pepstatin (# P-4265), benzamidine (# B 6506), aprotonin (# A-6279), leupeptin (# L-9783), PMSF(#P-7626), and phosphatases inhibitors NaF (# S 7920) and Na_3VO_4 (# S 6508). Salts EDTA (Sigma, # T-9285) and Tris (Sigma, # D-6750) were used as components of buffer solutions. Na-deoxycholate (Sigma, # 30970) was used as an ionic detergent.

3.2 Mammalian cell culture protocol

Mouse Embryonic Fibroblast (MEF) cells with stable expression of GFP light chain 3 (LC3) protein (a kind gift from Prof. Noboru Mizushima, Tokyo University, Japan) and wild type MEF cells (a kind gift from Dr. Robea Ballo, University of Cape Town, South Africa) were cultured in Dulbecco's modified Eagle's medium (DMEM) (Life Technologies, #41965-039) supplemented with 10% fetal bovine serum (Biochrom, #S-0615), 1% Antibiotic-Antimycotic (Life Technologies, #15240-062); 100 U/mL of penicillin, 100 μg/mL of streptomycin and 250 ng/mL of Fungizone® antimycotic, and maintained in a humidified atmosphere in the presence of 5% CO_2 at 37°C. The sub-culturing of MEF cells involved trypsinisation (Life Technologies, #25200-072) to dissociate adherent cells from the flask. Culturing medium was removed and washed with phosphate-buffered saline (PBS) (NaCl 137 mmol/L, KCl 2.7 mmol/L, Na_2HPO_4 10 mmol/L, KH_2PO_4 1.8 mmol/L, pH 7.4) and trypsinised using either a T25 (Porvair, # 500030), T75 (Porvair, # 500029) or T75 (Porvair, # 500028) depending cell culturing needs. Following trypsinisation, cells were collected in a 50 mL falcon tube (Biocom Biotech, # 50050) and DMEM was added in a 2:1 ratio. Cells were centrifuged (Eppendorf Centrifuge 5804R) at 1500 rpm for three minutes at room temperature. The supernatant was discarded and cells re-suspended in DMEM. Cells were reseeded in culturing flasks, petri-dishes (Sterlin # 90032), an 8-chamber cover slip-based dish (Nunc, Lab-Tek, #155411) or a CYTOO chamber single well plate (CYTOO, #30-010) for experimental purposes.

3.3 Protein extraction

For protein extraction, the medium was quickly removed and cells were rinsed twice with cold PBS. 300 μL of RIPA buffer (Tris-HCl: 50 mM, pH 7.4, NP-40 (1%), Na-deoxycholate (0.25%), 150 mM NaCl, 1 mM EDTA, 1 mM PMSF, 1 mM Na_3VO_4, 1 mM NaF, leupeptin, aprotonin and benzamidine (1 μg/mL), pepstatin (10ug/mL)) were added per petri-dish and cells scraped off using a cell scraper (Porvair, #500034). Lysates were collected, samples sonicated using a Mixsonic

(S-4000), and centrifuged at 8 000 rpm at 4°C for 10 min (Spectrafuge 16M). Supernatant was collected and stored at -80°C.

3.4 Protein concentration determination

The Bradford protein assay was used to determine the protein concentration of the lysates. First a protein standard was generated using bovine serum albumin (BSA) (Roche #10 735 078 001). BSA concentrations ranged from 0 to 2 μg/ul. The protein standard was treated with Bradford reagent (Coomassie Brilliant blue 50 mg/L, methanol 50 mL/L, phosphoric acid (85% stock solution) 100 mL/L, and dH2O 850 mL/L) for five minutes in the dark and absorbance was measured at 595nm with a universal microplate reader (EL800). Absorbance value for 0 μg/μL was subtracted from the respective standard range concentrations absorbance values. A standard curve was generated by plotting absorbance values against protein concentration. Protein samples were assayed as described above and absorbance measured at 595nm was used to determine the protein concentration of the samples.

3.5 Western blotting

For Western blotting 40 μg of protein mixed with LaemmLi buffer (6.5 mM Tris-HCl pH 6.8, 2% sodium dodecyl sulphate (SDS), 5% -mercaptoethanol, 10% glycerol, 0.01% Bromophenol blue) in a 2:1 ratio was boiled at 95°C for 5 min. Proteins were separated on a 4–15% Mini-PROTEAN® TGX Stain-Free™Precast gel (Bio-rad, #456-8084) and transferred onto a Transfer Pack™PVDF membrane (bio-rad, #170-84156) using Trans-Blot® Turbo™(Bio-rad, # 170-4155). Membranes were blocked with 5% milk in TBS-T (137 mM sodium chloride, 20 mM Tris, 0.1% Tween-20 at pH 7.6) for 1 hour. Thereafter membranes were washed with TBST three times for five minutes and incubated with primary antibodies overnight at 4°C. The primary antibodies used include mouse monoclonal anti-GFP (Sigma, #G-1546), rabbit anti-LC3 (Sigma, # L-8918), anti-mTOR (Sigma, # T-2949),

anti-phospho-mTOR Ser2448 (Sigma, # SAB-4504476), anti-p62 (Abcam, # ab-56416), anti-β-actin (Cell Signalling, # 4970) and anti-GAPDH (Sigma, # G-9545). Membranes were rinsed with TBST three times for five minutes and then incubated with either peroxidase linked anti-mouse IgG (Sigma, # A-9044) or anti-rabbit IgG (Sigma, # A-0545) for one hour at room temperature and visualized using Clarity^{TM}Western ECL substrate and the ChemiDoc^{TM}MP System.

3.6 Mass spectrometry

Total amino acid content of free amino acids was determined by mass spectrometry. Protein extract was treated with the Waters AccQ Tag^{TM}Ultra Derivatization Kit, placed in a heating block at 55°C, for ten minutes. Waters API Quattro Micro Waters mass spectrometry was used in the positive electrospray ionization mode. Nitrogen was used as a drying agent. Desolvation gas flow was 350 L/h, and the cone gas flow was maintained at 50 L/h. Desolvation temperature was 350°C and the source temperature was 120°C. The capillary voltage was 3.5 kV and the cone voltage 15 V.

3.7 Microscopy

3.7.1 Fluorescence microscopy

3.7.1.1 Experimental set-up

Initial protocol MEF cells were seeded onto an sterile 8-chamber cover slip-based dish at a density of 2x10^4 cells per well containing DMEM. Cells were incubated over night in a humidified atmosphere in the presence of 5% CO_2 at 37°C. The 8-chamber cover slip-based dish was then enclosed in IX-81 stage of the fluorescent microscope in the presence of 5% CO_2 for the duration of the experiment.

Modified protocol MEF cells were seeded onto a sterile cover-slip patterned with large Fibronectin discs (CYTOO, #10-003-10) in a CYTOO chamber single well plate. Cells were seeded at a density of $2x10^4$ cells and incubated for 30 minutes. Thereafter the chamber was rinsed several times using DMEM until all adherent cells in the non-patterned regions were washed off. The cells were maintained for 2 hours prior to the experiment in DMEM, containing 75 nM LysoTracker® (Life Technologies, #L-7528), in a humidified atmosphere in the presence of 5% CO_2 at 37°C. The chamber plate was then enclosed in IX-81 stage of the fluorescent microscope in the presence of 5% CO_2 for the duration of the experiment.

Experimental hardware and software set-up An Olympus IX81 inverted fluorescent microscope (Olympus Biosystems GMBH) was used with automated z-stack control to determine the total autophagosomal and lysosomal pool size in a single cell. The raw image stacks were acquired using a high NA objective (Olympus Plan APO N 60x/1.42 Oil/0.17/FN26.5) and a 500 nm step width between the image frames.The slides containing MEF cells were placed in a heated chamber at 37°C that encases the IX-81 stage of the microscope. Exposure time and illumination excitation outputs were chosen using a 492 nm GFP excitation filter and 572 nm TxRed excitation filter with a UBG triple-bandpass emission filter cube (Chroma) to ensure an optimal signal/noise ratio with minimal saturation, using a Xenon-Arc burner (Olympus Biosystems GMBH) as a light source. Images were processed using Cell® imaging software and exported to automated counting software, ImageJ with WatershedCounting3D plug in [63], to count the green and red puncta using voxel dimension 0.08 for both x and y as the search parameters.

3.7.1.2 Puncta analysis

Puncta count and morphometric analysis was performed using the WatershedCounting3D plugin of ImageJ. Images were converted to RGB colour format and processed WatershedCounting3D. Puncta count and surface area was determined for each respective colour puncta from the output file generated. Surface area, A_c,

was used to determine the radius using eqn. 3.1, assuming the vesicle to be circular in nature.

$$r = \sqrt{\frac{4\pi}{A_c}} \tag{3.1}$$

Volume of the sphere, V_s, was calculated using eqn. 3.2.

$$V_s = \sqrt{\frac{4}{3}\pi r^3} \tag{3.2}$$

Using the calculated volume data the total surface area of spheres was determined by multiplying the surface area of the sphere, A_s, which is calculated using eqn. 3.3, with the total puncta count.

$$A_s = 4\pi r^2 \tag{3.3}$$

3.7.2 Transmission electron microscopy (TEM)

3.7.2.1 Sample preparation

Cell harvesting. MEF cells were seeded into a T-25 flasks at a density of 5x10^5 cells and grown to approximately 90% confluency. Groups were divided and treated as described in treatment protocol. After incubation, cells were harvested by trypsinisation. After centrifugation at 1500 rpm for three minutes at 37°C, the trypsin and media was decanted and cells were re-suspended in PBS to remove trypsin and media. Cells were then centrifuged at 1500 rpm for three minutes and PBS was decanted. Cells were re-suspended in 2.5% glutaraldehyde (Sigma, # G5882) fixative, centrifuged, and transferred to Tygerberg Hospital where TEM analysis was performed by the National Health Laboratory Service.

Preparation, sectioning and image capturing. A dissecting microscope was used to cut the pellets into 1 mm sections. Samples were rinsed in phosphate buffer and incubated in 3% osmium tetroxide for 1 hour. Thereafter samples were stored in a 10% formalin solution in order to reduce the osmium tetroxide. Samples were then transferred to an automated tissue processor, and immersed in the following

solution: 10% uranyl acetate for 15 minutes, 70% ethanol twice for 10 minutes. Thereafter samples were subjected for 20 minutes to 10% uranyl nitrate, and for 15, 20 and 30 minutes to 100% ethanol. Samples were immersed for 90 minutes in a 1:1 ratio of 100% ethanol and Spurr's resin solution, followed by an incubation for 60 minutes in Spurr's resin. Samples were embedded in gelatin capsules overnight at 60°C and cut into 20 nm sections using a Leica EM UC7. Sections were stretched with chloroform and placed onto copper grids. Images were captured with a JEOL JEM 1011 transmission electron microscope, using an ITEM soft imaging analysis program.

3.7.2.2 Morphometric analyses

Morphometric analyses were performed using ImageJ. Images were imported into ImageJ and the brightness and contrast was adjusted. Vacuolar structures were demarcated and thereafter, using the brightness and contrast panel, the background was set to white so that the demarcated areas became visible. The 'analyse particles' function of ImageJ was used to count and measured the surface areas of the vacuolar structures. Furthermore, vacuolar structures volume and surface area was determined as described in section 3.7.1.2.

3.8 Treatment protocol

Cells were divided into seven groups: a control group (Con), a 30 minute bafilomycin A_1-treated group (Baf 30min), a two hour bafilomycin A_1-treated group (Baf 2hrs), a 30 minute rapamycin-treated group (Rapa 30min), a four hour rapamycin-treated group (Rapa 4hrs), a four hour rapamycin-pretreated group followed by a 30 minute bafilomycin A_1-treated group (Rapa Baf 30min), a four hour rapamycin-pretreated followed by a two hour bafilomycin A_1-treated group (Rapa Baf 2hrs). The control group represented basal steady state conditions, whereas the four hour rapamycin-treated group represented the rapamycin induced steady state. The 30 minutes rapamycin-treated group represented and early transition time point be-

tween the two steady states. The bafilomycin A_1 and rapamycin concentration used was 400 nM and 25 nM respectively.

3.9 Determining flux dynamics: Experimental procedure

A fundamental part of the protocol was the initial counting of autophagosomes over time without the use of any fusion inhibitors in order to determine whether the system was in a steady state. A steady state was verified over several time points when the rate of change of the number of autophagosomes/cell (n_A), did not change over time (see Fig. 2.9). Cell images were acquired at predetermined time points, the first experimental time points were 0, 1, 2, 2.5, 3, 4, 5, 6, 7, 8, 8.5, 9 and 10 hours, whereas the modified experiment time points were 0, 1, 2, 2.5, 3, 4, 5, 6.5, 6, and 8 hours. Cells were treated with 100 nM, 200 nM, 400 nM and 800 nM bafilomycin A_1. The autophagosomal pool size was monitored for two hours post-inhibition and images acquired at 30 minutes intervals.

The basal flux, J_{basal}, was determined by allowing the autophagic system to reach a steady state under basal conditions; basal flux was the initial slope of the progress curve at the point of inhibition of fusion. Multiple cells were assessed ($n = 10$) simultaneously using a stage control. Furthermore, the transition time, τ, was calculated from the ratio n_A/J of the autophagosome pool size and autophagosome flux, and indicated the turnover time of the autophagosome pool at steady state. Therefore, the smaller τ becomes the less time is required to completely replenish the autophagosome pool at steady state.

3.10 Statistical analysis

Statistical analysis was performed with Prism 5 software using a one way ANOVA with the Bonferroni post-test. Significance was indicated at $p < 0.05$. All results were presented as means $\pm$ SEM's.

Chapter 4

Results and Discussion

As discussed in Section 2.7, we define autophagic flux as a rate of flow of material through the autophagic pathway (Fig. 2.9). This chapter describes a fluorescence microscopy technique for measuring this flux in terms of the initial rate of accumulation of autophagosomes after the fusion between autophagosomes and lysosomes is completely inhibited. This method was used to compare the autophagic flux under basal conditions with that which obtains after induction of autophagy by rapamycin. Preliminary experiments were done to prove the concept, after which the method was further refined to yield more reliable and accurate measurements of autophagic flux.

At selected time points during the progress of these experiments autophagic flux was also assessed with traditional methods used in autophagic research such as Western blot analysis and electron microscopy. The data generated by these methods could be used as a context for assessing the usefulness of the data generated by our novel approach. Since amino acids are the end-products of the autophagic process, their concentrations were also measured at these selected time points.

Furthermore, a mathematical model that describes the autophagic system was parameterised with the experimental data obtained by the fluorescence microscopy experiments. With this parameterised model we could study the dynamic behaviour of the autophagic system and the degree to which the different steps control the autophagic flux. Our model of autophagy is described in Chapter 5.

4.1 Preliminary measurement of autophagic flux (proof of concept)

In the preliminary experiments described here we tested the approach of quantifying autophagic flux in terms of the initial rate of increase in the number of autophagosomes in a single cell after complete inhibition of fusion of autophagosomes with lysosomes.

4.1.1 Quantifying autophagic flux by inhibiting autophagosomal and lysosomal fusion with bafilomycin A_1

Fluorescence microscopy was performed to measure the initial rate of increase in autophagosome count after inhibition of fusion by bafilomycin A_1, and to confirm that inhibition of fusion was complete at 400 nM bafilomycin A_1, as suggested by our Western blot experiments (which are described in section 4.2.1 with results in Fig. 4.7) described above. Fig. 4.1 shows a representative time lapse image sequence of MEF GFP-LC3 cells treated with bafilomycin A_1. Each image is a superposition of z-stack image frames, while the total count of puncta in the cell is the sum of puncta counts in each such a layer (co-localised puncta shared between two layers are counted as one). Fig. 4.2 shows the effect of incremental increases in bafilomycin A_1 concentration on the rate of green puncta accumulation. Conventionally, green puncta are equated to autophagosomes, but it is more correct to equate green puncta to vacuolar structures that contain GFP-LC3, i.e., autophagosomes and autophagolysosomes. Here we adhered to this convention, so that the total number of puncta per cell was regarded as equivalent to the total number of autophagosomes per cell (n_A). After 2 hr with 800 nM bafilomycin A_1 treatment the majority of cell population exhibited cell death.

What is also clear from Fig. 4.1 is that under basal conditions the background noise is very high, especially in the perinuclear region where autophagosomes are known to congregate; this complicates the counting of green puncta, probably

underestimating their number considerably.

At all four bafilomycin A_1 concentrations (100, 200, 400 and 800 nM) there was a significant increase in n_A 60 min after treatment with bafilomycin A_1, while the initial rate of increase in n_A after bafilomycin A_1 treatment reached a maximum at 400 nM (46 autophagosomes/hr/cell at 100 nM, 52 autophagosomes/hr/cell at 200 nM, 54 autophagosomes/hr/cell at 400 nM, 54 autophagosomes/hr/cell at 800 nM). We therefore regard the initial rate of increase in n_A per cell after treatment with 400 nM bafilomycin A_1 as our measure of the autophagic flux. What we measure here is the basal autophagic flux, J_{basal}, which in this experiment is 54 autophagosomes/hr/cell. However, since autophagolysosomes also in principle show up as green puncta, these values may not be a true reflection of autophagic flux.

In Fig. 4.1, n_A at 0 hr is considerably lower than n_A in the steady state between 1–2 hr. A possible explanation could be that the change from 5% CO_2 in the culture atmosphere to the virtual absence of CO_2 (0.04%) in the ambient atmosphere that prevails under the experimental conditions causes induction of autophagy through stress caused by an increase in pH (as indicated by the pH indicator phenol red in the culture medium). Section 4.2 describes modifications to the experimental protocol that overcame this problem. However, the fact that in all cases a steady state was reached after 1 hr (within experimental error) still allowed for a reliable assessment of the bafilomycin A_1 concentration required for

the complete inhibition of autophagosome and lysosome fusion.

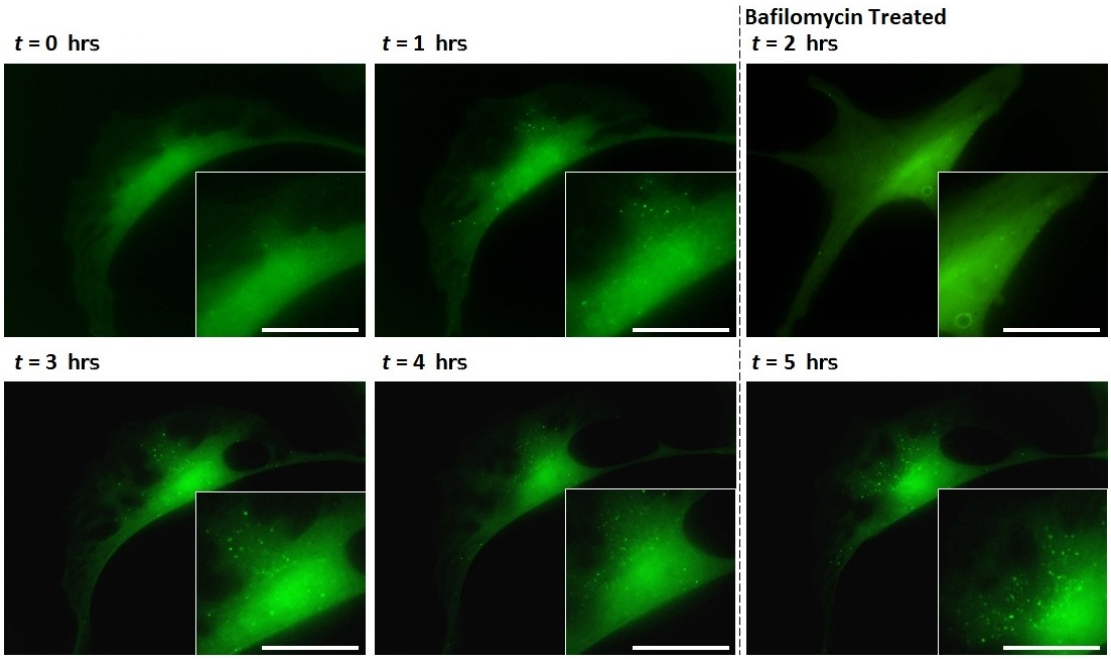

Figure 4.1: Representative time lapse images of basal autophagy. At 2 hr cells were treated with 400 nM bafilomycin A_1. Each image is a superposition of z-stack image frames obtained by scanning vertically through the cell. Scale bar: 20 μm.

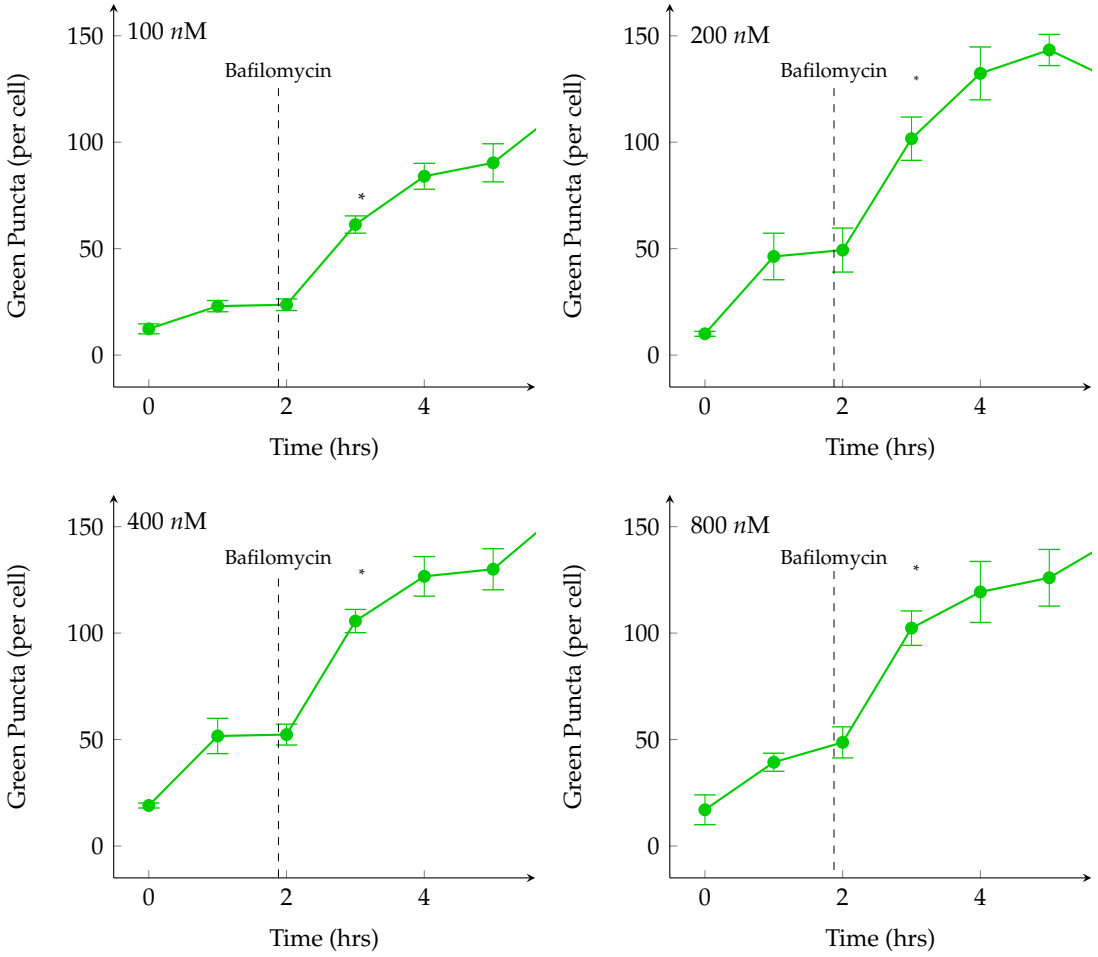

Figure 4.2: Time series of autophagosomal pool size (n_A) at the basal state of the autophagic system and after treatment at 2 hr with 100 nM, 200 nM, 400 nM or 800 nM bafilomycin A_1. $*$ vs. 2 hr, $p < 0.05$; $(n = 3)$.

4.1.2 Induction of the synthesis of autophagosomes with rapamycin

This section describes preliminary experiments to study the effect of induction of autophagy by rapamycin on both the autophagosomal pool size and the autophagic flux.

Figure 4.3 shows a representative time-lapse image sequence from which the change in autophagosomal pool size before and after induction by rapamycin could be measured by counting the green puncta. Figure 4.4 combines the results of a series of six such experiments. As before, the autophagic flux was calculated from the initial rate of increase in n_{A} after the complete inhibition of lysosomal and autophagosomal fusion by 400 nM bafilomycin A_1.

Before rapamycin treatment the basal autophagosomal pool size ($n_{\text{A-basal}}$) was in steady state (that this experiment does not show the initial increase in n_{A} observed in Fig. 4.2 is due to equilibration to ambient atmosphere prior to the first measurement). After treatment with 50 nM rapamycin (2–8 hr) n_{A} increased from its average basal value of 33 autophagosomes/cell until it approached a new steady state at 4 hr with an average value of 142 autophagosomes/cell during the 4–8 hr period (a 4.3-fold increase in n_{A}). However, during the 2–8 hr period the control n_{A} varied significantly, casting doubt on the accuracy of this calculation of the fold-increase in n_{A}. In the next section we discuss refinements in the experimental conditions that yielded more accurate results.

Following treatment with bafilomycin A_1, n_{A} increased rapidly and significantly relative to the induced steady-state n_{A}. The induced autophagic flux (J_{induced}) was calculated as before as the initial rate of increase in n_{A} after bafilomycin A_1 treatment (using the first time point after bafilomycin A_1 treatment, here at 1 hr, for the calculation) and had a value of 143 autophagosomes/hr/cell, but as with the calculation of the fold-increase in n_{A} after induction, variation in the control casts doubt on the accuracy of this value of J_{induced}. The next section describes a more accurate measurement of J_{induced}.

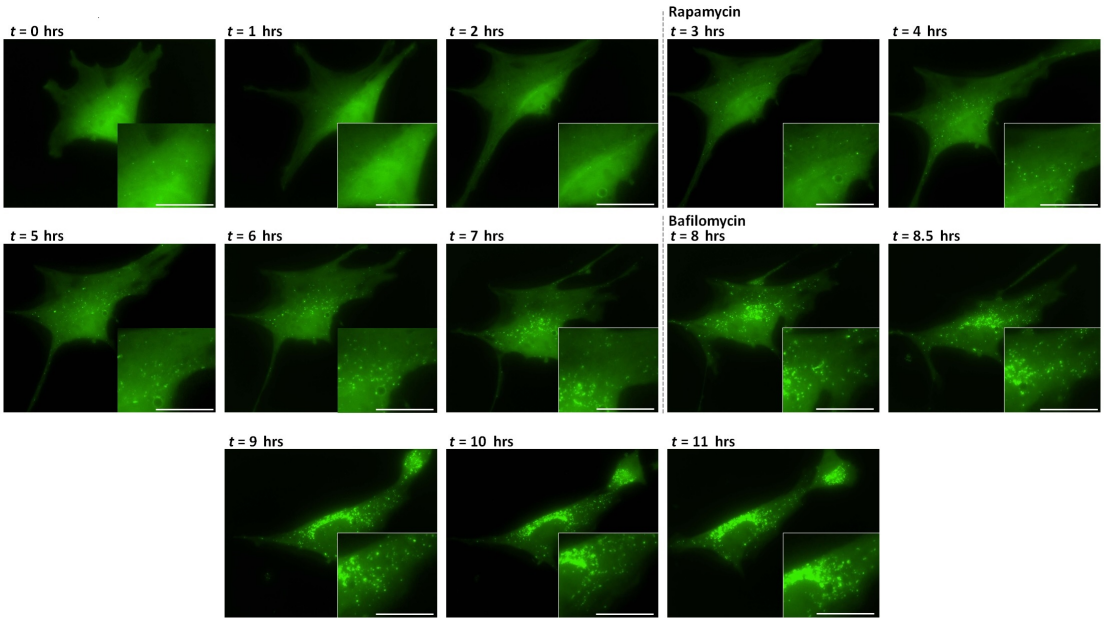

Figure 4.3: Time lapse image sequence that shows changes in the autophagosomal pool size (n_{A}) after induction of autophagy with 50 nM rapamycin at 2 hr. At 8 hr cells were treated with 400 nM bafilomycin A_1. Each image is a superposition of z-stack image frames. Scale bar: 20 μm.

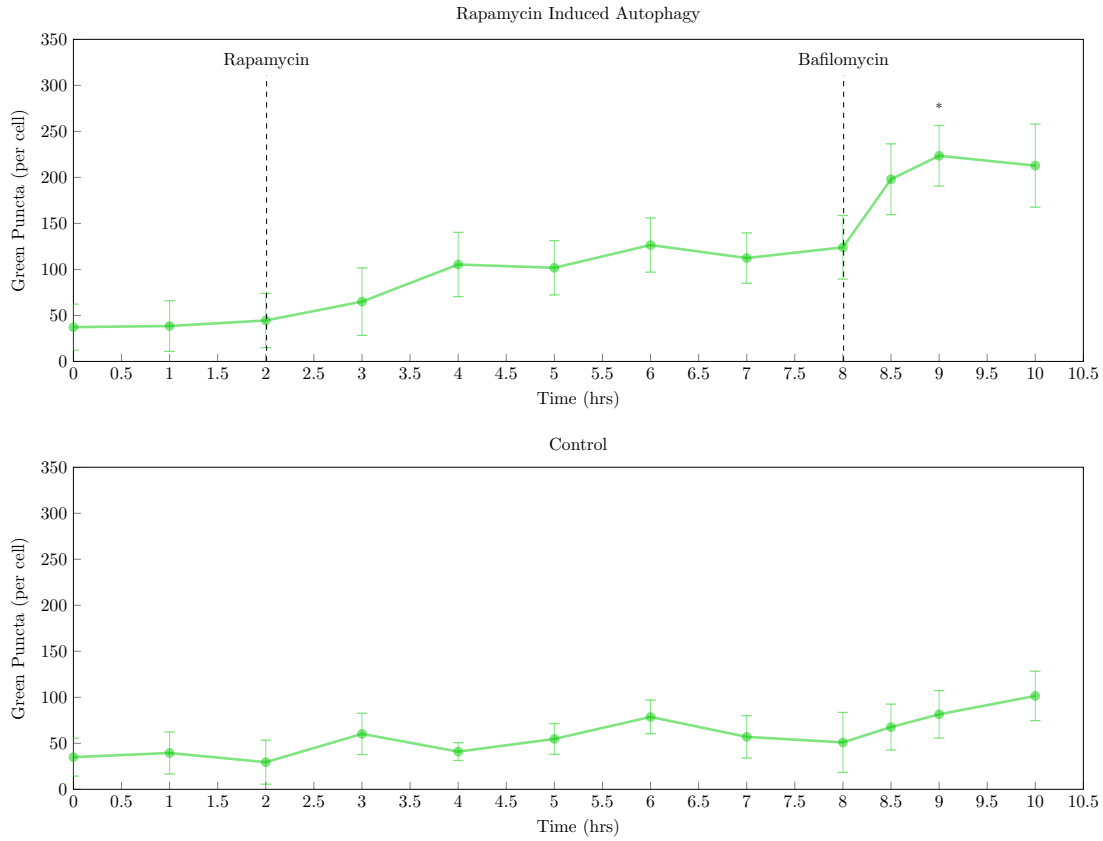

Figure 4.4: Monitoring autophagosome pool size before and after induction of the autophagic system with 50 nM rapamycin at 2 hr. Fusion was inhibited at 8 hr with 400 nM bafilomycin A_1. $*$ vs. 8 hr, $p < 0.05$ ($n = 6$).

4.2 Refined measurement of autophagic flux

In the preliminary experiments described above, changes in gas composition and changes in cell volume and shape not only made it challenging to track the cells, but also increased the variability in puncta counts as time progressed since variation in cell volume affected the number of autophagic vesicles a cell can accommodate. The experimental conditions under which basal and rapamycin-induced autophagy was studied were modified as follows in an effort to counteract these problems and produce consistent and reliable results.

The possible effects caused by changes in the gas composition between culture and experiment discussed in Section 4.1.1 were eliminated by keeping the cells inside the XI81 microscope case at 37 °C in a humidified atmosphere with the CO_2 maintained at 5% while measuring autophagic progress. Humidification prevented a possible stress-inducing increase in osmotic potential caused by evaporation and the concomitant decrease in the volume of culture medium during the experiment. Furthermore,the problem of changes in cell shape (see Fig. 4.3) as the cells migrated over the surface of the slide chamber was overcome by using micro-patterning (CYTOO, see section 3.7.1), which anchored the cells to the chamber using micro-patterned fibronectin discs and so prevented variations in cell shape.

Another refinement was the use of Lysotracker dye that allowed us to visualise the intermediates of the autophagic pathway, namely, autophagosomes (green puncta), lysosomes (red puncta), and autophagolysosomes (yellow puncta). The Lysotracker dye diffuses into both autophagosomes and lysosomes, but only fluoresces red in the acidic environment of the lysosomal lumen, so that lysosomes show up as red puncta, while autophagosomes still show up as green puncta. After fusion into autophagolysosomes, which are also acidic, the co-localisation of green GFP-derived signal and red Lysotracker-derived signal causes autophagolysosomes to show up as yellow puncta. While is was easy to distinguish between and count the green and yellow puncta, the lysosomal red puncta were more difficult to identify since they varied in hue and occurred in very low numbers, typically 2–5 per cell.

4.2.1 The inhibition of autophagosomal and lysosomal fusion by bafilomycin A_1

As before, fluorescence microscopy was performed to measure the initial rate of increase in autophagosome count after inhibition of fusion by bafilomycin A_1, and to confirm that inhibition of fusion was complete at 400 nM bafilomycin A_1, as suggested by the preliminary experiments described in section 4.1.1.

Fig. 4.5 shows a representative time lapse image sequence of MEF GFP-LC3 cells treated with bafilomycin A_1. As before, each image is a projection of z-stack image frames, while the total count of puncta in the cell is the sum of puncta counts in each layer (co-localised puncta shared between two layers are counted as one). Fig. 4.6 shows the effect of incremental increases in bafilomycin A_1 concentration on the rate of autophagosome accumulation. In contrast to the preliminary experiment (Fig. 4.2), we were able to count both autophagosomes (n_A, green puncta) and autophagolysosomes (n_{AL}, yellow puncta). In these experiments we did not attempt to count the red lysosomal puncta, since they would not provide useful additional information. At all four bafilomycin A_1 concentrations (100, 200, 400 and 800 nM) there was a significant increase in n_A 30 min after treatment with bafilomycin A_1: the initial rates of increase were 25.8 ± 4.1 autophagosomes/hr/cell at 100 nM, 24.8 ± 4.9 autophagosomes/hr/cell at 200 nM, 25.4 ± 3.8 autophagosomes/hr/cell at 400 nM, 24.0 ± 2.2 autophagosomes/hr/cell at 800 nM. The initial rate of increase in n_A after bafilomycin A_1 treatment had therefore already reached a maximum at 100 nM. This was in contrast to what was observed in the preliminary experiments which suggested that, to be absolutely sure that fusion was completely inhibited, 400 nM bafilomycin A_1 was needed. Even though the experiments described here suggested that we could use a lower bafilomycin A_1 concentration to inhibit fusion, we decided to keep on using 400 nM bafilomycin A_1.

At all four bafilomycin A_1 concentration we observed an increase in the total puncta count (green plus yellow). This was obviously due to the rate of decrease in yellow puncta being lower than the rate of increase in the green puncta, which is to be expected, at least partly, for the following reason: after inhibi-

tion of fusion autophagosomes continue to be produced at a constant rate, while the concentration-dependent rate of degradation of autophagolysosomes decreases because of decreasing numbers of autophagolysosomes.

Fig. 4.6 shows that the rate of autophagosome accumulation and of autophagolysosome depletion apparently increases in the period following the 30 min time point after bafilomycin A_1 treatment and could be interpreted as a further increase in autophagic flux. This could be due to additional stress-induced autophagy, but a more likely reason is the following: the fluorescent Lysotracker dye is acidotrophic and, under normal conditions, accumulates in the low-pH lumen of acidic vesicles such as lysosomes. Treatment with bafilomycin A_1 causes inhibition of fusion by inhibiting the V-ATPases in the (autophago)lysosomal membrane that maintain the low pH in the lumen of these vesicles, thereby causing de-acidification and concomitant leaching of the dye from both lysosomes and autophagolysosomes. When vesicles, in particular autophagolysosomes, that show up as yellow puncta lose the Lysotracker dye in this manner, they will turn green and be included in the autophagosome count, thereby overestimating it and underestimating the autophagolysosome count.

From these experiments we were therefore able to calculate from the initial rate of increase in n_A after treatment with 400 nM bafilomycin A_1 a value of 25.4 autophagosomes/hr/cell for the basal autophagic flux, J_{basal}. This value was substantially lower than the value calculated from our preliminary experiment, and can be attributed to the fact that we measured only autophagosomes and that we measured at 30 min after inhibition of fusion, instead of at 1 hr as in our preliminary experiment.

We also assessed the inhibition of autophagosomal and lysosomal fusion in MEF GFP-LC3 cells by bafilomycin A_1 with Western blot analysis. No significant differences could be discerned between the LC3 II band intensities at 30 min after 200, 400 or 800 nM bafilomycin A_1 treatment (Figure 4.7).

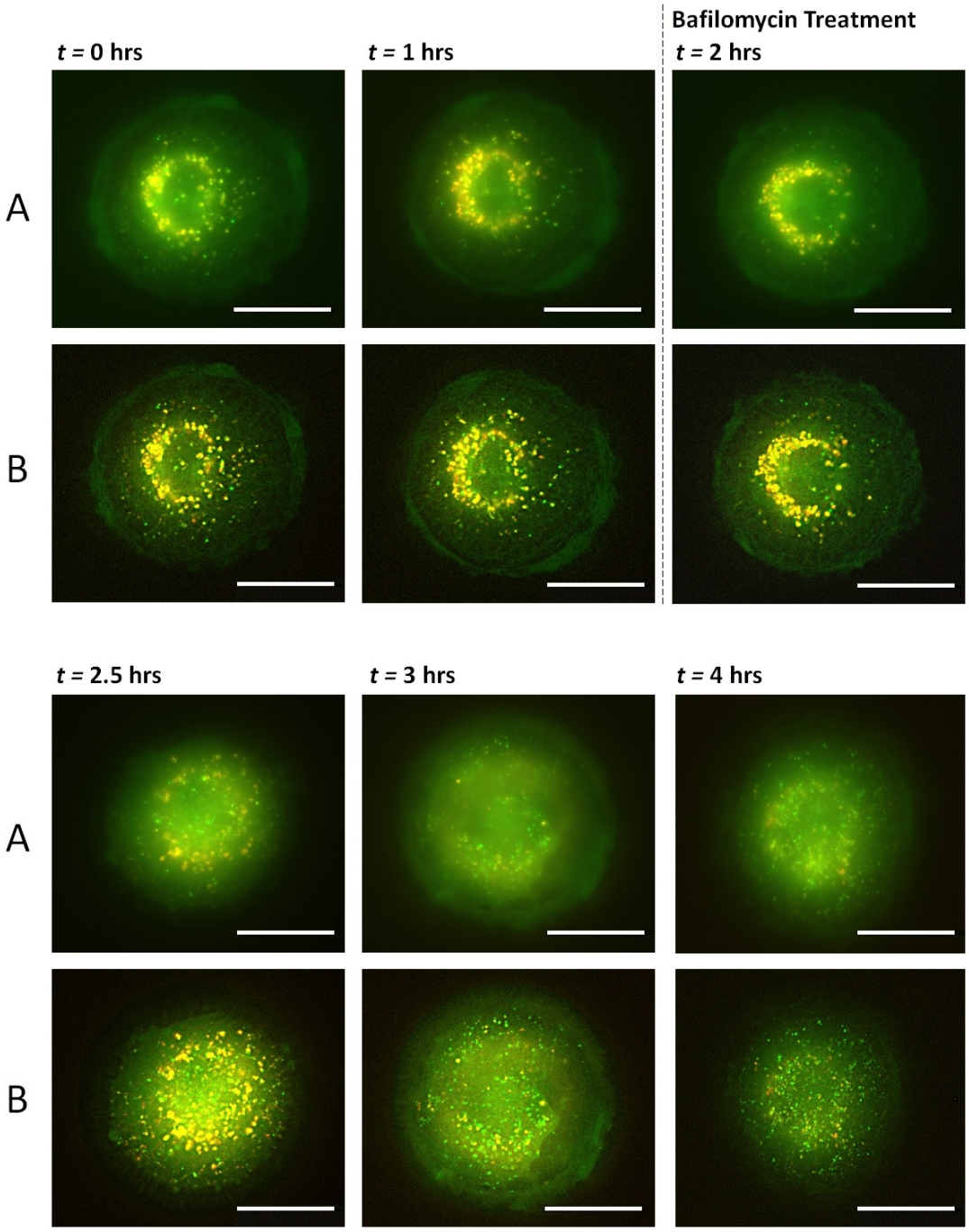

Figure 4.5: Time lapse image sequence of autophagy at basal state with refined method. At 2 hr cells were treated with 400 nM bafilomycin A_1. Puncta are counted as autophagosomes (●), lysosomes (●) and autophagolysosomes (●). Cells were micro-patterned and z-stack images were projected. (A) raw data; (B) deconvolved images. Scale bar: 20 μm.

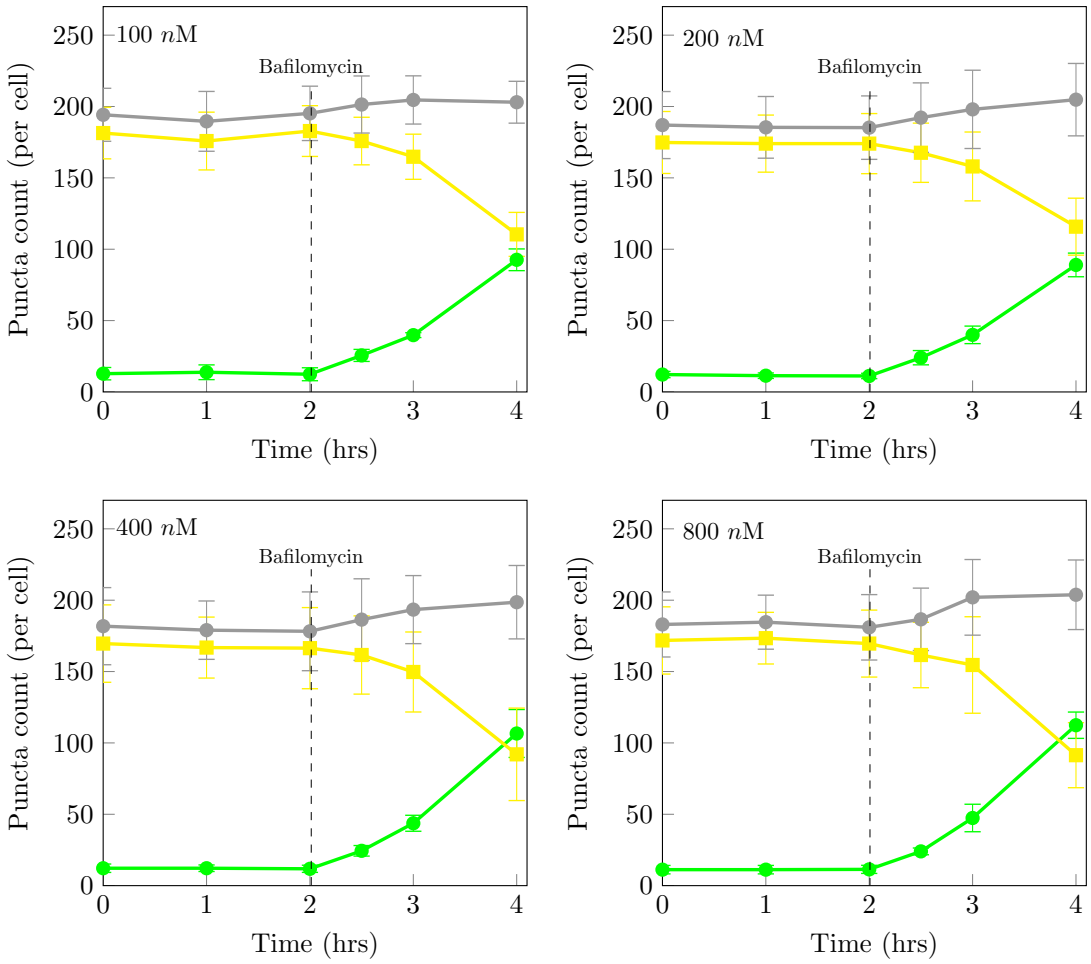

Figure 4.6: Time series of autophagosomal (n_{A}) and autophagolysosomal (n_{AL}) pool size at the basal state of the autophagic system and after treatment at 2 hr with 100 nM, 200 nM, 400 nM or 800 nM bafilomycin A_1. Autophagosomes (●), autophagolysosomes (●) and total puncta (●). ($n = 5$).

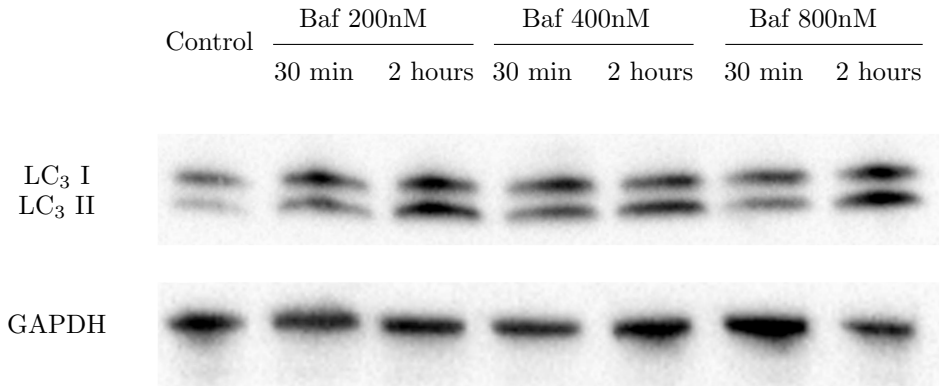

Figure 4.7: Determining the concentration of bafilomycin A_1 required to achieve full inhibition of the autophagosomal and lysosomal fusion process using Western blot analysis. Treatment with 400 nM bafilomycin A_1 resulted in a substantial increase in LC3 protein level at 30 min relative to the control. The difference in the LC3 increase between 400 nM and 800 nM bafilomycin A_1 treatment was negligible. Glyceraldehyde phosphate dehydrogenase (GAPDH) was used as a loading control.

4.2.2 Measuring autophagosomes, autophagolysosomes and lysosomes under the induction of the autophagic system

The effect of rapamycin on autophagic flux was assessed with our modified fluorescence microscopy technique. As before, autophagic flux was calculated from the initial rate of increase in green puncta after the complete inhibition of lysosomal and autophagosomal fusion. However, since we could here distinguish between autophagosomes and autophagolysosomes, we were more certain that, at least for 30 min after inhibition of fusion, the green puncta represented only autophagosomes, and that their increase with time was a more accurate measure of autophagic flux.

Fig. 4.8 shows a time-lapse image series of autophagy over a 8 hr period (the control), while Fig. 4.5 shows the effect on autophagy of inhibition of fusion by bafilomycin A_1 at 2 hr. Fig. 4.9 shows the increase in n_A following rapamycin induction of autophagy at 2 hr and, again, that following inhibition of fusion by bafilomycin A_1 at 6 hr (note that the image at $t = 8$ hr is blurred compared to the other images; this was observed in all cases and made counting of puncta difficult). A comparison between these three figures and Fig. 4.4 clearly shows the improvement in standardisation of the technique for assessing changes in autophagy in a single cell. Micro-patterning standardised cell shape, while deconvolution of the images improved puncta analysis (see the B-panels in Figs. 4.8–4.9).

Fig. 4.10 is a quantitative visualisation of data obtained from the raw fluorescent z-stack images. In the control (Fig. 4.10C) the basal number of autophagosomes ($n_{\text{A-basal}}$), autophagolysosomes ($n_{\text{AL-basal}}$), and lysosomes ($n_{\text{L-basal}}$) remained in steady state throughout the 8 hr duration of the experiment with no significant variation in levels. Lysosomal count was very low, varying between one and five per cell, averaging 1.6 ± 0.5. The puncta counts for autophagosomes and autophagolysosomes averaged at 22.7 ± 2.9 and 167.5 ± 15.6 respectively.

In the experiments where fusion was inhibited by bafilomycin A_1 the average $n_{\text{A-basal}}$ was 12.1 ± 2.5 autophagosomes per cell for non-induced autophagy

(Fig. 4.10A) and 14.3 ± 1.5 autophagosomes per cell for rapamycin-induced autophagy (Fig. 4.10B). These differences are insignificant, but they do differ significantly from the $n_{\text{A-basal}}$-value of 22.7 ± 2.9. This difference, which can be ascribed to the fact that a single cell is chosen for counting and that individual cells do differ from each other, is however irrelevant, since the control study was only done to show that autophagic steady-state persisted for the 8 hr duration of the experiments.

After an hour of induction with rapamycin, n_{A} nearly doubled to 23.1 ± 2.8 autophagosomes per cell and slowly decreased as it approached an $n_{\text{A-induced}}$ of 16.7 ± 1.7 autophagosomes per cell (a 1.3-fold increase relative to the basal level). The average $n_{\text{AL-basal}}$ was 164.5 ± 15.5 autophagolysosomes per cell, which upon induction of autophagy with rapamycin gradually increased until the new induced steady state was established at 6 hr with an average $n_{\text{AL-induced}}$ of 251.2 ± 15.8 autophagolysosomes per cell (a 1.5 fold increase in n_{AL} relative to the basal level). $n_{\text{L-basal}}$ averaged at 1.2 ± 0.3 lysosomes per cell, decreasing upon induction to 0.9 ± 0.2 lysosome per cell and slowly increasing as it approached $n_{\text{L-induced}}$ of 2.0 ± 0.3 lysosomes per cell. Our data showed that under basal condition autophagosomes constituted only a small fraction (7.5%) of the total GFP-LC3 positive puncta, the rest (92.5%) being associated with the autophagolysosomes. This of course means that in our preliminary experiments, which used only GFP-LC3 as marker, we actually measured the sum of autophagosomes and autophagolysosomes; this in turn means that we overestimated autophagic flux. Our refined protocol allowed a more reliable calculation of J_{basal} as 25.4 autophagosomes/hr/cell and J_{induced} as 105.4 autophagosomes/hr/cell (compared to 54 and 143 autophagosomes/hr/cell in our preliminary experiments), a four-fold increase in autophagic flux. As before we used the first time point (30 min) after bafilomycin A_1 treatment for the calculation of the initial rate (at 2.5 hr for basal autophagy and 6.5 hr for induced autophagy).

One would expect the profile of changes in the puncta count for autophagosomes and autophagolysosomes after bafilomycin A_1 treatment to be the same for basal autophagy (Fig. 4.10A) and rapamycin-induced autophagy (Fig. 4.10B). However, at 8 hr in Fig. 4.10B the increase in green puncta did not match the

decrease in yellow puncta, as they did at 4 hr in Fig. 4.10A. The reason for this is not quite clear, but could be due to the unreliability of counting puncta in the consistently blurry images at the 8 hr time point mentioned above.

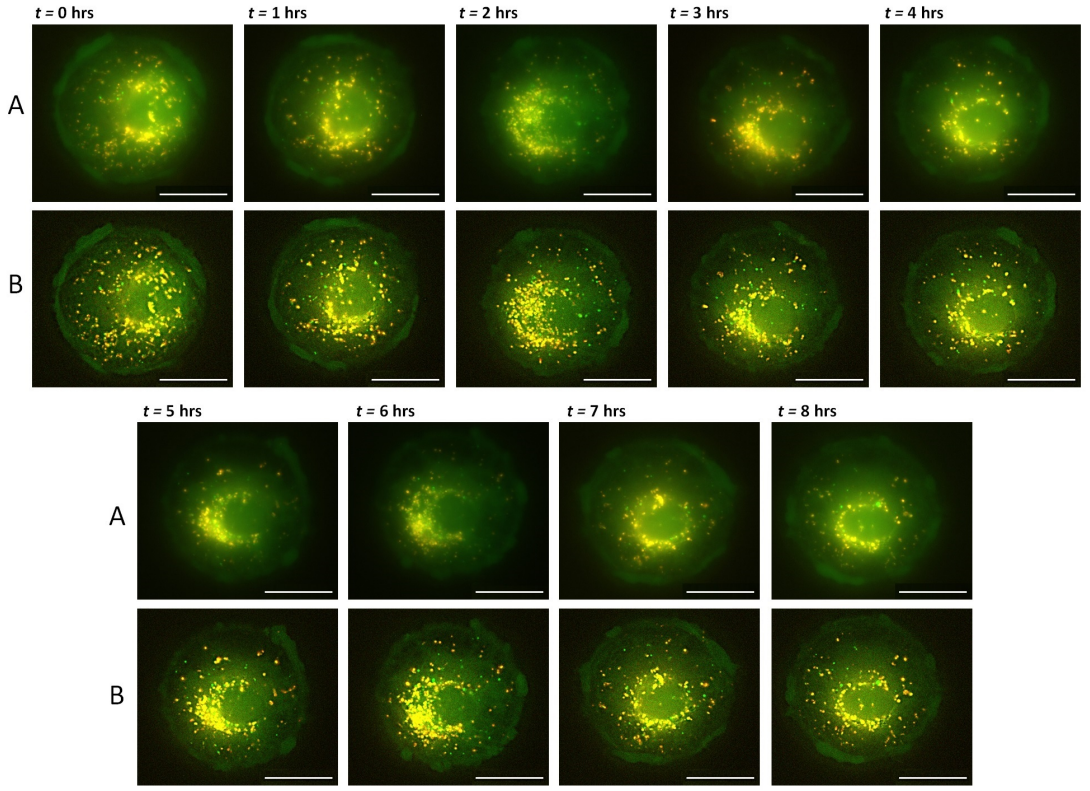

Figure 4.8: Time lapse image sequence of basal autophagy (control). Autophagosomes (●), lysosomes (●) and autophagolysosomes (●). (A) raw data; (B) deconvolved images. Scale bar 20 μm.

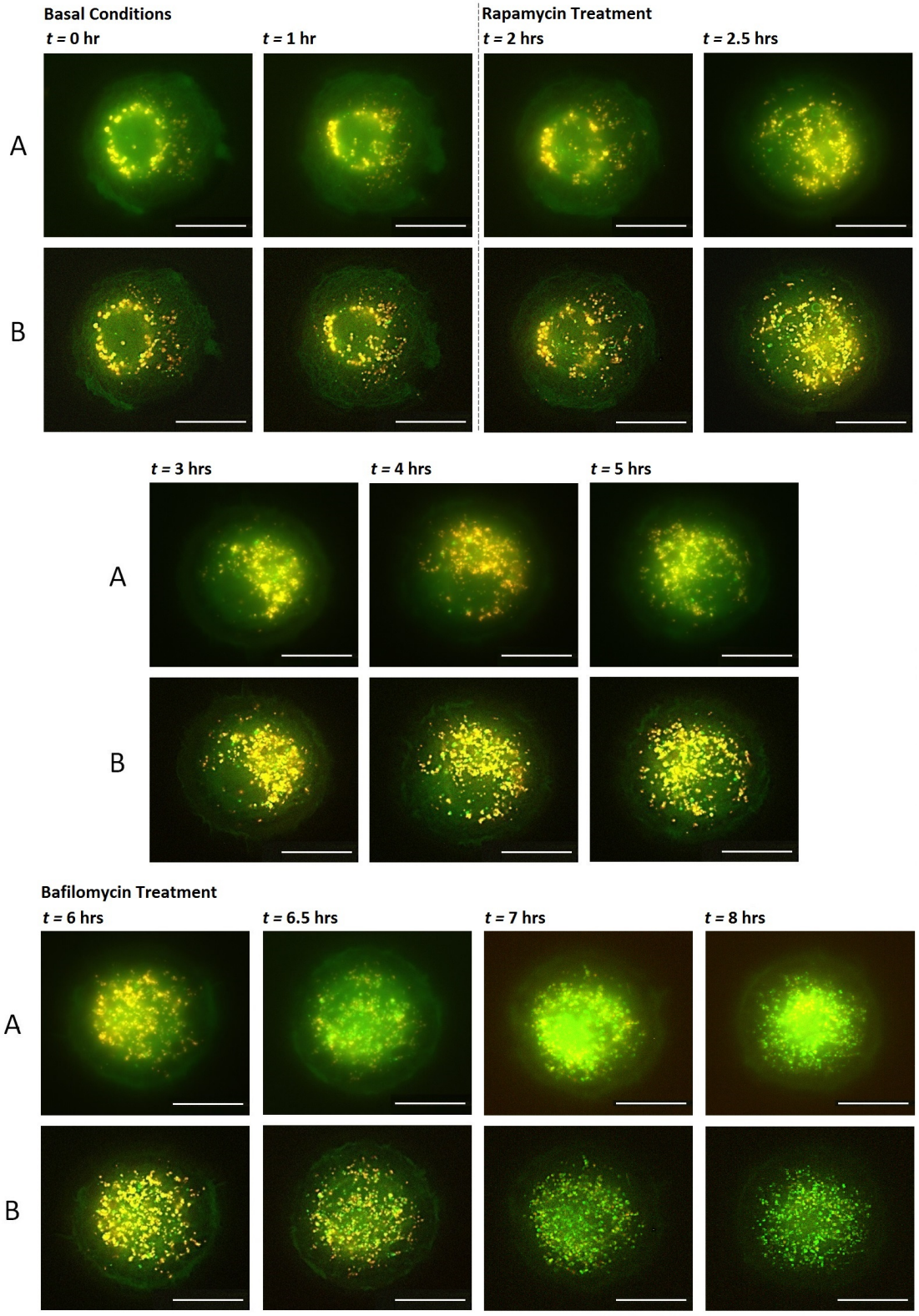

Figure 4.9: Time lapse images of autophagy before and after induction with 25 nM rapamycin at 2 hr, and after inhibition of fusion with 400 nM bafilomycin A_1 at 6 hr. Autophagosomes (●), autophagolysosomes (●) and lysosomes (●). Cells were micropatterned and z-stack images were superimposed. (A) raw data; (B) deconvolved images. Scale bar: 20 μm.

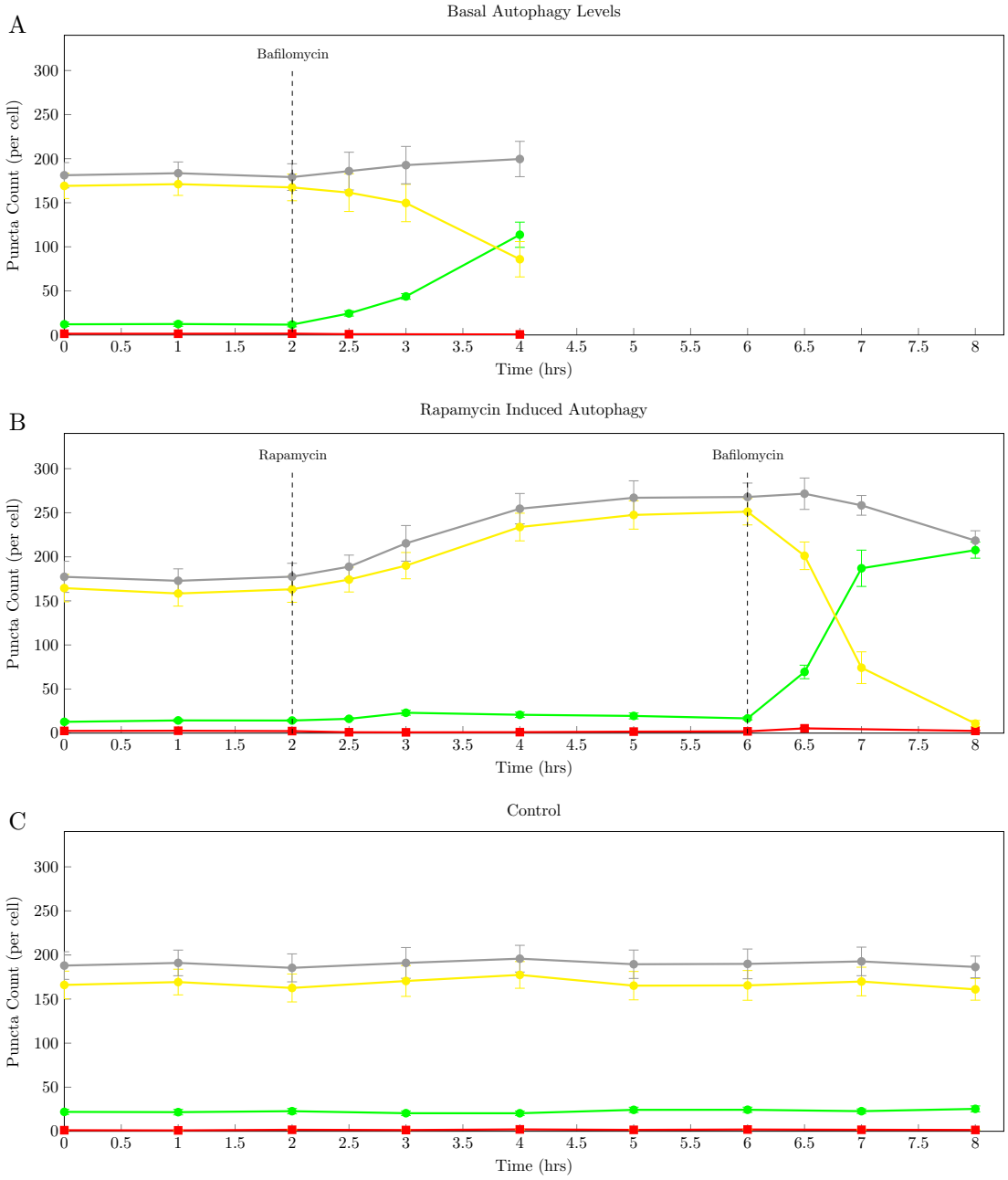

Figure 4.10: The change over time in autophagosomes (●), autophagolysosomes (●), lysosomes (●) and total green and yellow puncta (●). (A) Pool sizes of the three autophagic intermediates under non-induced basal conditions (0–2 hr) and after inhibition of fusion with 400 nM bafilomycin A_1 at 2 hr; (B) Enhanced autophagy after 25 nM rapamycin treatment at 2 hr and after inhibition of fusion with 400 nM bafilomycin A_1 at 6 hr; (C) Control: pool sizes of the three autophagic intermediates under non-induced basal conditions (0–8 hr). ($n = 10$)

In the experiments described in the rest of this chapter data was collected at specific points during the time-course of either basal autophagy or rapamycin-induced autophagy. Fig. 4.11 shows these time points and the names by which they will be referred to on a cartoon of the graphs shown in Fig. 4.10.

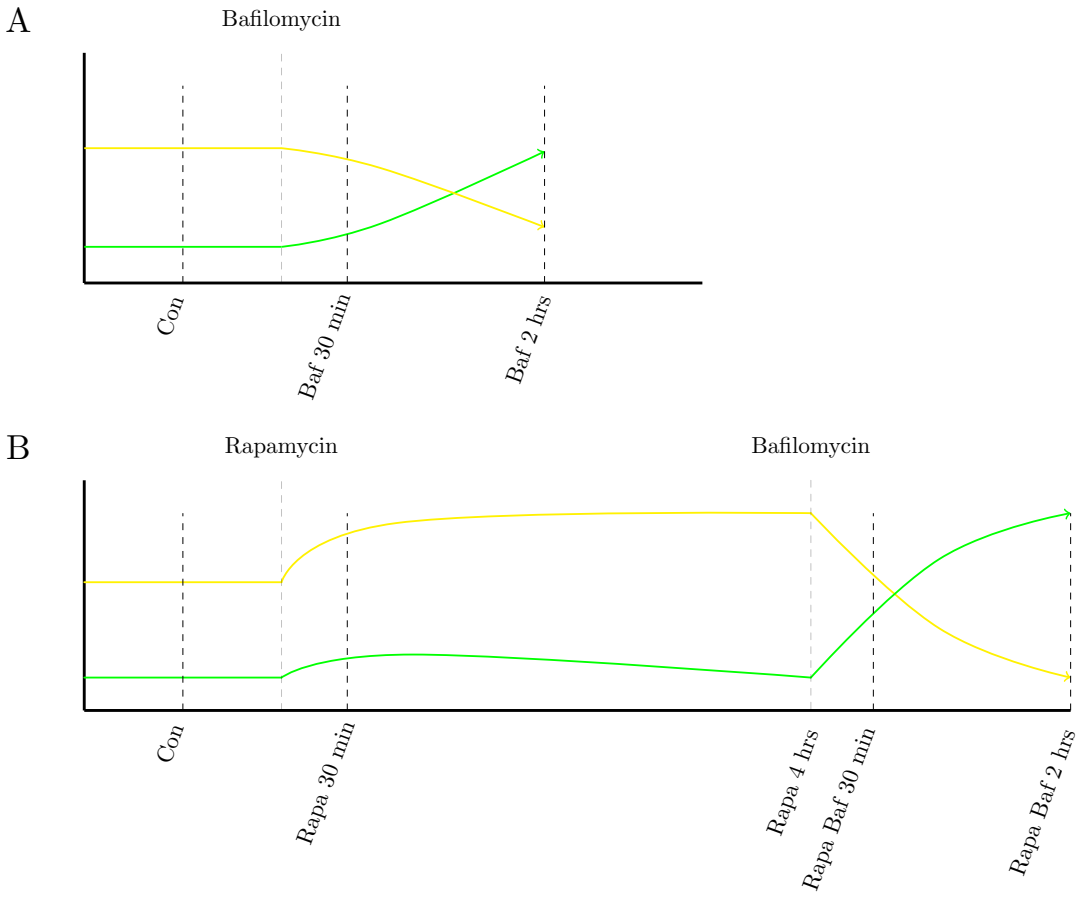

Figure 4.11: Time points at which autophagic variables are measured in (A) basal and (B) rapamycin-induced states.

4.3 Morphometric analyses of autophagosomes, autophagolysosomes and vacuolar structures

Electron microscopy (EM) is an established method for studying the morphology of autophagic vesicles, and is still considered the gold standard in autophagy research. This section describes the use of EM to assess the time-dependent morphometric changes in the vacuolar structures of the autophagy system, and compares it to similar assessments of puncta using FM (as described in section 4.2). Fig. 4.12 compares representative electron microscopic and fluorescence microscopic images of various time points during a measurement of rapamycin-induced autophagy and inhibition of fusion with bafilomycin A_1. Since EM does not allow live cell imaging, the time points selected corresponded to key points in the FM measurements of autophagy (see section 3.8 for the treatment protocol). However, the generic EM protocol used in this study only identifies vacuolar structures and therefore cannot distinguish between autophagosomes and autophagolysosomes, although it can identify lysosomes. In contrast, the method used in the previous section, which utilises GFP-LC3 in MEF cells in conjunction with Lysotracker dye, is able to distinguish between all three entities. The morphometric analyses are divided in three sections: (1) puncta/vacuolar structures count and the average area of a punctum or a vacuole (Fig. 4.13), (2) the size distribution (in percentage) of the puncta/vacuolar structures (Fig. 4.14), and (3) the average volume of a punctum/vacuole and the total surface area of the puncta/vacuole, assuming it to be circular (Fig. 4.15). In comparing EM and FM we considered a vacuole to be equivalent to a punctum. Lysosomes were not included in the analysis because of the low numbers observed.

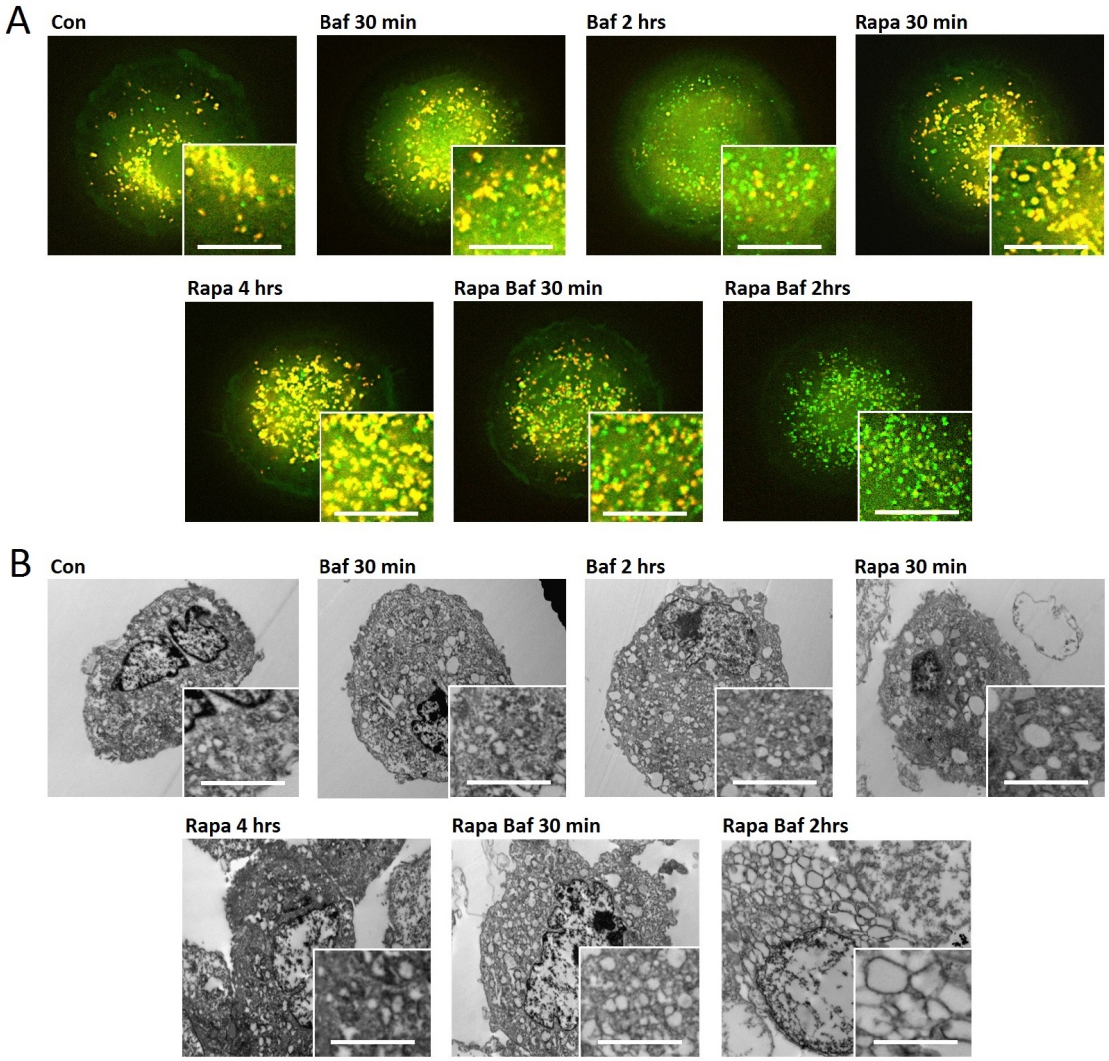

Figure 4.12: Representative images of the autophagic process acquired at the time points shown in Fig. 4.11 with (A) fluorescence microscopy and (B) electron microscopy. Con: control; Baf: bafilomycin A_1; Rapa: rapamycin. Scale bar: 10 μm.

4.3.1 Puncta/vacuolar structures count and the average surface area of a punctum/vacuole on a micrograph

Fig. 4.13 shows the number of puncta or vacuolar structures and the average surface area of a punctum or a vacuole on a micrograph at various time points during control, basal, and induced autophagy.

Puncta/vacuole counts (Fig. 4.13). The striking difference in the number of puncta or vacuoles counted with the two methods was due to the fact that FM made use of an automated stage control that allowed for the acquisition of multiple z-stack images of a single cell and thus counted the total number of puncta in the cell, while EM acquired an image at a single plane, and therefore only counted the vacuoles in a single cell layer (note that with EM the sum of autophagosomes and autophagolysosomes is counted, while, as described earlier, the combination of GFP-LC3 and Lysotracker allowed for the separate FM counting of autophagosomes and autophagolysosomes). Moreover, FM allowed the visualisation of viable cells, and therefore did not introduce fixation related changes. Following bafilomycin A_1 treatment at basal steady state the FM total puncta count did not change significantly, while the EM vacuole count did increase significantly. Fig. 4.13C shows that, following bafilomycin A_1 treatment, n_A increased while n_{AL} decreased, as expected. The sum of these two opposite effects accounted for the constancy of the total puncta count observed in Fig. 4.13A. The contrary increase in vacuoles observed with EM was most probably due to the difficulty of distinguishing autophagy-specific vacuoles from other structures with similar appearance, and the fact that only a single slice of the cell was used in the measurement.

In cells treated with rapamycin there was a 1.5-fold increase in puncta (FM) and a 2.5-fold increase in vacuoles (EM) 4 hr after rapamycin treatment. However, after subsequent inhibition of fusion with bafilomycin A_1 the number of puncta decreased, while the number of vacuoles increased (similar to the increase in vacuoles observed without rapamycin). As discussed in the previous section, the decrease in the total number of puncta can most probably be ascribed to unreliable puncta count in the consistently blurry images at 8 hr in rapamycin-induced autophagy.

Average surface area of a punctum/vacuole (Fig. 4.13). The average area of a punctum remained constant following rapamycin treatment (30 min and 4 hr) and following 30 min bafilomycin A_1 treatment of both the control and rapamycin pretreated cells. However, two hours after bafilomycin A_1 treatment a decrease in the average area of a punctum for both the basal and rapamycin-induced cells was observed. Compared to FM data, the average area of vacuoles varied considerably and showed no discernible trend, which again emphasises the unreliability of EM data for quantifying the entities of autophagy. Furthermore, the average surface area of an autophagosome was four times smaller than that of an autophagolysosome, and this size difference remained constant in the various treatment conditions. In Fig. 4.13A the apparent decrease in the average surface area of a punctum 2 hr after bafilomycin A_1 treatment was a result of the displacement of the larger autophagolysosome with the smaller autophagosome following the inhibition of the formation of autophagolysosomes by bafilomycin A_1.

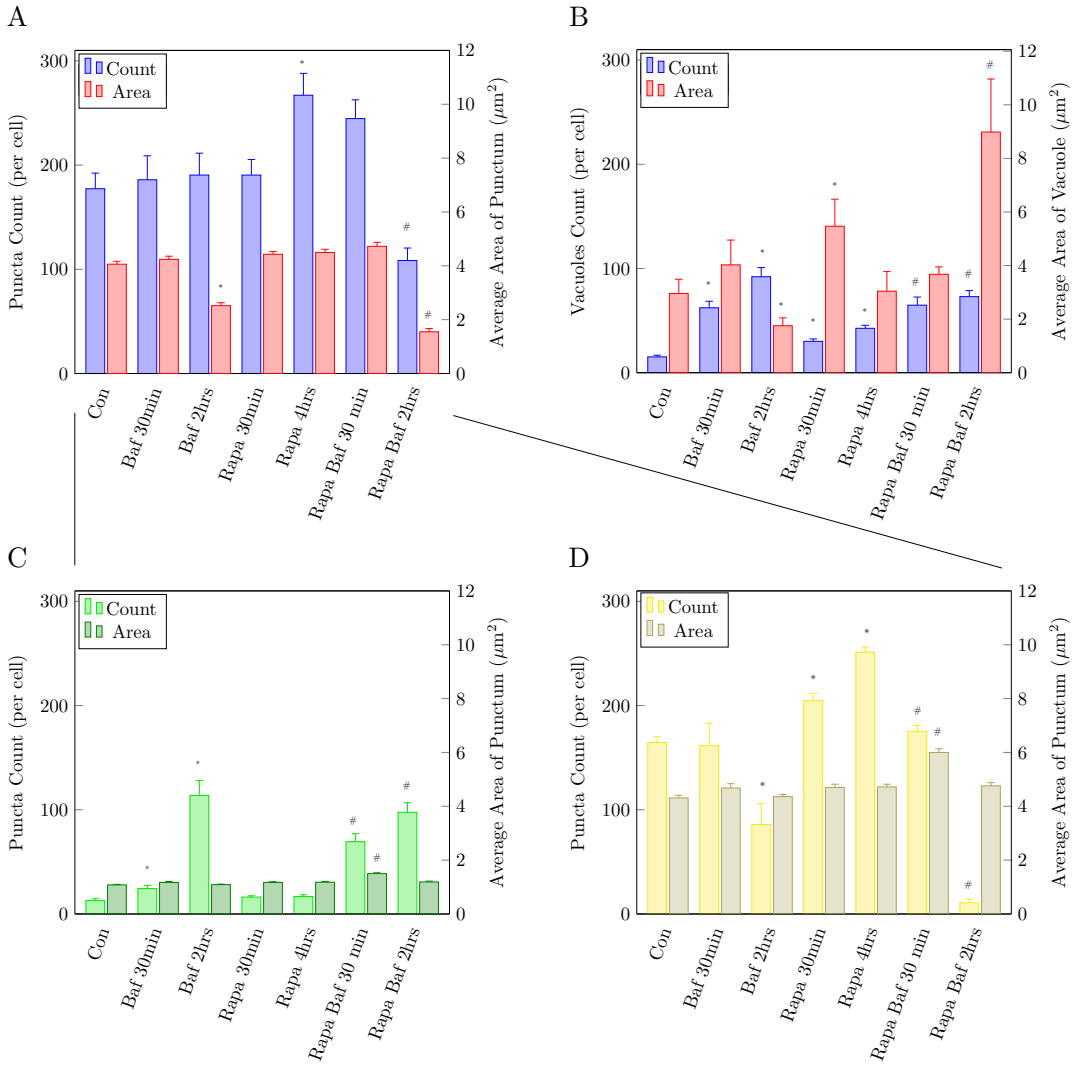

Figure 4.13: Quantification of the number of puncta and vacuolar structures, as well as the area of a punctum or vacuole averaged over all the puncta/vacuoles in a micrograph, from images derived from fluorescence and electron microscopy. (A) Fluorescence microscopy data (total puncta) and (B) electron microscopy data. (A) Can be separated into (C) autophagosomes and (D) autophagolysosomes. $*$ vs. Con $p < 0.05$, # vs. Rapa 4hr $p < 0.05$ ($n = 10$).

4.3.2 Size distribution

Fig. 4.14 shows the size distribution of puncta/vacuoles derived from the FM and EM studies based on three size classes.

The sizes of most of the puncta fell in the mid-sized range of 4–8 μm^2, except after inhibition with bafilomycin A_1 where there was an increase in small puncta (both in basal and rapamycin-induced conditions). As already mentioned above, this was due to the increase in the number of (smaller) autophagosomes relative to (larger) autophagolysosomes following inhibition of fusion. However, the size distribution of autophagosomes Fig. 4.14C and autophagolysosomes Fig. 4.14D remained constant under all treatment conditions. The distribution of autophagosomes in the small, mid and large size classes was 67.2%, 32.4% and 0.4%, while that of autophagolysosomes was 9.7%, 76.1% and 14.2%.

The majority of the vacuoles were smaller than 4 μm^2 (Fig. 4.14B). Whether the apparent shift in vacuolar size immediately after rapamycin treatment was real or, as surmised above, due to the unreliability of EM data, is unclear.

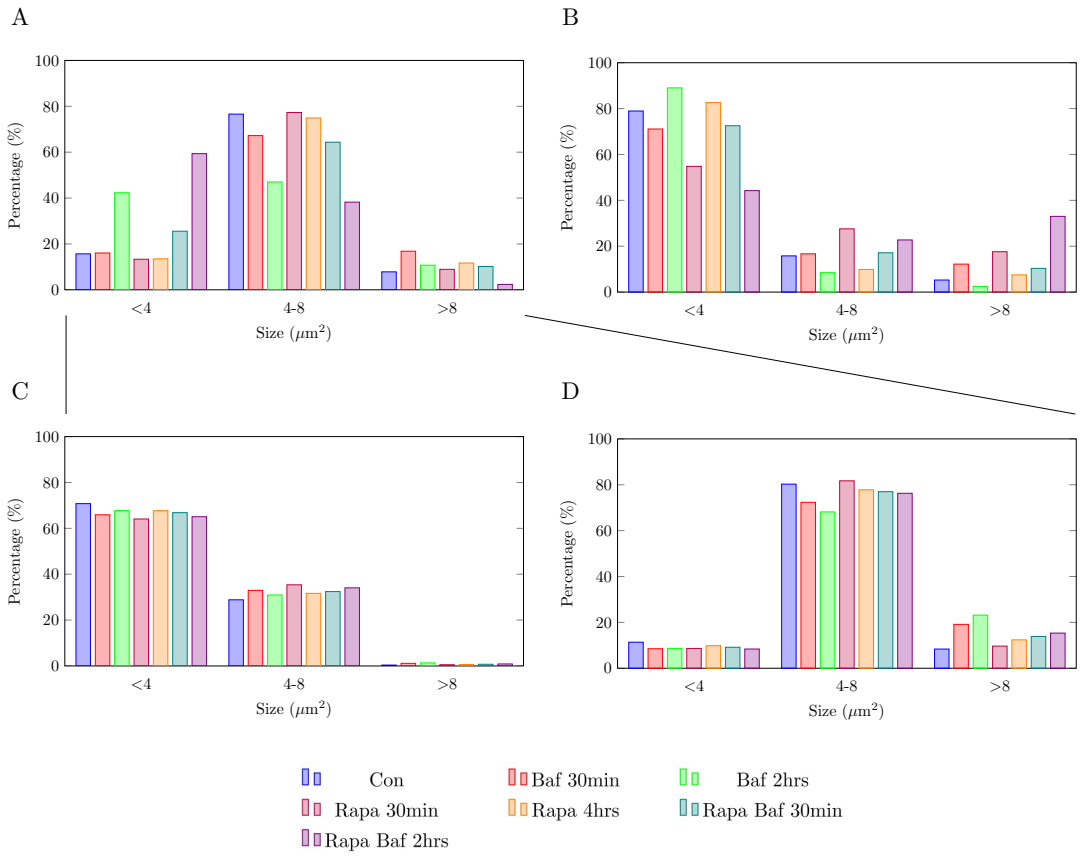

Figure 4.14: Size distribution of puncta/vacuolar structures, expressed as the percentage occurrence in one of three size classes: $< 4\mu m^2$, 4–$8\mu m^2$, $> 8\mu m^2$. (A) Total puncta observed using fluorescence microscopy; (B) Vacuoles using electron microscopy. Puncta are divided into (C) autophagosomes and (D) autophagolysosomes ($n = 10$).

4.3.3 Average punctum/vacuole volume and the derived total sphere surface area of puncta/vacuoles

The volume of a punctum or vacuole was calculated by assuming it to be spherical and that the experimentally measured area could be used to calculate the radius of the sphere. Using the radius, the volume and the surface area of an individual punctum or vacuole could therefore be calculated. Using the count of puncta or vacuoles in one cell the total combined surface area of autophagosomes and autophagolysosomes at any time point could also be calculated. The total surface area was equated to the combined total vesicular membrane area of autophagosomes and autophagolysosomes. Fig. 4.15 shows the average punctum/vacuole volume and the calculated total surface area of puncta/vacuoles.

Because the volume and surface area of the assumed sphere were derived from the puncta/vacuole count and area no additional information could in principle be deduced from these data, which therefore cannot add to that which was discussed in the previous section. The reason that volumes and total surface area are reported here is that they can be used to calculate the rate at which cytoplasmic volume and cellular membrane was consumed in the formation of autophagosomes, which we propose as new and potentially useful functional variables of autophagy (see Section 4.5).

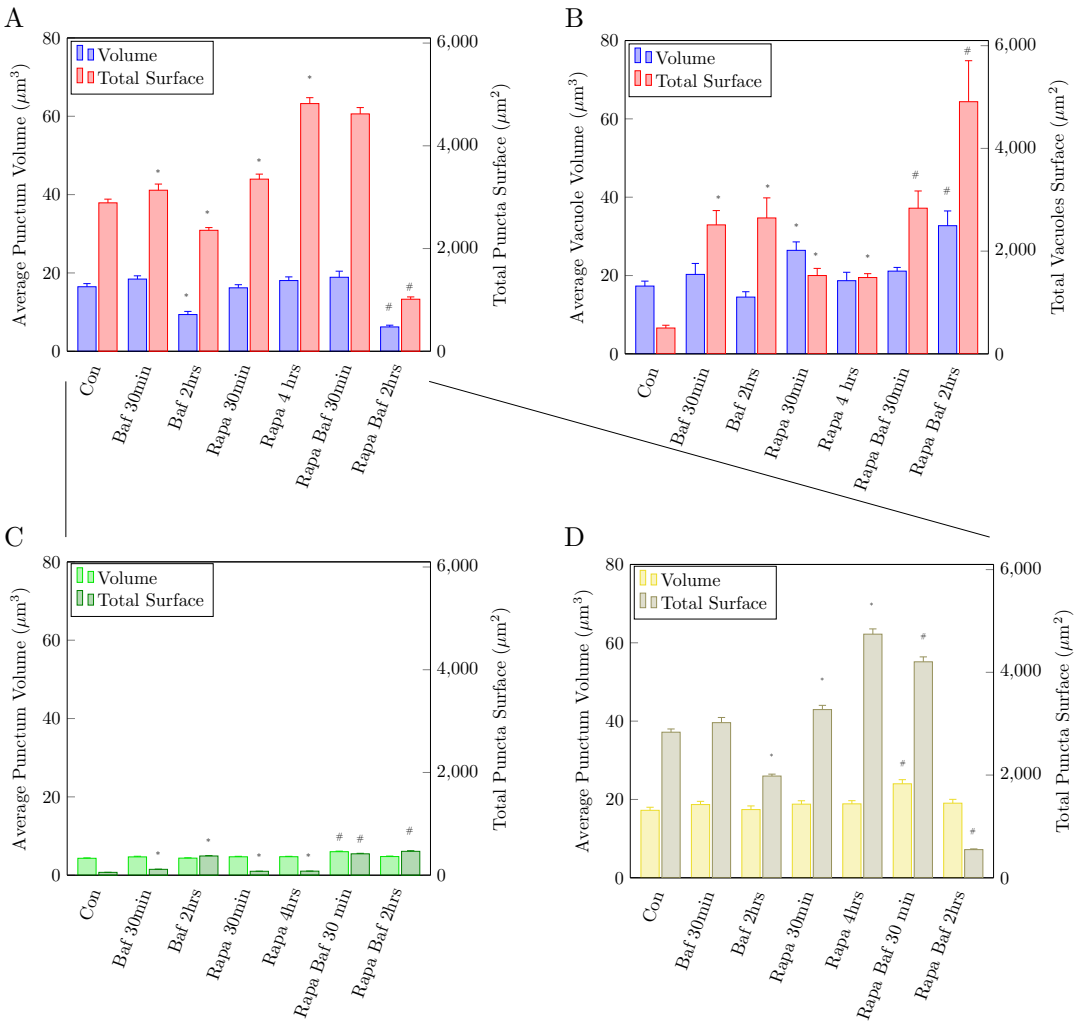

Figure 4.15: Average puncta volume and total puncta surface area of autophagosomes plus autophagolysosomes assessed by (A) fluorescence microscopy and (B) electron microscopy. The same variables are shown for (C) autophagosomes on their own and for (D) autophagolysosomes on their own. $*$ vs. Con, $p < 0.05$; # vs. Rapa 4hr, $p < 0.05$ ($n = 10$).

4.4 Assessing key autophagy-related proteins

In reporting autophagic activity, Western blot analysis forms part of the standard protocol used today to assess autophagy-related proteins, particularly LC3 and p62 [167]. LC3 II is used as an autophagy vesicle marker, since it is a structural component of the autophagosomal membrane. p62 is used to assess the degradative capacity of the autophagic system due to its mediating role between autophagosomal cargo and LC3 II, a role that facilitates protein degradation. LC3 I, LC3 II and p62 levels were measured at the time points shown in Fig. 4.11. Furthermore, pmTOR and total mTOR (mTOR+pmTOR) levels were also assessed, since rapamycin induces autophagy by preventing phosphorylation of mTOR. Two cell lines were used: GFP-LC3 MEF cells in live cell imaging (see section 4.1.1 and 4.2) and wild type MEF cells (to serve as a control against our transgenic cell line). The Western blots of LC3, p62, pmTOR and mTOR are shown in Fig. 4.16 together with histograms of the band intensities that quantify the proteins.

4.4.1 Analyses of phospho-mTOR and total mTOR

Western blot analyses using antibodies specific to phosphorylated mTOR (pmTOR) and antibodies that recognise mTOR irrespective of its phosphorylation status (i.e., total mTOR) showed that upon treatment with rapamycin there was a decrease in pmTOR (as a fraction of the total mTOR) as compared to the basal condition (Con) (Fig. 4.16 A). The decrease in pmTOR was associated with the increase in n_{A}, n_{AL} and autophagic flux as assessed by fluorescence microscopy (Fig. 4.10), which agrees with its role as negative regulator of autophagy.

4.4.2 Analyses of LC3 I and II

The most widely used assay for assessing autophagic activity involves Western blot analysis of LC3 before and after treatment with a fusion inhibitor such as bafilomycin A_1. Fig. 4.16B and C show the Western blot analysis of LC3 I and II in GFP-LC3 MEF cells and wild type MEF cells respectively. Note that for the GFP-LC3 MEF cells (Fig. 4.16B) the Western blots only show LC3 I and II

that are not coupled to GFP, which, as discussed in Chapter 6, complicates the interpretation of the results. As an example, we expected LC3 II, a membrane component of autophagosomes, to increase after rapamycin induction and after bafilomycin A_1 treatment since we had observed an increase in the number of autophagosomes for such experiments (Fig. 4.10A and B). Wild type MEF cells clearly showed these trends (Fig. 4.16C), whereas GFP-LC3 MEF cells showed an initial decrease and subsequent increase in LC3 II following bafilomycin A_1 treatment and no increase upon rapamycin induction, although bafilomycin A_1 treatment of induced autophagy did show the expected increase in LC3 II.

Standard Western blot analysis of LC3 was used to assess whether autophagic flux increased or not relative to a control condition. Measuring LC3 II band densities before and after inhibition of fusion with bafilomycin A_1 was used to indirectly assess the time-dependent accumulation of autophagosomes. Based on the differences between the relative increases in LC3 II band densities after bafilomycin A_1 treatment of control and rapamycin-treated cells, we could conclude that the cells treated with rapamycin had a two-fold higher autophagic flux compared to the control (Fig. 4.16C compares the relative difference between Con and Baf 30min to that between Rapa 4hr and Rapa Baf 30min).

Cytoplasmic LC3 I is not directly associated with autophagosomes and it is not known whether variations in its level can be linked with changes in the number of autophagosomes. What is clear from Fig. 4.16C is that in our experiments with wild type MEF cells there was no correlation between variations in LC3 I and II. The data in Fig. 4.16B have no clear interpretation.

4.4.3 Analyses of p62

Fig. 4.16 D and E show the Western blot analysis of p62 of GFP-LC3 MEF and wild type MEF cell lines respectively. The p62 blots showed the same trends as the LC3 blots of both GFP-LC3 and wild type MEF cells, which is not surprising since p62, which occurs in the lumen of autophagosomes, associates with LC3 II and would thus be expected to vary with it.

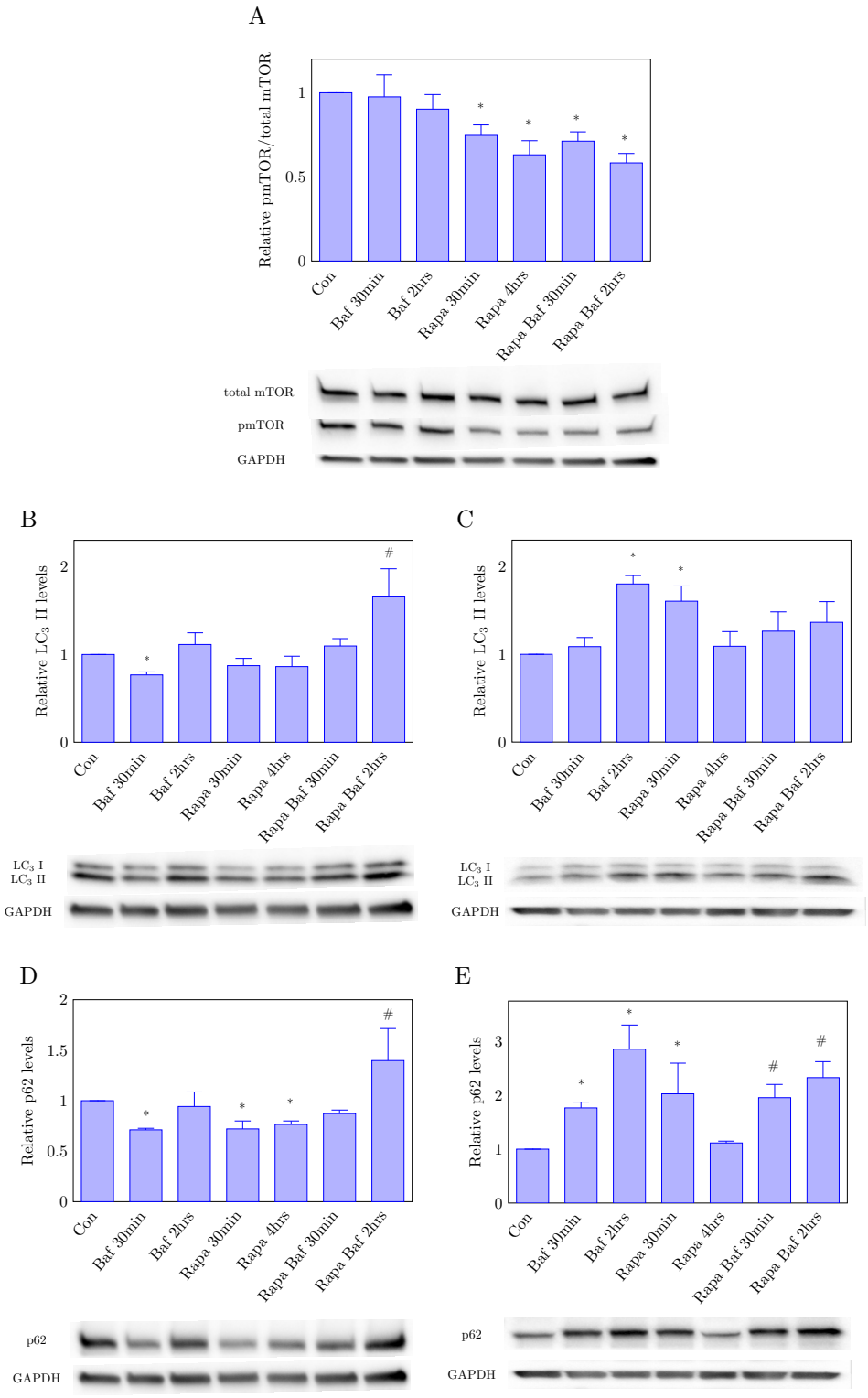

Figure 4.16: Western blot analysis of autophagy related proteins. (A) mTOR; (B) LC3 in GFP-LC3 MEF cells; (C) LC3 in wild type MEF cells; (D) p62 in GFP-LC3 MEF cells; (E) P62 in wild type MEF cells. Glyceraldehyde phosphate dehydrogenase (GAPDH) was used as a loading control. A representative blot is shown. $*$ vs. Con, $p < 0.05$; # vs. Rapa 4hr, $p < 0.05$ ($n = 3$).

4.5 Autophagic variables

From the data obtained by the experiments described above, we were able to quantify a number of autophagic variables. Traditional methods such as Western blot analysis and electron microscopy allowed the measurement of variables associated with vacuolar structures, but without making any distinction between autophagosomes and autophagolysosomes (Table 4.1). Our new fluorescence microscopy approach allowed us to make this distinction, while at the same time providing more reliable and accurate assessments of a number of autophagic variables (Table 4.2)

Autophagic flux is commonly assessed with Western blot analysis of LC3 with and without the inhibition of fusion between autophagosome and lysosomes (described in section 2.6.2.1); the relative increase in LC3 levels after treatment with a fusion inhibition such as bafilomycin A_1 is used to describe autophagic flux. As indicated in Table 4.1 we measured a 2.15-fold increase in autophagic flux with this method, compared to the 4.14-fold increase measured with our fluorescence microscopy method (see Table 4.2).

With electron microscopy, vacuolar flux, J_{vac}, in the basal and induced states was measured as the rate of increase in the number of vacuoles, n_{vac}, after inhibition of fusion (Baf 30 min and Rapa Baf 30 min in Fig. 4.11). The decrease in the vacuolar flux after rapamycin induction was in stark contrast to the increase in autophagosomal flux observed with fluorescence microscopy, and demonstrates that vacuolar flux is a poor measure of autophagic flux. This is to a large part due to the fact that the number of vacuoles counted in a single EM section is probably a poor indicator of the total number of vacuoles in a cell. Although we calculated the vacuolar transition time τ_{vac} as the ratio of $n_{\text{vac}}/J_{\text{vac}}$, we cannot deduce much from these values. Induction by rapamycin had little effect on the average volume of a vacuole, but the total membrane area of the vacuoles in an EM section increased about 28-fold.

The measurement of n_{A} and J with our fluorescence microscopy technique allowed us to calculate the transition time $\tau = n_{\text{A}}/J$, which is the time required to turn over the autophagosomal pool in the system; the autophagolysosomal transition time τ_{AL} is similarly calculated as n_{AL}/J (Table 4.2). Both τ_{A} and τ_{AL}

respectively decreased 3-fold and 2.8-fold after induction. The average volume of an autophagosome was not affected by induction, while the cytoplasmic volume consumption rate increased by a factor of 4.5, while the autophagosomal membrane flux increased by a factor of 5.9. Fig. 4.17 summarises these results graphically.

Table 4.1: Functional variables of autophagy as measured by traditional methods (Vac: vacuolar structures counted in a single EM section). Derived variables are shown in italics.

Variable	**Unit**	**Basal**	**Induced**
		Western blot	
Relative flux, J_{rel}	dimensionless	1	2.15
		Electron microscopy	
Vacuolar flux, J_{vac}	Vac/hr/section	92.3	61.6
Number of vacuoles, n_{vac}	Vac/section	15.2	42.6
Average volume of a vacuole	fL	17.3	18.7
Total membrane area	μm^2	52.8	1486
Vacuolar transition time, τ_{vac}	hr	0.16	0.69

Table 4.2: Functional variables of autophagy as measured by the new fluorescence microscopy method (A: autophagosomes; AL: autophagolysosomes). Derived variables are shown in italics.

Variable	**Unit**	**Basal**	**Induced**
Autophagic flux, J	A/hr/cell	25.4	105.4
Number of autophagosomes, n_{A}	A/cell	13.4	16.7
Number of autophagolysosomes, n_{AL}	AL/cell	164.5	251.2
Average volume of an autophagosome	fL	4.3	4.7
Average volume of an autophagolysosome	fL	17.3	18.8
Autophagosomal transition time, τ_{A}	hr	0.53	0.16
Autophagolysosomal transition time, τ_{AL}	hr	6.7	2.4
Cytoplasmic volume consumption rate, J_{vol}	fL/hr/cell	109	495
Autophagosomal membrane flux, J_{mem}	μm^2/hr/cell	1397	8268

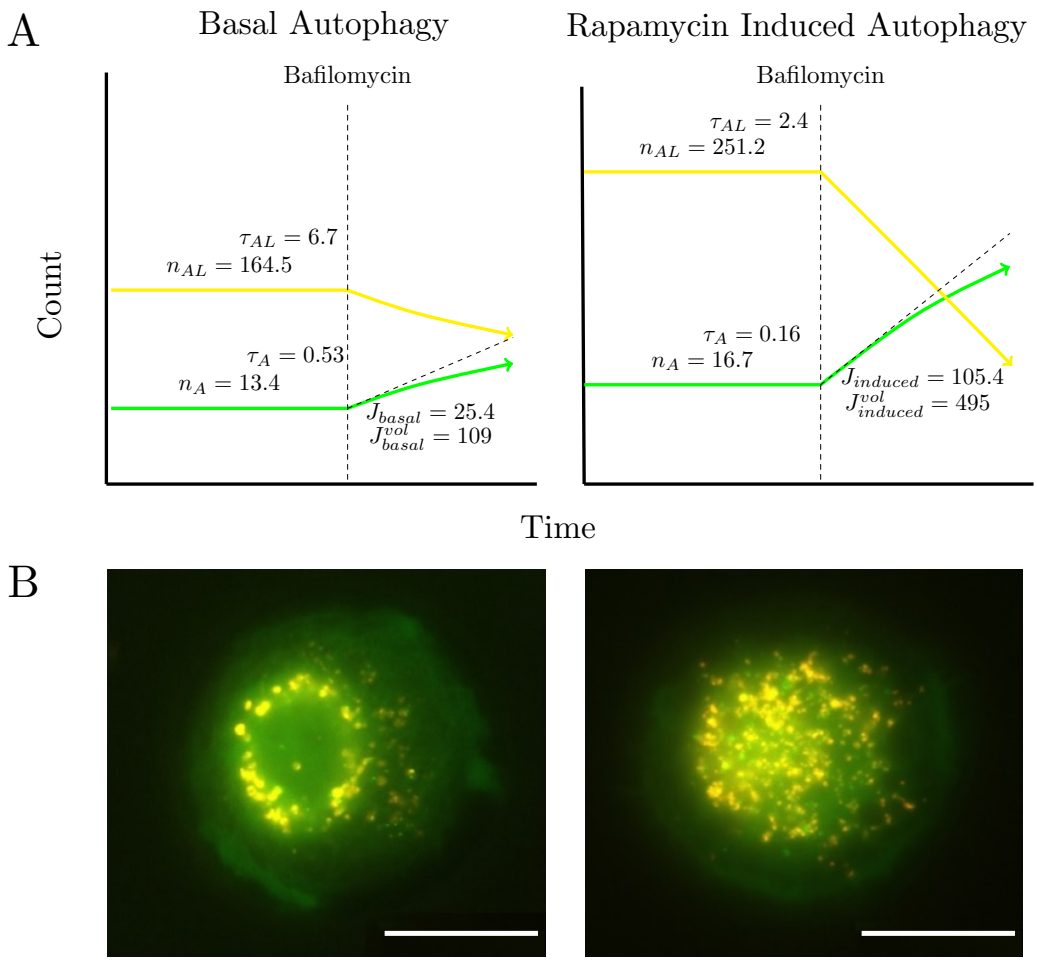

Figure 4.17: Basal and rapamycin-induced autophagy variables. (A) shows a cartoon of basal and induced autophagy variables. (B) depicts representative image of basal and rapamycin-induced autophagy. J = autophagosomes/hr/cell, n_i = number of steady state species , τ_i = hr and J_i^{vol} = pL/hr/cell.

4.6 Amino acid and protein levels under basal and induced autophagy

4.6.1 Single amino acids

A complete amino acids analysis was performed on the treatment groups described in Fig. 4.11. Fig. 4.18 shows the amino acid profiles for each treatment condition (Fig. A in Appendix A shows the quantitative analysis of individual amino acids).

Glutamic acid and arginine were the only amino acids that showed significant changes between treatment groups (Fig. 4.19), although the changes in arginine were marginal compared to those in glutamic acid. The trend in the arginine change profile (Fig. 4.19B) was shared by all the other amino acids analysed. The most likely explanation for the high glutamic acids levels after rapamycin treatment is an increase in amino acid catabolism which leads to an increase the production of nitrogen waste, glutamic acid being a key intermediate in the nitrogen waste disposable pathway. This increase in amino acid metabolism is discussed in more detail in section 6.7. Rapamycin mimics starvation induced-autophagy by preventing the negative feedback by high amino acids levels on autophagy [197]. Therefore, no conclusions about the regulation of autophagy by amino acids can be drawn from experiments in which rapamycin is used to induce autophagy, such as described in this thesis.

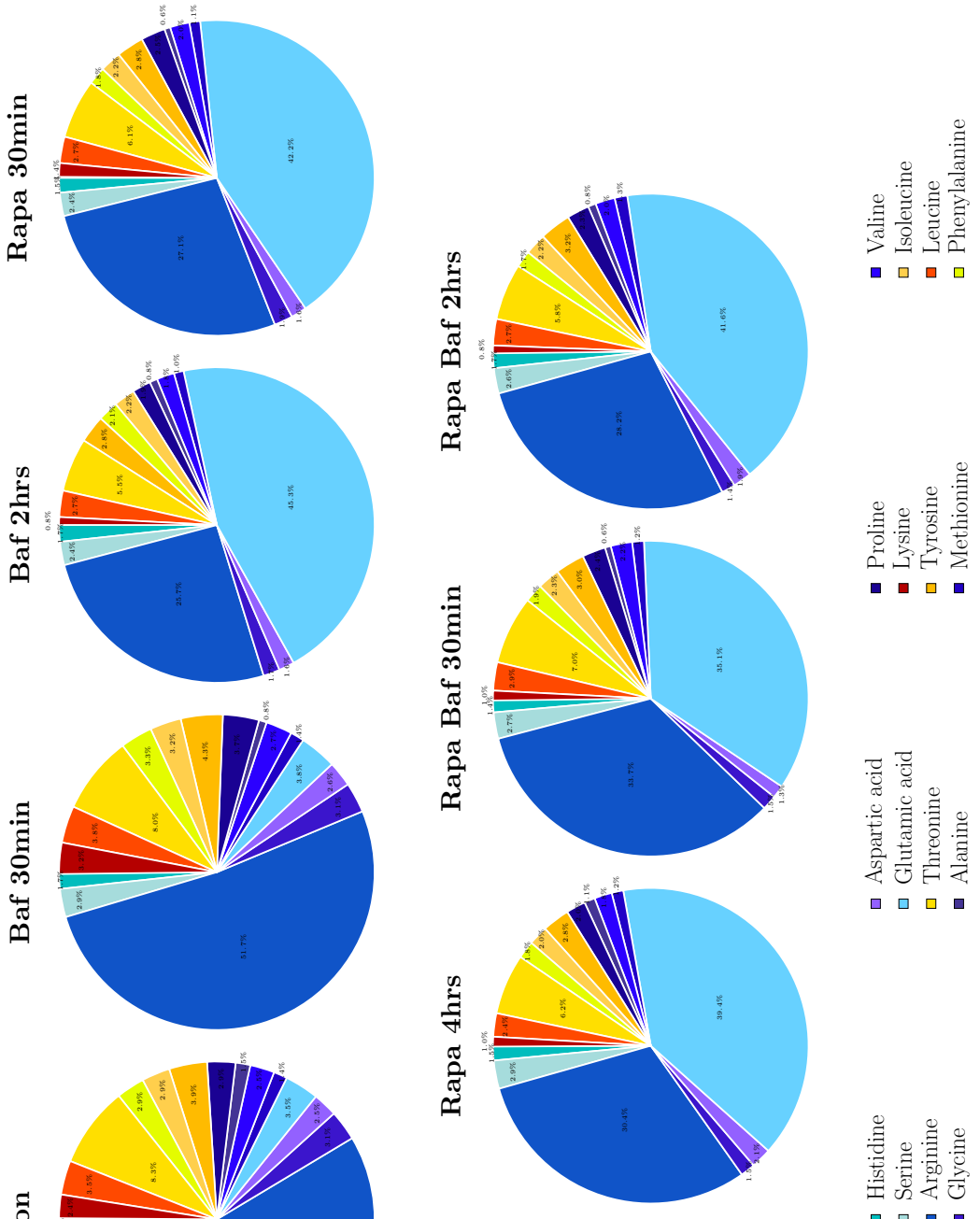

Figure 4.18: Pie-charts showing the amino acid profiles under various treatment conditions. Glucogenic amino acids are shaded in blue, ketogenic amino acids are shaded in red whereas amino acids that are both glucogenic and ketogenic are shaded in yellow ($n = 3$).

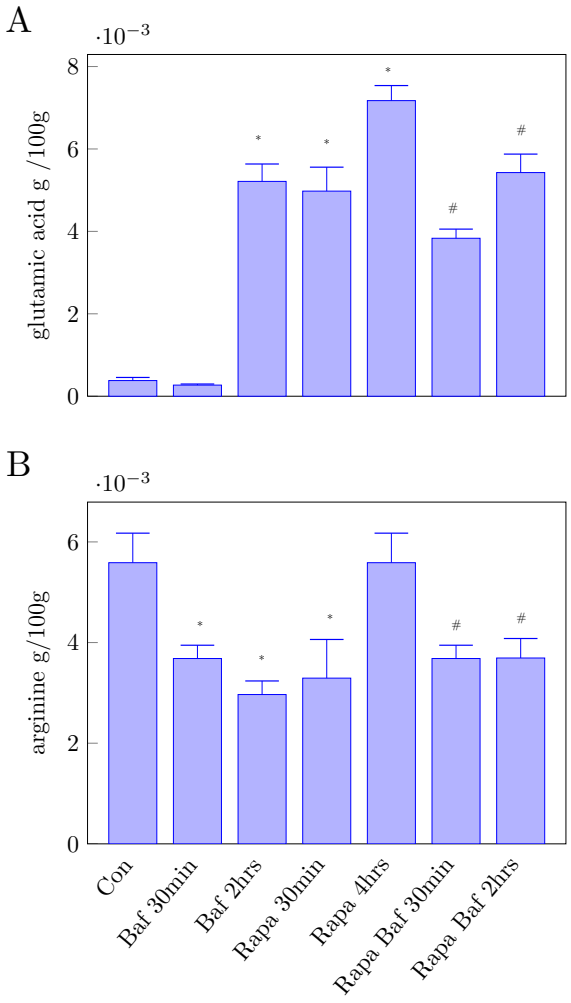

Figure 4.19: Quantitative measurements of (A) glutamic acid and (B) arginine. $*$ vs. Con, $p < 0.001$; # vs. Rapa 4hr, $p < 0.001$ ($n = 3$).

4.6.2 Glucogenic and ketogenic amino acids

Amino acids can be grouped on the basis of how they feed into energy metabolism. Glucogenic amino acids feed into the gluconeogenesis pathway through pyruvate. Ketogenic amino acids contribute to the synthesis of ketone bodies and fatty acids. Some amino acids are metabolised through both ketogenic and glucogenic pathways. Figs. 4.20A and 4.20B respectively show the ketogenic and glucogenic amino

acid levels for the different treatment groups, while Fig. 4.20C shows that of amino acids that are both ketogenic and glucogenic. Ketogenic amino acids and amino acids that are both ketogenic and glucogenic show similar trends after induction and inhibition of autophagy. An increase in glucogenic amino acids was observed in the rapamycin-induced steady state (Rapa 4 hr), to which glutamic acid was the major contributor.

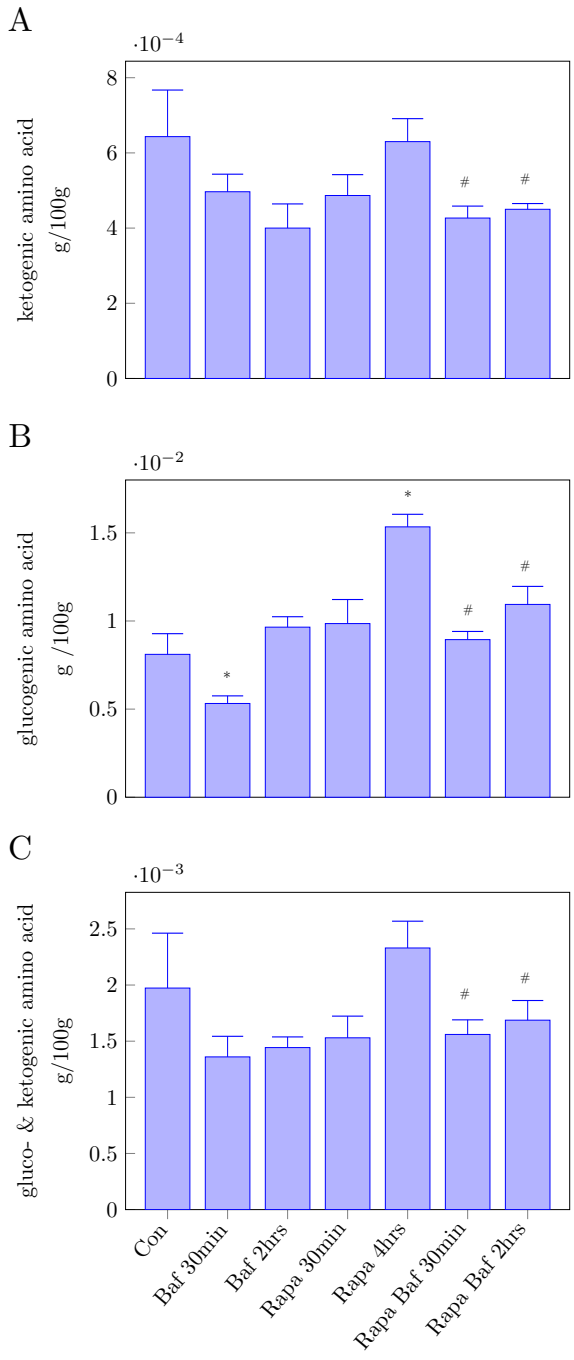

Figure 4.20: Quantitative analysis of (A) ketogenic amino acids, (B) glucogenic amino acids, and (C) amino acids that are both ketogenic and glucogenic. $*$ vs. Con, $p < 0.05$; # vs. Rapa 4hr, $p < 0.05$ ($n = 3$).

4.6.3 Total amino acid and total protein profiles

Cytoplasmic proteins serve as substrates for the autophagic system; amino acids are the end products of the degradation of proteins through autophagy. We therefore measured total amino acid and total cellular protein levels during basal and rapamycin-induced autophagy (Fig. 4.21). Following induction of the autophagic system protein levels decreased while the amino acid level increased, as expected. After inhibition of fusion, and the subsequent suppression of autophagic flux, amino acid levels descreased significantly, while the observed decrease in proteins levels was not significant according to one-way Anova with Bonferoni post-test. The decrease in amino acids was to be expected, but the observed decrease in protein level was contrary to expectation. We do not know why, but we cannot exclude the possibility that this was just due to experimental error.

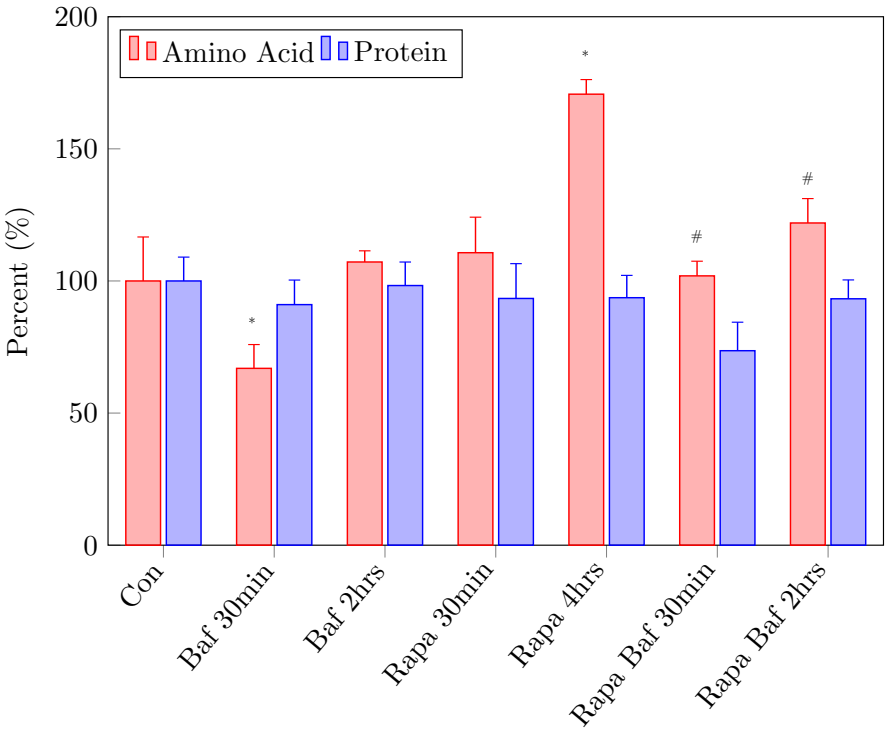

Figure 4.21: Total amino acid and protein levels. Graph shows control (Con), 30 min (Baf 30min) and 2 hr (Baf 2hr) bafilomycin A_1 treatment, and 30 min (Rapa 30 min) and 4 hr (Rapa 4hr) rapamycin treatment, as well as cells pretreated for 4 hr with rapamycin followed 30 min (Rapa Baf 30min) and 2 hr (Rapa Baf 2hr) bafilomycin A_1 treatment. $*$ vs. Con, $p < 0.05$; # vs. Rapa 4hr, $p < 0.05$ ($n = 3$).

Chapter 5

A kinetic model of autophagy

The autophagic pathway is a stepwise series of transformations of membrane-bound vesicles along which there is a flow of cytoplasmic material, which is degraded during the process. We have defined autophagic flux as the rate of flow through the pathway at steady state [142]. This definition of autophagic flux is similar to that of flux in metabolic studies, where metabolic flux refers to the rate of flow of metabolites along a metabolic pathway in steady state. Presently, combinations of assays such as Western blot analysis, fluorescence and transmission electron microscopy are used to assess the autophagic degradative capacity [167]. Although these techniques do generate invaluable data for deciphering aspects of autophagy, they do not generate the type of data that allow a study of the continuous time-dependent behaviour of autophagy.

As described in Chapter 4, we have developed a fluorescence microscopy technique with which we can quantitatively measure the changes with time in the number of autophagosomes, autophagolysosomes and lysosomes in a single cell during basal and rapamycin-induced autophagy. Inhibiting the fusion of autophagosomes and lysosomes with bafilomycin A_1 and measuring the rate of accumulation of autophagosomes allowed us to calculate the steady-state autophagic flux. This chapter describes the development of a kinetic model, similar to the type of models used to study metabolism, that simulates the time-course of the autophagic vesicles during the process of autophagy, with and without induction.

Our modelling strategy was to start with the simplest possible model of autophagy with the simplest possible rate equations, and then to extend the network scheme and modify the kinetics step by step in order to achieve a near-perfect fit of our experimental data. This afforded us a deep understanding of the contribution of each part of the autophagic network to its time-dependent behaviour.

In recent years computer modelling has become an integral tool for the analysis of the behaviour, control and regulation of reaction networks that underlie cellular processes. There are many software platforms for building such models, one of which we have developed, namely PySCeS (the Python Simulator for Cellular Systems [191], http://pysces.sourceforge.net), a console-based simulation platform written in the Python programming language (http://www.python.org). PySCeS uses the Numerical Python (NumPy) and Scientific Libraries for Python (SciPy), which are collections of mathematical algorithms for science and engineering applications. The kinetic model of autophagy described in the next section was developed using PySCeS.

5.1 The kinetic model

The first step in the modelling process is to create a model object that describes a model in terms of its stoichiometry and rate equations. This is done by defining the model in a text file, which is parsed and converted into the model object. In the process PySCeS checks the validity of the model and automatically performs a structural analysis of the stoichiometry matrix that describes the topology of the reaction network. PySCeS can then simulate the dynamical behaviour of the system over time, calculate the steady state, do 1, 2, or n-dimensional parameter scans and bifurcation analyses, and investigate the control and regulation of cellular systems with a metabolic control analysis (MCA) module that calculates elasticity coefficients, flux and concentration-control and response coefficients.

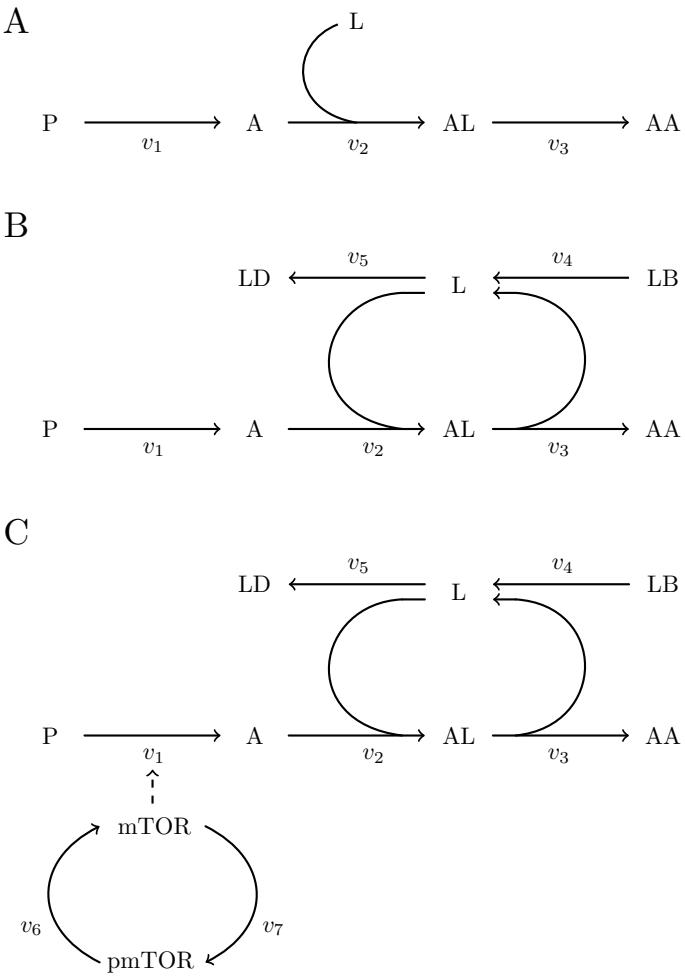

Figure 5.1: Network representation of the autophagic process: (A) The minimal model describes autophagosome synthesis, fusion with lysosomes, and autophagosome breakdown with the release of amino acids. Lysosomes are regarded as fixed. (B) The model is extended with the biogenesis and degradation of lysosomes, which are now regarded as variable. (C) The mTOR/pmTOR cycle is added, with mTOR incorporated into the rate equation for step 1. P: phagophores, A: autophagosomes, AL: autophagolysosomes, AA: amino acids, L: lysosomes, LB: biogenesis of lysosomes, LD: lysosome degradation. LB and LD are dummy variables necessary for defining the models.

Fig. 5.1 shows the schemes used to describe the autophagic process. Our strategy was to describe each step in autophagy as a chemical reaction in which the "reactants" were the autophagic intermediate vesicles. The pathway shown in

Fig. 5.1A is a simple representation of autophagy and served as a starting point for modelling the dynamics of autophagy. This minimal kinetic model was extended to include lysosomal biogenesis and degradation (Fig. 5.1B), and the mTOR/pmTOR system (Fig. 5.1C).

The PySCeS model input files for the reaction schemes in Fig. 5.1 define the reactions, rate equations and parameters as well as variable initializations (the input files are listed in Appendix C). All steps were assumed to be irreversible and product-insensitive. The rate equations were all based on mass-action kinetics. The model input files incorporated an event that simulated the complete inhibition of the fusion of A and L at a specified time point. An induction event was also created to simulate rapamycin induction of the autophagic system.

Our modelling strategy was to start with the simplest possible kinetics, assuming the rate equations of the minimal model in Fig. 5.1A to be first-order with respect to all species:

$$\begin{aligned} v_1 &= k_1[P] \\ v_2 &= k_2[A][L] \\ v_3 &= k_3[AL] \end{aligned}$$

Kinetic parameters of the rate reactions were set as follows to simulate the experimental basal flux: $P = 1.0$, $L = 1.0$ (average experimental basal value), $AA = 0.0$, $k_1 = 25.4$ hr^{-1}, $k_2 = 25.4/13.0$ hr^{-1}, $k_3 = 25.4/165.0$ hr^{-1}. Initial values of A and AL were set to zero entities/cell. The rationale for choosing the values of k_1, k_2 and k_3 was the following:

- Since the first step in the pathway (the biogenesis of autophagosomes from phagophores) was assumed to be irreversible and insensitive to downstream events, it is rate-limiting and completely determines the steady-state autophagic flux under all conditions. Setting k_1 to 25.4 hr^{-1} (with $P = 1.0$) therefore set the autophagic flux to the average basal flux as measured experimentally (calculated from $v_1 = k_1[P] = k_1(1.0) = 25.4$).

- The average experimental basal steady-state value of A was 13 autophagosomes/cell. The rate v_2 of step 2 in the basal steady-state had to be equal to the steady-state flux set by step 1, i.e., 25.4 hr^{-1}. In order to set A to 13.0, k_2 was be set to 25.4/13.0 hr^{-1} (calculated from $v_2 = k_2[A][L] = k_2(13.0)(1.0) = 25.4$).

- The average experimental basal steady-state value of AL was 165 autophagolysosomes/cell, which, similarly, required k_3 to be set to 25.4/165.0 hr^{-1} (calculated from $v_3 = k_3[AL] = k_3(165.0)(1.0) = 25.4$).

The time-dependent behaviour of the system with these parameter values was simulated with PySCeS. At $t = 2$ hr the inhibition of fusion by bafilomycin A_1 was simulated by setting k_2 to zero. Fig. 5.2A shows that with these parameter settings the simulated data were a reasonably good fit to the experimental data up to 30 min after bafilomycin A_1 treatment. After that there are processes that change the rates of autophagosome formation and autophagosome degradation which our model (and all the extensions discussed below) could not account for.

The induction of autophagy by rapamycin and subsequent inhibition of fusion by bafilomycin A_1 when the new induced steady state had been established was simulated by increasing P to 105.4/25.4 at $t = 2$ hr and k_2 to zero at $t = 6$ hrs. The experimentally-determined induced autophagic flux was 105.4 autophagosomes/hr/cell, and to set that value P had to be increased by the factor 105.4/25.4. As Fig. 5.2B shows, the induced flux was well-simulated (the experimental and simulated slopes at $t = 6$ hrs were equal), but the induced steady-state values of A and AL were too high ($A = 54$ instead of 17, $AL = 385$ instead of 251). The only way to lower these values without affecting the basal and induced flux was by adjusting the kinetic orders of A and AL in the rate equations for step 2 and 3 respectively. We therefore introduced terms for these kinetic orders in our rate

equation definitions:

$$\begin{aligned} v_1 &= k_1[P] \\ v_2 &= k_2[A]^{h_2}[L] \\ v_3 &= k_3[AL]^{h_3} \end{aligned}$$

These alterations of course implied that k_2 and k_3 also needed to be recalculated as $k_2 = 25.4/13.0^{h_2}$ and $k_2 = 25.4/165.0^{h_3}$. By trial and error we arrived at the values $h_2 = 5$ and $h_3 = 3.4$, which lowered A and AL to the required 17 and 251 respectively. Using these modifications to our minimal model we were able to bring our simulation very close to the experimental profile (Fig. 5.2D). The simulation of basal flux (Fig. 5.2C) was virtually indistinguishable from that in Fig. 5.2A, except that the decrease in AL in the 30 min period after bafilomycin A_1 treatment was better approximated with the incorporation of h_2 and h_3.

Where our simulation still did not match the experimental profile was in the two-hour period after induction with rapamycin, during which A nearly doubled to 23 autophagosomes/cell and then decreased to its new steady-state value of 17. This initial increase in A after induction was accompanied by a slower increase in AL. The only way to introduce this effect was by making the lysosome pool variable as in the extended scheme in Fig. 5.1B. It was important that not only regeneration of lysosomes in step 3 was included, but also de novo biogenesis and degradation of lysosomes (steps 4 and 5):

$$\begin{aligned} v_1 &= k_1[P] \\ v_2 &= k_2[A]^{h_2}[L] \\ v_3 &= k_3[AL]^{h_3} \\ v_4 &= k_4[LB] \\ v_5 &= k_5[L] \end{aligned}$$

The properties of steps 4 and 5 had to be set to values that ensured both that L returned to a value of 1 in the induced steady state and that the initial increase in

A after induction (and the concomitant decrease in L and slower increase in AL) occurred during the two hours after induction. The first criterion was satisfied if, at an LB-value of 1, $k_4 = k_5$. Note that in steady state, $v_1 = v_2 = v_3$, which implies that $v_4 = v_5$ (for L to be in steady state), and therefore that $k_4(1.0) = k_5[L]$. For L to be 1 in steady state, k_4 therefore had to equal k_5. By trial and error we found that the second criterion was satisfied if $k_4 = k_5 = 80.0$.

Fig. 5.2F shows that, although we could now simulate the initial overshoot of A after induction it was too fast. This was due to our making the induction event instantaneous, whereas in reality it would be a slower process that depends on the rate of dephosphorylation of pmTOR to mTOR, which is the species that activates autophagy. We therefore incorporated the pmTOR/mTOR cycle into our model (Fig. 5.1C). In the rate equation for step 1 mTOR appears as a reactant, so that the rate of autophagy depends linearly on mTOR concentration. This served our purpose, but is probably too simple and a more realistic rate equation will be developed in the future.

$$\begin{aligned} v_1 &= k_1[P][mTOR] \\ v_2 &= k_2[A]^{h_2}[L] \\ v_3 &= k_3[AL]^{h_3} \\ v_4 &= k_4[LB] \\ v_5 &= k_5[L] \\ v_6 &= k_6[pmTOR] \\ v_7 &= k_7[mTOR] \end{aligned}$$

When $P = 1$ and $mTOR = 1$ the set k_1-value of 25.4 ensured the correct basal autophagic flux. Instead of increasing P by a factor of 105.4/25.4 to simulate induction, we now had to ensure that $mTOR$ increased with time from a value of 1.0 to 105.4/25.4 (with P now set to 1.0). The simplest way of accomplishing this was to set k_6 to 1.0 and k_7 to 105.4/25.4. Because in steady state $v_6 = v_7$, this ensured that mTOR and pmTOR had steady-state concentrations of 1.0 and 105.4/25.4 respectively. We therefore initialised $mTOR$ and $pmTOR$ to these values. Because the mTOR/pmTOR cycle is a moiety-conserved cycle, i.e., the

sum of $mTOR$ and $pmTOR$ is constant, switching the k_7/k_6 ratio from 105.4/25.4 to 25.4/105.4 switched $mTOR$ and $pmTOR$ to 105.4/25.4 and 1.0 respectively, i.e., $mTOR$ increased by the required factor of 105.4/25.4. This switch in k_7/k_6 was done by multiplying k_6 with the factor $(105.4/25.4)^2$.

We now had to also multiply k_6 and k_7 by the same time-scaling factor to simulate the rate of the induction process itself, i.e., the time taken for $mTOR$ to change from 1.0 to 105.4/25.4. A factor of 0.08 (determined by trial and error) gave the desired result. Fig. 5.2G and H show that with all these extensions of and modifications to our simple model we now had a near-perfect simulation of our experimental data for both basal and induced autophagy.

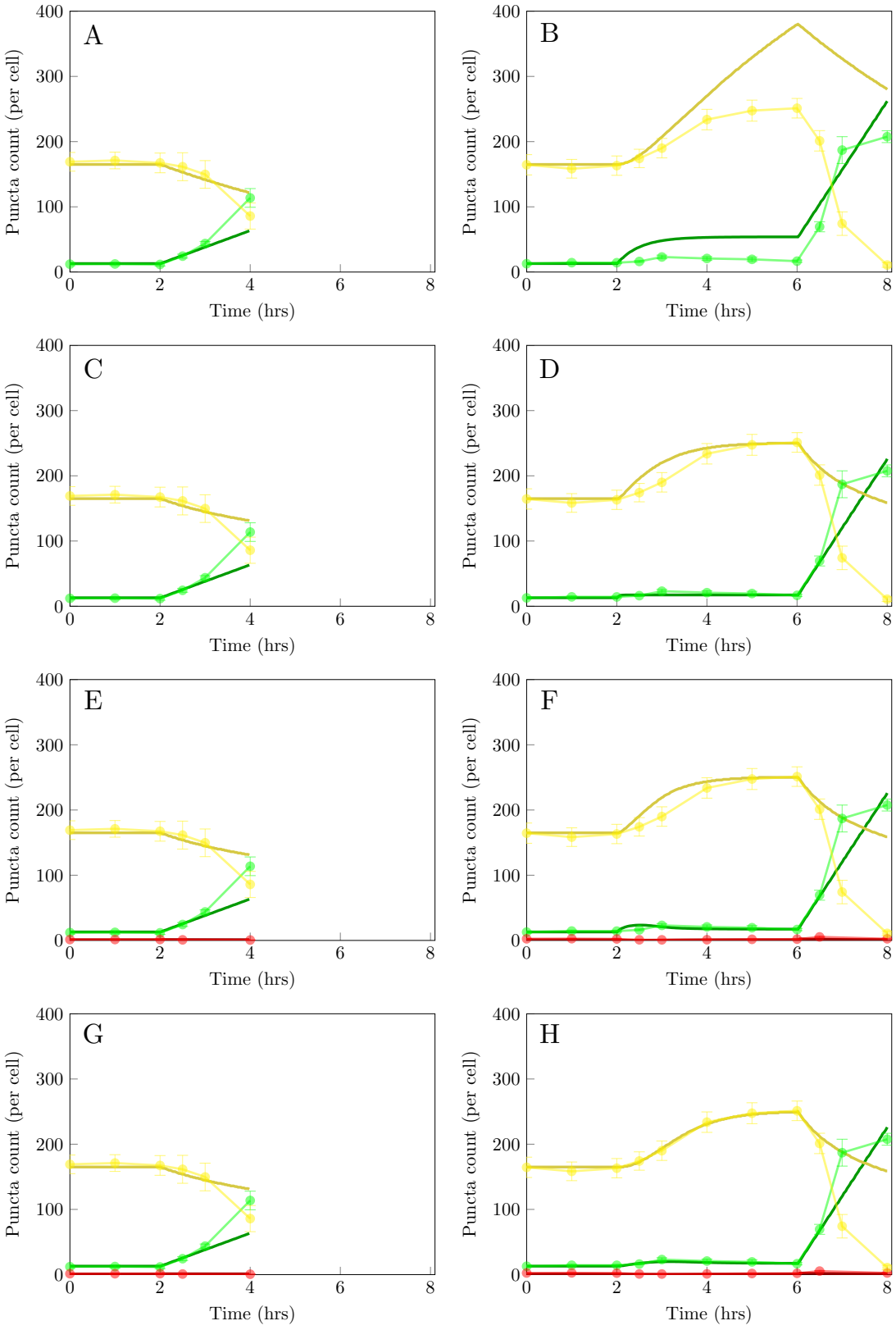

Figure 5.2: Fitting simulation curves to experimental data. Left-hand graphs: determination of basal flux; right-hand graphs: determinations of induced flux. (A,B) the minimal model of autophagy in Fig. 5.1A with first-order rate equations; (C,D) the minimal model of autophagy in Fig. 5.1A with higher-order rate equations; (E,F) the minimal model expanded to include lysosomal formation and degradation (Fig. 5.1B); (G,H) further addition of the mTOR/pmTOR system(Fig. 5.1C). The autophagosomal (—), autophagolysosomal, (—), and lysosomal (—) time courses were simulated.

5.1.1 Control analysis

PySCeS also allows the calculation of control and elasticity coefficients of a steady state. Appendix B lists these coefficients for the basal steady state of the kinetic model of autophagy described above. In our model full control of the autophagic flux is trivially in the first step ($C_{v_1}^{J_{\text{basal}}} = 1.0$), since its rate equation is defined to be insensitive to downstream intermediates (A and AL). Future refinements of the model will include negative feedback by amino acids on the synthesis of autophagosomes so that flux-control will at least be shared between step 1 and the demand for amino acids. Step 6 and 7 also control the autophagic flux through changes in mTOR, which is a multiplier in the rate equation of step 1, but the magnitude of the control coefficients of these two steps is proportional to the flux-control coefficient of step 1. Similarly, because of the way the rate equations are defined, step 4 has full control over the flux through the lysosomal pool.

Concentration control of A by step 1 and 2 (0.2 and -0.2 respectively) is completely determined by the elasticity coefficient of step 2 with respect to A, because step 1 is insensitive to A. $C_{v_1}^{A}$ and $C_{v_2}^{A}$ are the positive and negative reciprocals of $\varepsilon_{A}^{v_2} = 5.0$. Similarly, concentration control of AL by step 1 and 3 (0.29 and -0.29 respectively) is completely determined by the elasticity coefficient of step 3 with respect to AL, where $C_{v_1}^{AL}$ and $C_{v_3 2}^{AL}$ are the positive and negative reciprocals of $\varepsilon_{AL}^{v_3} = 3.4$.

At this stage of the development of our kinetic model of autophagy it is premature to make confident statements about the control of autophagic flux and concentration of autophagic vesicles. Too much depends on how we defined the rate equations.

Chapter 6

General discussion

6.1 Introduction

Conventional methods used in autophagy research, most notably Western blotting and electron microscopy, generate invaluable information about the mechanistic behaviour of autophagy, but they lack the ability to accurately measure autophagic flux. Therefore, the first aim of this study was to develop a new approach to quantifying autophagic flux and to compare it to the conventional methods. The quantification of autophagic flux was done at a single cell level using live cell fluorescence imaging. The experimental protocol was to establish an autophagic steady state, and then to block the fusion of autophagosomes and lysosomes; autophagic flux was then calculated as the initial rate at which the number of autophagosomes increased after inhibition of fusion. The second aim was to create a kinetic model of the autophagic process and to analyse its dynamics and the control of its steady states.

6.2 Assessing and distinguishing between autophagic intermediates

It is well established that after induction of the autophagic system there is an increase in GFP-LC3 puncta [36, 129, 146, 161, 167, 255, 263, 265]. However, only a

few of these studies distinguish between autophagosomal and autophagolysosomal pool size and their changes after induction [36, 255, 265]; these studies assessed the autophagic vesicles with either LAMP2 anti-body staining [36] or with Lysotracker dye for live imaging [255, 265] (Lysotracker is a red fluorescent acidotropic probe for labelling and tracking acidic organelles). Staining for autophagosomes, autophagolysosomes and lysosomes provided a more complete picture of the autophagic system and its dynamic behaviour. The results of these studies accord with what we observed (Fig. 4.5), namely that autophagosomes only constitute a small fraction of GFP-LC3 puncta.

It is generally assumed that GFP-LC3 only identifies autophagosomes, since it is to be expected that the low pH in autophagolysosomes would immediately quence the pH-sensitive GFP fluorescence, and that, in the longer term, GFP protein would be degraded by lysosomal proteases. However, the addition the red Lysotracker dye shows that this is not the case, since the majority of puncta in a cell are yellow (which is due to a co-localisation of green and red puncta) and therefore indicate autophagolysosomes. If green GFP were quenched or degraded immediately upon fusion, autophagolysosomes would show up as red puncta and would be indistinguishable from red lysosomal puncta. This means that, contrary to received wisdom, green puncta in the absence of a lysosomal marker actually indicate either autophagosomes or autophagolysosomes so that the total green puncta count indicates the sum of autophagosomes and autophagolysosomes.

However, most of the scientific community still seems to accept that GFP-LC3 puncta are appropriate indicators of autophagosomes and base their conclusions on this surmisal (see, for example, [129, 146, 263]). The studies cited above and our own data suggest that this could potentially lead to misconceptions about the autophagy system during basal and diseased states, since both induced autophagy and impaired autophagosome/lysosome fusion would result in an increase in GFP-LC3 puncta. We therefore suggest that in future research the methodology should distinguish between autophagosomes, autophagolysosomes and lysosomes.

Since our data and the studies discussed above indicate that GFP is not immediately degraded after fusion, this opens the possibility of measuring the rate of

protein degradation within autophagolysosomes. Recent advancements in fluorescence microscopy and software allow for automated tracking of fluorescing puncta and measuring time-dependent changes in fluorescence intensities of individual puncta. Therefore, the decay in the GFP fluorescent signal of a punctum can in principle be used to determine the turnover rate of autophagosomal cargo after fusion with lysosomes. Free soluble GFP has been suggested as a marker for autophagosomal cargo, since it seems to be more stable within autophagolysosome [182]. Such studies could be complemented with morphometric analysis of autophagolysosomes throughout the degradation of the cargo; we observed that after fusion yellow puncta slowly changed colour to orange (due to the decrease in green GFP signal) and finally to red, completing degradation and the recycling to lysosomes—during the degradative process these puncta slowly became larger, and after completion of the degradative phase rapidly became small and red.

6.3 Quantifying autophagic flux

6.3.1 Determining the concentration of bafilomycin A_1 required for the inhibition of the autophagosome fusion with lysosome

A crucial part of the protocol to assess autophagic flux requires the complete inhibition of the autophagosomal and lysosomal fusion process. Previous autophagic studies [32, 158, 166, 182] have used concentrations ranging from 10 to 100 nM bafilomycin A_1. Typically, the effect of bafilomycin A_1 is assessed either by measuring LC3 Western blot band intensities or by counting the numbers of fluorescent puncta 6 hrs [182] or more (even up to several days [104]) after treatment with bafilomycin A_1. Our data, discussed below, show that a new steady state can already be established after 4 hrs (Fig. 4.10); this means that these studies actually measure the new steady-state autophagosomal pool size after inhibition of fusion. However, studies such as [182] suggest that bafilomycin A_1 concentrations lower than 100 nM probably result in only partial inhibition of autophagosome

and lysosome fusion (see Fig. 6.1B).

We approached the determination of the concentration of bafilomycin A_1 that causes complete inhibition of fusion differently by measuring the initial rate of increase in autophagosomes in a single cell after treatment with different bafilomycin A_1 concentrations (Fig. 6.1A). Our preliminary experiments suggested that 400 nM bafilomycin A_1 would completely block fusion (Fig. 4.2) and we used this concentration in all experiments in this study. Later in our study we repeated these experiments with our improved methodology and found no difference between the effects of 100, 200, 400 and 800 nM bafilomycin A_1, which suggests that 100 nM is enough to completely block fusion. In future studies we will reduce the bafilomycin A_1 concentration to either 100 (or, to be safe, 200 nM). These conclusions are further substantiated by the study of Yoshimori *et al.* [274] who found that 100 nM bafilomycin A_1 treatment of A431 cells resulted in significant de-acidification after 30 min, and complete de-acidification after 60 min. Similarly, Choi *et al.* [32] reported that 200 nM bafilomycin A_1 was sufficient to completely de-acidify lysosomes in HeLa cells. The difference in these results indicate that each cell line may require a unique concentration of bafilomycin A_1 for the complete inhibition of fusion.

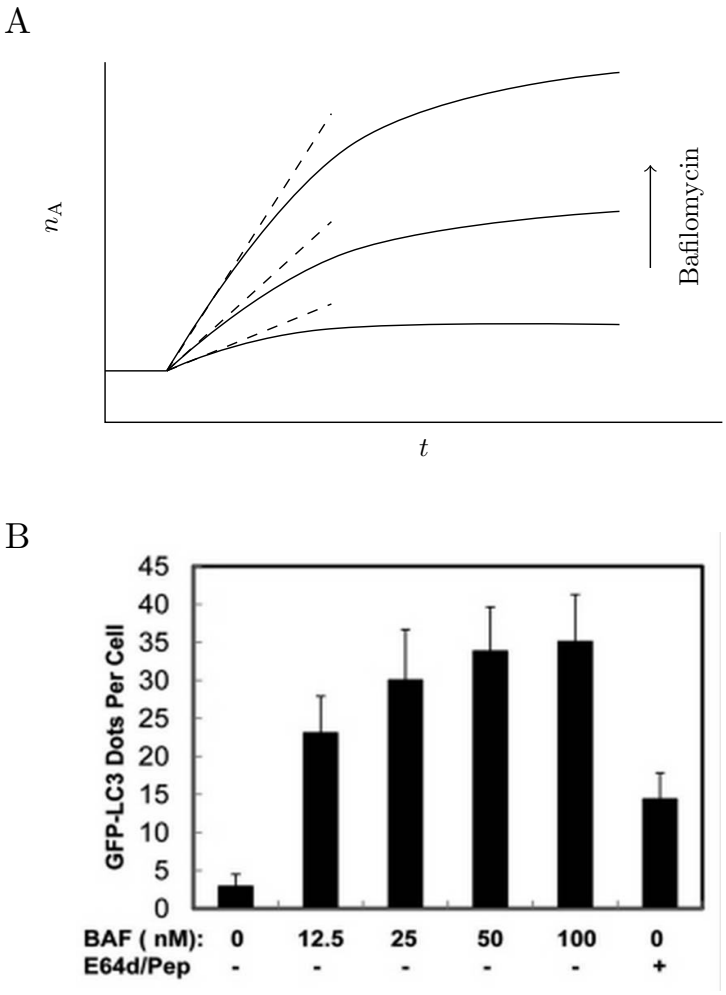

Figure 6.1: Methods for evaluating inhibition of fusion of autophagosomes and lysosomes by bafilomycin A_1. (A) Measuring the initial rate of increase of autophagosomes after treatment with different bafilomycin A_1 concentrations. (B) Measuring the increase in GFP-LC3 puncta 6 hrs after treatment with different bafilomycin A_1 concentrations [182].

.

6.3.2 Quantification of flux

Using our newly-developed fluorescence microscopy technique, we were able to numerically quantify both basal and rapamycin-induced autophagic flux, something which up to now has not been possible. The success of our method was due to our being able to distinguish between and measure the total pool sizes of autophagosomes, autophagolysosomes and lysosomes over time. This allowed us to characterise the autophagic steady state under basal and induced conditions, and also measure the changes in pool size of the three autophagic vesicles after the fusion between autophagosomes and lysosomes was inhibited. From these data we were able to quantitatively calculate the basal autophagic flux as 25.4 autophagosomes/hour/cell and the rapamycin-induced autophagic flux as 105.4 autophagosomes/hour/cell, which represented a four-fold increase.

Despite the clear utility of our new method, it does have shortcomings. Bafilomycin acts by inhibiting the membrane-bound V-ATPase, a proton-pump, which leads to the de-acidification of the lumen of vesicles, such as lysosomes, that contain this transporter. This means that in our system addition of bafilomycin A_1 de-acidifies both lysosomes and autophagolysosomes. In turn, de-acidification of lysosomes prevents their fusion with autophagosomes. The problem with using bafilomycin A_1 is that this de-acidification of lysosomes and autophagolysosomes results in the depletion of the red pH-dependent Lysotracker fluorescent dye, which changes the colour of autophagolysosomes from yellow to green, so leading to the false identification of autophagosomes, especially at later time periods following bafilomycin A_1 treatment. It would therefore be advisable to avoid pH-dependent fluorescent dyes, and to rather use fluorescently-tagged lysosomal proteins such as lysosome-associated membrane protein 2 (LAMP2). In an attempt to overcome this limitation of live-cell imaging, we generated a cell line that stably expressed RFP-LAMP2 (red) and GFP-LC3 (green), but due to high background noise and time constraints we abandoned this line of experimentation, and continued to use fluorescent dyes. In future work we plan to improve the cell line that expresses both RFP-LAMP2 and GFP-LC3. Alternatively, we may rather opt to fix cells at specific time points with acetone/methanol and quantify the autophagic intermedi-

ates using immunofluorescence, i.e., fluorescently-tagged antibodies that recognise proteins specific to autophagic vesicles. Fixing the cells would have an additional advantage, namely the avoidance of counting an autophagic vesicle twice: when acquiring multiple z-stack layer images of a cell, autophagic vesicles can potentially be counted twice, since they can move around in the cell during the acquisition time from on layer to the next.

Recent advances in FM have led to the development of novel techniques that have been employed to assess autophagic activity. One of the most accurate ways of indirectly assessing autophagic degradation is based on monitoring the decay of cytosolic proteins [116, 249]. These methods use cytosolic photo-activatable fluorescent proteins, that, once activated, can be used to measure the rate of decay of the fluorescence signal in the cytoplasm, which gives an indication of the rate of protein degradation in general [249]. From this the transition time, τ, can be calculated, which in this context is the time required for the complete turnover of the cytosolic protein pool, or more accurately, of the fluorescent protein pool. If the sole path of protein degradation is via autophagy, then the rate of protein degradation measured by this method could be regarded as an indication of autophagic flux. However, this method provides no data on the detailed dynamics of autophagy, such as the change over time in pool sizes of the autophagic vesicles. Consider the following two examples where this deficiency is pertinent. First, impaired autophagosome/lysosome fusion, such as can occur in a disease state, would result in an increase in autophagosomes and lysosomes, while the basal autophagic flux in the normal and diseased states as reported by photoswitchable proteins would be the same. As we have shown, this is due to the flux being determined by the rate of autophagosome synthesis and not to the rate of fusion. Photoswitchable protein decay would not be able to distinguish the diseased from the normal state. Second, during periods of autophagy arrest, protein degradation can be shifted towards selective protein degradation pathways, such chaperone-mediated autophagy [121, 180]. Therefore, although macro-autophagic flux may have decreased, the rate of fluorescent decay may remain the same, so that measuring fluorescent decay would not shed light on the impairment in the autophagic

system. In principle, given the cytosolic protein concentration and because our data allow the calculation of the cytoplasmic volume consumption rate, we should also be able to determine cytosolic protein turnover.

6.4 Morphometric analyses

In accordance with our findings, a number of groups have reported an increase in the vacuolar count observed by EM following induction of autophagy [51, 54, 145, 161, 186]. Various groups have also reported that, following an increase in the synthesis of autophagosomes, there was also an increase in the volume of autophagosomes and autophagolysosomes [54, 161, 273]. They made use of automated 3D Correlative Light and Electron Microscopy (CLEM) that made 3D rendering of autophagosomes and autophagolysosomes possible [54, 273]. In our study we also observed an increase in vacuolar volume, but we were not able to distinguished between autophagosomes and autophagolysosomes.

Although changes in the size of autophagic vesicles are usually based on EM, not on FM, we consider live cell FM images to be more accurate in representing the size of autophagosomes and autophagolysosomes compared to EM. By using FM we were able to distinguish between autophagosomes and autophagolysosomes and to assess their respective morphological characteristics. Images obtained by other groups that distinguished autophagosomes and autophagolysosomes show trends similar to those in our images [20, 36, 255, 265].

Groups that only assessed GFP-LC3 puncta (which do not distinguish between autophagic vesicles), found an increase in GFP-LC3 puncta size when the autophagic system was induced [129, 146, 263]. In contrast, our data showed the autophagosomal and autophagolysosomal volumes to remain constant (Figs. 4.15C and 4.15D). However, while the autophagolysosomal volume remained constant, the autophagolysosome pool size increased (Fig. 4.10). This explains the seeming increase in volume observed in GFP-LC3 puncta in the above-mentioned studies.

Inaccuracies in the counting of vacuoles due to plane-sectioning affect the observed numbers [273]. Like several other groups [26, 102, 224], we also had difficul-

ties in positively identifying autophagosomes, autophagolysosomes, lysosomes and endosomes in our EM images, and could only confidently distinguish autophagic vacuolar structures from other membrane-bound organelles. However, there are groups that have successfully used EM to identify autophagosomes, autophagolysosomes and lysosomes in HeLa cells and hepatocytes [53, 54, 186, 273]. Techniques such as CLEM and Immunogold staining (IGS) have recently been used to improve the identification of autophagosomes, autophagolysosomes and lysosomes in EM images. IGS is an EM staining technique that uses gold-labelled antibodies to mark proteins of interest, but it still relies on the sectioning of EM samples and therefore the analysis of a single plane. CLEM combines the advantages of both fluorescence microscopy and EM, allowing the identification of cellular structures using fluorescence probes in EM images and exploiting the high resolution of EM. The automated 3D-CLEM interface makes possible the 3D rendering of autophagosomes [54, 273], allowing for detailed morphometric analysis. In principle precise quantification of the total pool sizes of autophagosomes, autophagolysosomes and lysosomes should also be possible with this technique, but it remains to be done.

6.5 Western blotting

Western blot analysis forms part of the standard protocol used today to assess autophagic activity [167]. It is used to assess autophagy related proteins, particularly LC3 and p62. LC3 is one of the structural components of the autophagosomal membrane, and is involved in the development of the sequestering vesicle as well as the facilitation of cargo recognition via p62. p62 is involved in the formation of autophagosomes by linking proteins to be degraded with LC3; it is therefore regarded as a marker of autophagosomal cargo. Traditionally, Western blotting of LC3-II has been a particularly attractive means of assessing autophagic activity. The amount of LC3-II generally corresponds to the number of autophagosomes, or, more accurately, to the total autophagosomal membrane [98].

6.5.1 pmTOR and mTOR

Since it is involved in the signal transduction cascade that induces autophagy, the ratio pmTOR/mTOR, where pmTOR is the phosphorylated state of mTOR, is commonly used in the autophagy research field to indicate the level of induction of autophagy. The lower this ratio, the higher the level of induction.

Our Western blots revealed that pmTOR decreases upon treatment with rapamycin compared to basal conditions (Fig. 4.16A) and led to an increased autophagic flux as assessed by fluorescence microscopy (Fig. 4.10, summarised in Table 4.2). The inverse correlation between the pmTOR level and autophagic activity has been shown by various research groups [32, 35, 109, 179, 208, 208, 277]. In addition, other research groups have shown that autophagy can also be induced independently of the mTOR pathway [140, 219, 262].

Generally, a single measurement of pmTOR is made 1 hr [32] to several days [208] after induction [32, 35, 109, 179, 208, 208, 277]. We measured pmTOR 30 min and 4 hrs after induction by rapamycin, and since there was no significant difference between these measurements, were able to conclude that the decrease in pmTOR occurs within 30 min or shorter.

6.5.2 LC3

In accordance with published studies [32, 36, 46, 80, 166, 213], we observed an increase in LC3-II in the wild type MEF cells following bafilomycin A_1 treatment (Fig. 4.16C). However, several research groups have reported the converse [11, 208], similar to what we observed in the transgenic GFP-LC3 MEF cell line (Fig. 4.16B). In accordance with our data, the rate of LC3-II accumulation after inhibition of fusion by bafilomycin A_1 was greater for the rapamycin-induced autophagic state as compared to the basal state [14, 36, 104, 158, 167]. In contrast to these groups, who measured LC3-II 1 hr [14] to several days [104] after induction, we measured LC3-II 30 min after inhibition of fusion, which allowed us to make a more accurate assessment of autophagic flux compared to measuring of LC3-II after 2 hours inhibition. Furthermore, we found an increase in LC3-II 30 min after rapamycin

treatment, which then returned to basal levels. This dynamic response, which has not been seen before, corresponds to our FM results (Fig. 4.10).

LC3-II blots of GFP-LC3 MEF cells showed a decrease in LC3-II 30 min after bafilomycin A_1 treatment (Fig. 4.16B), but by 2 hrs after bafilomycin A_1 treatment LC3-II had increased relative to the control. In our studies with wild-type MEF cells and in other studies with endogenous LC3-II blots in the GFP-LC3 cell line [129, 146, 182, 255], this initial decrease in LC3-II levels after inhibition of fusion was not observed and was therefore unexpected. Even more unexpected was the decrease in LC3-II levels in blots of GFP-LC3 MEF cells at both 30 min at 4 hrs after rapamycin treatment.

However, after induction of autophagy in GFP-LC3 MEF cells the decreased LC3-II signal did increase as expected after bafilomycin A_1 treatment, showing that the autophagic flux had increased from its basal level, but not as much as was observed in Western blots of wild-type MEF cells (Fig. 4.16C) and in FM studies of GFP-LC3 MEF cells (Fig. 4.10). That previous studies did not observe these decreases in LC3-II could be due to the measurement of LC3-II levels six hours or longer after treatment with autophagy inducers or inhibitors, during which time autophagosomes, and hence endogenous LC3-II levels, could have increased back to or higher than basal levels.

It is generally accepted that blotting for endogenous LC3-II in GFP-LC3 cells allows the estimation of the magnitude of autophagic flux. However, our blots of endogenous LC3-II in GFP-LC3 cells showed that the band intensities do not accurately reflect the number of autophagosomes obtained with fluorescence microscopy. In using Western blots it is therefore advisable to follow the example of groups such as Morselli *et al.* [171] that measure GFP-LC3 I and II rather than endogenous LC3. We tried to blot for GFP-LC3 with an anti-GFP antibody, but, similar to other colleagues in the field [161], we were unable to resolve GFP-LC3 I and II.

A possible explanation for the initial decrease in LC3-II levels in GFP-LC3 MEF cells following either bafilomycin A_1 or rapamycin treatment (Fig. 4.16B) could be a preferential incorporation of GFP-LC3 instead of endogenous LC3. In

both cases the number of autophagosomes would be expected to increase: after 30 minutes of bafilomycin A_1 treatment the decline in amino acid levels could activate autophagosome synthesis through feedback onto the mTOR system, while 30 min after rapamycin treatment the increased flux would be accompanied by an increase in the number of autophagosomes. If GFP LC3-II is preferentially incorporated into autophagosomal membranes at the expense of endogenous LC3 this would explain both the observed decrease in endogenous LC3-II discussed above and the observed increased GFP LC3-II fluorescent signal.

This speculation is further substantiated by the decrease observed by FM in endogenous LC3-II 4 hrs after induction even though autophagosomal numbers return to just above basal levels (Figs. 4.10 and 4.13). Directly after administrating bafilomycin A_1, the residual rate of fusion that remains prior to achieving complete inhibition may keep on preferentially consuming already existing autophagosomes that are located closer to lysosomes in the paranuclear region. The observed decrease in LC3-II may therefore be associated with the newly synthesised "induced form of autophagosomes" since they may displace autophagosomes that existed before inhibition of fusion. In future a potential preferential incorporation of GFP-LC3-II into autophagosomal membranes could be evaluated by assessing the ratio LC3-II to GFP-LC3-II.

Currently, Western blot analysis of LC3-II forms part of the standard protocol to assess autophagic flux [36, 158, 161, 167], but it can only provide information about whether or not autophagic flux has increased or decreased. For potential clinical approaches this is a drawback: in order to determine whether and by how much autophagic flux needs to be altered one would need to have a quantitative measure for the basal autophagic flux in the tissues or cells under investigation, and Western blot analysis cannot provide this.

6.5.3 p62

Impairment of the fusion of autophagosomes and lysosomes leads to the accumulation of p62, which therefore is a useful marker for autophagic degradation. In our Western blots, at any experimental time point following inhibition of fusion

by bafilomycin A_1, the changes in the levels of p62 (Fig. 4.16D and E) and LC3-II (Fig. 4.16B and C) of both wild type and GFP-LC3 MEF cells were always correlated: both either increased or decreased together. Other groups have also reported this correlation between LC3-II and p62 levels when treating cells with bafilomycin A_1 [86, 235]. In contrast, treating cells with a drug such as Linifanib, which targets upstream signalling pathways and thereby leads to the induction of autophagosome synthesis and a concomitant increase in LC3-II, resulted in a decreased p62 after 24 hours treatment [169, 193, 256]. If bafilomycin A_1 was then added, p62 again increased with LC3-II as before [169].

In our experiments p62 only correlated with endogenous LC3-II and not with GFP-LC3. This may indicate steric hindrance of the binding between p62 and GFP-LC3-II because of the GFP tag. This could potentially affect the autophagic degradative capacity and consequently increase flux through a reduction in the level of amino acids in GFP-LC3 cells. If this hypothesis turns out to be correct, it would be advisable to determine autophagic flux in wild type cells by fixing them at key time points and performing LC3-II and LAMP2 immunofluorescence staining.

In summary, when the signalling pathways involved in the synthesis of autophagosomes are affected, both p62 and LC3-II levels are influenced, which in turn affects the degradative capacity of autophagy, since p62 is involved in cargo recognition. If these changes in p62 and LC3-II are independent, it would be possible for the regulation of p62 to modulate the degradative capacity independently of the autophagosomal number. However, this is still to be investigated.

6.6 Functional variables of autophagic flux

Although Western blot analysis provides a means of assessing autophagic activity, it only allows for the expression of autophagic activity relative to a basal level. Similarly, whereas EM provides high-resolution morphometric analysis of vacuolar structures at various stages of and conditions for autophagy, it cannot be used to assess autophagic flux accurately. With our new protocol we could quantity

basal as well as rapamycin-induced autophagic flux. Furthermore, we could also calculate functional variables of the autophagic system, such as transition times for the various pathway entities, as well as the flow of volume of cytoplasm through the autophagic pathway and the total membrane utilised per hour. These variables are new to the field of autophagy. Although there are techniques that can quantify the turnover rate of autophagic substrate, for instance through the measurement of decay of a fluorescent marker [116, 249], they do not measure autophagic flux in terms of the turnover in the autophagosomal pool.

The functional variables of the autophagic system described in this thesis could prove to be very useful in the comparison of different cell types and treatment interventions.

6.7 Amino acids

Amino acids are end-products of the autophagic degradation pathway; some are potent nutrient regulators of autophagy, inducing autophagy during periods of starvation. A great deal is known about the modulation of autophagy by the availability of amino acids [69, 100, 159, 172, 174, 183, 200, 270], implicating several key amino acids involved in feedback regulation of autophagy. Although the detailed mechanism is unknown, an increase in amino acid levels is accompanied by an increase in phosphorylated mTOR. Rapamycin mimics starvation induction of autophagy, thereby preventing the negative feedback of amino acids through a conformational change of mTOR that prevents its phosphorylation [197].

Individual amino acid levels. We found that glutamic acid was significantly increased after rapamycin treatment, whereas arginine was significantly decreased after bafilomycin A_1 treatment. Furthermore, aspartate and glutamate levels after 4 hours of rapamycin treatment were higher compared to other amino acids.

High levels of aspartate and glutamate have been reported to accompany high rates of protein degradation [143, 197, 204, 261]. Glutamate and aspartate act as carriers of the nitrogen waste products that are generated when amino acids

are processed by the citric acid cycle (TCA). During the initial breakdown of amino acids their α-amino group is transferred to α-ketoglutarate to yield glutamic acid. Glutamic acid acts as an intermediate in the α-amino disposal pathway by transferring the amino group to oxaloacetic acid to produce aspartic acid which acts as the penultimate carrier of the amino group before its incorporation into the urea cycle. The protein-nitrogen flux model created by Walsh and Wright showed that the flux of amino acids from proteins into the TCA cycle depends on the concentration of available amino acids [252]. Therefore it is likely that the high levels of aspartate and glutamate observed are the result of an increase in amino acids being fed into the TCA cycle and the concomitant build-up of nitrogen waste. These high levels of aspartate and glutamate have also been suggested by other groups to be the result of an increased rate of protein degradation [204], as well as the up-regulation of autophagy. This was observed in cancer cells, and it was suggested that these cells self-cannibalise through autophagy to produce glutamic acid and fatty acids, which can serve as energy sources [261].

Two hours after bafilomycin A_1 treatment of basal autophagy, there was an increase in glutamic acid similar to that observed in the rapamycin-treated cells. This may have been a result of a reverse in flow of TCA cycle intermediates to amino acids in order to compensate for the loss in the supply of amino acids. Glutamic acid plays a key role in the regeneration of non-essential amino acids [181]. Interestingly, our amino acid profiles (Fig. A) show that essential amino acids increased relative to non-essential amino acids. This may have been the result of up-regulation in the ubiquitin-proteasome system to compensate for the loss in supply of essential amino acids via autophagy [121, 180]. This could be assessed with kits such as the VIVAdetect 20S proteasome assay kit PLUS [211].

Increased glucogenic amino acids have been reported following the induction of autophagy [55, 192]. Our results support the notion that autophagy plays a key role in glucose homeostasis during periods of starvation by degrading proteins for gluconeogenesis, as mimicked by rapamycin treatment [122].

Total amino acid and protein levels. Autophagy is responsible for the sequestering of and the subsequent degradation and recycling of proteins. Our data showed that the induction of autophagy resulted in an increase in amino acids and a decrease in protein levels. Blocking autophagy by inhibiting fusion lead to a decrease in amino acids. These trends have also been reported by other groups [121, 204, 261]. Furthermore, other research groups have reported a decrease in protein synthesis upon induction of autophagy due to mTOR inactivation[136].

When Baf 30 min groups and Rapa Baf 30 min groups in Fig. 4.21 are compared, there was a greater decrease in amino acids in the rapamycin treated cells, which can also be interpreted as an increase in flux after rapamycin treatment. Although it is common procedure to measure the change in LC3-II after bafilomycin A_1 treatment, the concomitant changes in amino acids levels, as shown in our results, have not yet been previously measured.

Unexpectedly, we observed a decrease in protein levels after inhibition of the fusion between autophagosomes and lysosomes. In contrast, there is a report in the literature of the opposite observation, namely a decrease in protein degradation following partial inhibition of autophagy with 3-methyladenine [221]. Two possible reasons could account for our observation: first, within the first few minutes after inhibition of fusion autophagy is up-regulated to compensate for the decrease in amino acid supply, thereby leading to higher protein turnover; second, autophagy, the primary pathway responsible for protein degradation, occurs in parallel with chaperone-mediated autophagy, and during autophagy arrest, protein degradation can be shifted towards chaperone-mediated autophagy [121, 180]. Moreover, a combination of both of these responses may occur directly after inhibition that temporarily increases protein turn over.

6.8 Kinetic modelling of autophagy

There are a number of papers in the autophagy literature that describe computer models of aspects of autophagy. The most comprehensive of these are the models of the Choi group [70–73]. The network on which their minimal autophagy

model is based is the same as that in our simple model (Fig. 5.1A), but they also include protein synthesis from the amino acids released from autophagolysosomes and non-autophagic protein degradation. However, the aim of their model is to "[investigate the] hypothesis that autophagy mediates cellular phase transitions and demonstrate that the autophagic phase transitions are essential to the maintenance of normal cellular functions and critical in the fate of a cell, i.e., cell death or survival" [72]. Their model does not attempt to simulate experimentally obtained data such as that obtained in our studies, but rather to find a set of parameters that allow the bifurcations and oscillations required by their hypothesis.

Phagosym is available as a Java program [125] that simulates the creation of omegasomes and phagosomes in response to a stimulus. The paper does not explain the mathematics behind the model and only shows the results of the simulations, which purport to shows that autophagosomes are formed within omegasomes, which are membrane sites on the endoplasmic reticulum. They conclude that "having a transient precursor permits a bigger dynamic range of the autophagic response and allows a more efficient approach to steady state after autophagy stimulation".

While these studies are interesting in their own right, they were of peripheral interest to our own modelling efforts.

One aspect of our model that needs further comment is the necessity for having to use variable kinetic orders for autophagosomes and autophagolysosomes in the rate equations for fusion and for autophagolysosomal degradation to fit the simulated curve to the experimental data. This suggests that other factors are involved in these processes.

Various factors play a key role in autophagic degradation; one such factor is the transport of autophagosomes to the perinuclear region where they fuse with lysosomes to form autophagolysosomes—these transport processes are associated with microtubules [157], dynein motors [52] and a number of fusion proteins [268]. Microtubules are involved in the organization of intracellular structures and form an intracellular transport "road network", whereas dynein motors are responsible for the physical transport of vesicles such as autophagosomes along micro-tubules

[52]. Furthermore, the clearance of autophagolysosomes could be affected by factors such variation in protease activity.

In future developments of our kinetic model we plan to incorporate the details of these factors. This is important because they have been suggested to form part of the pathogenesis of neurodegenerative diseases [93, 111, 115, 157, 185, 205].

There are already methods available for the quantitative description of microtubule networks (FibrilTool) [19], *in vitro* motility assays of the microtubule motors, kinesin and dynein [144], as well as lysosomal protease degradation [182]. Such an expansion in our approach could greatly improve our understanding of the autophagy system and how to target the autophagic machinery for therapeutic purposes.

6.8.1 WatershedCounting3D analysis software

The segmentation and counting of organelles is mostly derived by using the global thresholding method [63]. Such methods rely on homogeneous background intensity values within a cell, which is not always the case. WatershedCounting3D, developed by Gniadek and Warren [63], makes use of a modified watershed algorithm to more accurately identify intracellular structures in an inhomogeneous background. The WatershedCounting3D algorithm has been implemented as a Java-based plug-in for ImageJ. Recently, we, in collaboration with Gniadek, expanded on the WatershedCounting3D allowing for high through-put processing power. The new through-put WatershedCounting3D allows for multiple images with respective image masks to be uploaded and analysed, generating a text output file. In conclusion, the combination of the high through-put WatershedCounting3D and Python/Java scripts to process generated text file can be used for the high through-put analysis and quantification, including statistical analysis of puncta in images.

6.9 Future work

The main aims of the work described in this thesis were to develop and perfect a technique for measuring autophagic flux and construct a kinetic model that fits the experimental data generated by our determination of autophagic flux under basal and induced conditions, i.e., a model that could simulate the steady state and time-dependent behaviour of the system. With this new method it is now possible to conduct an experimental supply-demand analysis [84, 85] of autophagy around the autophagosome pool. This would entail perturbing the system both upstream and downstream from the autophagosome pool. The first of these perturbations has already been done through the induction of autophagy by rapamycin. The downstream perturbation would require us to increase, or decrease, the rate of fusion between autophagosomes and lysosomes. We already have the tool for doing so in bafilomycin A_1, which in our flux determination is used to completely inhibit fusion. Here we would first have to change the demand of autophagosomes by partially inhibiting fusion using a low concentration of bafilomycin A_1, wait for a new steady state to be established, and then completely inhibiting fusion so as to measure the new steady-state autophagosomal pool size and steady-state flux.

Other future work will be to measure autophagic flux and autophagic variables in other cell types, both in healthy and diseased states. Such information could be very useful in both research and clinical settings, since it would provide insight into the dynamic behaviour of autophagy in different situations, which in turn could identify potential therapeutic targets and so assist the development of new therapeutic strategies. Our technique could be used to screen drugs and characterise their effects on autophagy.

Although the kinetic model that we developed was based on a simplification of the autophagic process, it still gave an excellent fit to our experimental data. Our model will serve as a starting point for further work: we plan to include other signalling pathways that regulate autophagy, the negative feedback effects of amino acids on the biogenesis of autophagosomes, and the degradative processes that occur in the lumen of the different autophagic vesicles, which will allow us to also simulate the substrate clearance flux. An important aspect of future work is

the validation of the kinetic model with experimental data obtained at autophagic states other than that used to parameterise our current model. Ultimately, we envisage the combination of data obtained from different cell types in healthy or diseased states into a unified kinetic model of autophagy.

Appendix A

Changes in amino acid levels during autophagy

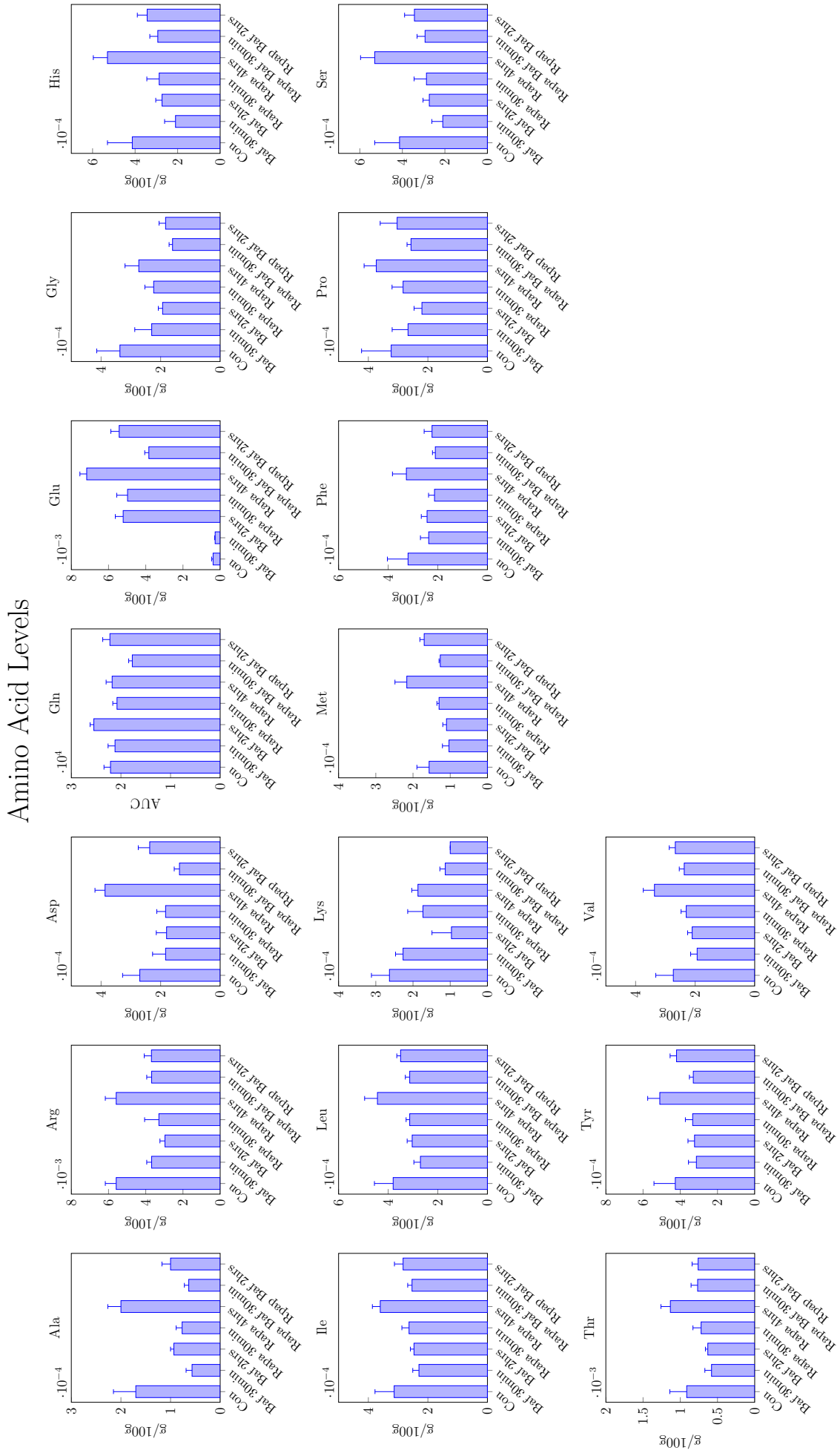

Appendix B

Control and elasticity coefficients

The coefficients of a control analysis of basal steady state of the extended autophagy model described by the PySCeS input file listed in Appendix C.2. *Only the coefficients with non-zero values are shown.*

B.1 Flux-control coefficients

Flux-control coefficients for the basal autophagic flux (J_{basal}), mTOR/pmTOR cycle (J_{mTOR}) and lysosomal flux (J_{lyso}):

Autophagic flux (J_{basal})

$$C_{v_1}^{J_{\text{basal}}} = 1.0$$
$$C_{v_6}^{J_{\text{basal}}} = 0.81$$
$$C_{v_7}^{J_{\text{basal}}} = -0.81$$

Lysosomal flux (J_{lyso})

$$C_{v_4}^{J_{\text{lyso}}} = 1.0$$
$$C_{v_5}^{J_{\text{lyso}}} = 0.0$$

mTOR/pmTOR cycle (J_{mTOR})

$$C_{v_6}^{J_{\text{mTOR}}} = 0.81$$
$$C_{v_7}^{J_{\text{mTOR}}} = 0.19$$

B.2 Concentration-control coefficients

Autophagosomes (A)

$$C_{v_1}^{A} = 0.20$$
$$C_{v_2}^{A} = -0.20$$
$$C_{v_4}^{A} = -0.20$$
$$C_{v_5}^{A} = 0.20$$
$$C_{v_6}^{A} = 0.16$$
$$C_{v_7}^{A} = -0.16$$

Autophagolysosomes (AL)

$$C_{v_1}^{AL} = 0.29$$
$$C_{v_3}^{AL} = -0.29$$
$$C_{v_6}^{AL} = 0.24$$
$$C_{v_7}^{AL} = -0.24$$

Lysosomes (L)

$$C_{v_4}^{L} = 1.0$$
$$C_{v_5}^{L} = -1.0$$

mTOR

$$C_{v_6}^{mTOR} = 0.81$$
$$C_{v_7}^{mTOR} = -0.81$$

pmTOR

$$C_{v_6}^{pmTOR} = -0.19$$
$$C_{v_7}^{pmTOR} = 0.19$$

B.3 Elasticity coefficients

Step 1

$$\varepsilon_{mTOR}^{v_1} = 1.0$$

Step 2

$$\varepsilon_{A}^{v_2} = 5.0$$
$$\varepsilon_{L}^{v_2} = 1.00$$

Stepo 3

$$\varepsilon_{AL}^{v_3} = 3.4$$

Appendix C

PySCeS-input files

C.1 Minimal model of autophagy

```
# Autophagy model

#           L
#           |
# P ---> A ---> AL ---> AA

# P: supply of autophagosomes
# A: autophagosomes
# L: lysosomes
# AL: autophagolysosomes

FIX: P L AA

R1: P = A
k1*P

R2: A + L = AL
k2*(A**h2)*L
```

```
R3: AL = AA
k3*AL**h3

#Init
P  = 1.0
AA = 0.0
L  = 1.0

#InitPar
h2 = 5.0
h3 = 3.4
k1 = 25.4
k2 = 25.4/(13.0**5.0)
k3 = 25.4/(165.0**3.4)

#InitVar
A  = 13.0
AL = 165.0

# Event 1 - Simulating Rapamycin Induction
Event: Induction, _TIME_ > 2, 0 {P = 105.4/25.4}
# Event 2 - Simulating Inhibiton with Bafilomycin
Event: Inhibition, _TIME_ > 6, 0 {k2 = 0.0}
```

C.2 Extended model of autophagy

```
# Extended autophagy model

#            LD <----  L <---- LB
#                 |        |
#       P  ---> A ---> AL ---> AA
#           ^
#        -> T  -
#       |       |
#        - pT <-

# P:  supply of autophagosomes which is controlled by T/pT
# A:  autophagosomes
# L:  lysosomes
# AL: autophagolysosomes
# AA: amino acids
# pT: phosphorylated mTOR
# T:  mTOR
# LD: lysosome degradation
# LB: lysosome biosynthesis

FIX: P AA LB LD

R1: P = A
k1*P*T

R2: A + L = AL
k2*L*A**h2

R3: AL = AA + L
k3*AL**h3

R4: LB = L
```

```
k4*LB

R5: L = LD
k5* L

R6: pT = T
k6*pT

R7: T = pT
k7*T

#Init
P  = 1.0
LB = 1.0
D  = 0.0
LD = 0.0
AA = 0.0

#InitPar
h2 = 5.0
h3 = 3.4
k1 = 25.4
k2 = 25.4/(13.0**5.0)
k3 = 25.4/(165.0**3.4)
k4 = 80.0
k5 = 80.0
k6 = 0.08*1.0
k7 = 0.08*(105.4/25.4)

#InitVar
A  = 13.0
AL = 165.0
L  = 1.0
```

```
pT = 105.4/25.4
T  = 1.0

# Event 1 - Simulating Rapamycin Induction
Event: Induction, _TIME_ > 2, 0 {k6 = 0.08*(105.4/25.4)*(105.4/25.4)}
# Event 2 - Simulating Inhibiton with Bafilomycin
Event: Inhibition, _TIME_ > 6, 0 {k2 = 0.0}
```

Bibliography

[1] Abedin, M. J., Wang, D., McDonnell, M. A., Lehmann, U. and Kelekar, A. [2007] "Autophagy delays apoptotic death in breast cancer cells following DNA damage." *Cell Death Differ.* **14**, 500–510.

[2] Ahlberg, J., Berkenstam, A., Henell, F. and Glaumann, H. [1985] "Degradation of short and long lived proteins in isolated rat liver lysosomes. Effects of pH, temperature, and proteolytic inhibitors." *J. Biol. Chem.* **260**, 5847–5854.

[3] Aita, V. M., Liang, X. H., Murty, V., Pincus, D. L., Yu, W., Cayanis, E., Kalachikov, S., Gilliam, T. C. and Levine, B. [1999] "Cloning and genomic organization of Beclin 1, a candidate tumor suppressor gene on chromosome 17q21." *Genomics* **59**, 59–65.

[4] Amaravadi, R. K., Yu, D., Lum, J. J., Bui, T., Christophorou, M. A., Evan, G. I., Thomas-Tikhonenko, A. and Thompson, C. B. [2007] "Autophagy inhibition enhances therapy-induced apoptosis in a Myc-induced model of lymphoma." *J. Clin. Invest.* **117**, 326.

[5] Arrasate, M., Mitra, S., Schweitzer, E. S., Segal, M. R. and Finkbeiner, S. [2004] "Inclusion body formation reduces levels of mutant huntingtin and the risk of neuronal death." *Nature* **431**, 805–810.

[6] Ashford, T. P. and Porter, K. R. [1962] "Cytoplasmic components in hepatic cell lysosomes." *J. Cell Biol.* **12**, 198–202.

[7] Atkinson, D. E. and Walton, G. M. [1967] "Adenosine triphosphate conservation in metabolic regulation rat liver citrate cleavage enzyme." *J. Biol. Chem.* **242**, 3239–3241.

[8] Atwal, R. S. and Truant, R. [2008] "A stress sensitive ER membrane-association domain in Huntingtin protein defines a potential role for Huntingtin in the regulation of autophagy." *Autophagy* **4**, 91–93.

[9] Axe, E. L., Walker, S. A., Manifava, M., Chandra, P., Roderick, H. L., Habermann, A., Griffiths, G. and Ktistakis, N. T. [2008] "Autophagosome formation from membrane compartments enriched in phosphatidylinositol 3-phosphate and dynamically connected to the endoplasmic reticulum." *J. Cell Biol.* **182**, 685–701.

[10] Azad, M. B., Chen, Y., Henson, E. S., Cizeau, J., McMillan-Ward, E., Israels, S. J. and Gibson, S. B. [2008] "Hypoxia induces autophagic cell death in apoptosis-competent cells through a mechanism involving BNIP3." *Autophagy* **4**, 195–204.

[11] Balgi, A. D., Fonseca, B. D., Donohue, E., Tsang, T., Lajoie, P., Proud, C. G., Nabi, I. R. and Roberge, M. [2009] "Screen for chemical modulators of autophagy reveals novel therapeutic inhibitors of mTORC1 signaling." *PLoS One* **4**, 7124.

[12] Beaulaton, J. and Lockshin, R. A. [1977] "Ultrastructural study of the normal degeneration of the intersegmental muscles of Antheraea polyphemus and Manduca sexta (Insecta, Lepidoptera) with particular reference to cellular autophagy." *J. Morphol.* **154**, 39–57.

[13] Behrends, C., Sowa, M. E., Gygi, S. P. and Harper, J. W. [2010] "Network organization of the human autophagy system." *Nature* **466**, 68–76.

[14] Bellot, G., Garcia-Medina, R., Gounon, P., Chiche, J., Roux, D., Pouysségur, J. and Mazure, N. M. [2009] "Hypoxia-induced autophagy is mediated through hypoxia-inducible factor induction of BNIP3 and BNIP3L via their BH3 domains." *Mol. Cell. Biol.* **29**, 2570–2581.

[15] Bergamini, E. [2005] "Targets for antiageing drugs." *Expert Opin. Ther. Targets* **9**, 77–82.

[16] Bjorkoy, G. [2005] "p62/SQSTM1 forms protein aggregates degraded by autophagy and has a protective effect on huntingtin-induced cell death." *J. Cell Biol.* **171**, 603–614.

[17] Bolender, R. P. and Weibel, E. R. [1973] "A morphometric study of the removal of phenobarbital-induced membranes from hepatocytes after cessation of treatment." *J. Cell Biol.* **56**, 746–761.

[18] Botti, J., Djavaheri-Mergny, M., Pilatte, Y. and Codogno, P. [2006] "Autophagy signaling and the cogwheels of cancer." *Autophagy* **2**, 67–73.

[19] Boudaoud, A., Burian, A., Borowska-Wykret, D., Uyttewaal, M., Wrzalik, R., Kwiatkowska, D. and Hamant, O. [2014] "Fibriltool, an ImageJ plug-in to quantify fibrillar structures in raw microscopy images." *Nature Protocols* **9**, 457–463.

[20] Burnett, J. W. and Calton, G. J. [1977] "The chemistry and toxicology of some venomous pelagic coelenterates." *Toxicon* **15**, 177–196.

[21] Carew, J. S., Nawrocki, S. T., Kahue, C. N., Zhang, H., Yang, C., Chung, L., Houghton, J. A., Huang, P., Giles, F. J. and Cleveland, J. L. [2007] "Targeting autophagy augments the anticancer activity of the histone deacetylase inhibitor SAHA to overcome Bcr-Abl–mediated drug resistance." *Blood* **110**, 313–322.

[22] Chalkiadaki, A. and Guarente, L. [2012] "Sirtuins mediate mammalian metabolic responses to nutrient availability." *Nature Reviews Endocrinology* **8**, 287–296.

[23] Chan, E. Y., Longatti, A., McKnight, N. C. and Tooze, S. A. [2009] "Kinase-inactivated ULK proteins inhibit autophagy via their conserved C-terminal domains using an Atg13-independent mechanism." *Mol. Cell. Biol.* **29**, 157–171.

[24] Chang, Y.-Y. and Neufeld, T. P. [2009] "An Atg1/Atg13 complex with multiple roles in TOR-mediated autophagy regulation." *Mol. Biol. Cell* **20**, 2004–2014.

[25] Chen, J.-L., Lin, H. H., Kim, K.-J., Lin, A., Forman, H. J. and Ann, D. K. [2008] "Novel roles for protein kinase Cδ-dependent signaling pathways in acute hypoxic stress-induced autophagy." *J. Biol. Chem.* **283**, 34432–34444.

[26] Chen, S., Zhou, L., Zhang, Y., Leng, Y., Pei, X.-Y., Lin, H., Jones, R., Orlowski, R. Z., Dai, Y. and Grant, S. [2014] "Targeting SQSTM1/p62 induces cargo loading failure and converts autophagy to apoptosis via NBK/Bik." *Mol. Cell. Biol.* **34**, 3435–3449.

[27] Chen, Y., McMillan-Ward, E., Kong, J., Israels, S. J. and Gibson, S. B. [2007] "Oxidative stress induces autophagic cell death independent of apoptosis in transformed and cancer cells." *Cell Death Differ.* **15**, 171–182.

[28] Cheong, H., Lindsten, T., Wu, J., Lu, C. and Thompson, C. B. [2011] "Ammonia-induced autophagy is independent of ULK1/ULK2 kinases." *Proc. Natl. Acad. Sci. U.S.A.* **108**, 11121–11126.

[29] Cheong, H., Nair, U., Geng, J. and Klionsky, D. J. [2008] "The Atg1 kinase complex is involved in the regulation of protein recruitment to initiate sequestering vesicle formation for nonspecific autophagy in Saccharomyces cerevisiae." *Mol. Biol. Cell* **19**, 668–681.

[30] Chin, R. M., Fu, X., Pai, M. Y., Vergnes, L., Hwang, H., Deng, G., Diep, S., Lomenick, B., Meli, V. S., Monsalve, G. C., Hu, E., Whelan, S. A., Wang, J. X., Jung, G., Solis, G. M., Fazlollahi, F., Kaweeteerawat, C., Quach, A., Nili, M., Krall, A. S., Godwin, H. A., Chang, H. R., Faull, K. F., Guo, F., Jiang, M., Trauger, S. A., Saghatelian, A., Braas, D., Christofk, H. R., Clarke, C. F., Teitell, M. A., Petrascheck, M., Reue, K., Jung, M. E., Frand, A. R. and Huang, J. [2014] "The metabolite α-ketoglutarate extends lifespan by inhibiting ATP synthase and TOR." *Nature* **510**, 397–401.

[31] Choi, A. M., Ryter, S. W. and Levine, B. [2013] "Autophagy in human health and disease." *N. Engl. J. Med.* **368**, 651–662.

[32] Choi, Y. J., Park, Y. J., Park, J. Y., Jeong, H. O., Kim, D. H., Ha, Y. M., Kim, J. M., Song, Y. M., Heo, H.-S., Yu, B. P., Chun, P., Moon, H. R. and Chung, H. Y. [2012] "Inhibitory effect of mTOR activator MHY1485 on autophagy: Suppression of lysosomal fusion." *PLoS ONE* **7**, 43418.

[33] Ciechomska, I., Goemans, G., Skepper, J. and Tolkovsky, A. [2009] "Bcl-2 complexed with Beclin-1 maintains full anti-apoptotic function." *Oncogene* **28**, 2128–2141.

[34] Clark, S. L. [1957] "Cellular differentiation in the kidneys of newborn mice studied with the electron microscope." *J. Biophys. Biochem. Cytol.* **3**, 349–362.

[35] Cohen, A. and Hall, M. N. [2009] "An amino acid shuffle activates mTORC1." *Cell* **136**, 399–400.

[36] Criollo, A., Niso-Santano, M., Malik, S. A., Michaud, M., Morselli, E., Mariño, G., Lachkar, S., Arkhipenko, A. V., Harper, F., Pierron, G., Rain, J.-C., Ninomiya-Tsuji, J., Fuentes, J. M., Lavandero, S., Galluzzi, L., Maiuri, M. C. and Kroemer, G. [2011] "Inhibition of autophagy by TAB2 and TAB3.." *EMBO J.* **30**, 4908–4920.

[37] Cuervo, A. M., Bergamini, E., Brunk, U. T., Dröge, W., Ffrench, M. and Terman, A. [2005] "Autophagy and aging: the importance of maintaining "clean" cells." *Autophagy* **1**, 131–140.

[38] Cuervo, A. M., Stefanis, L., Fredenburg, R., Lansbury, P. T. and Sulzer, D. [2004] "Impaired degradation of mutant α-synuclein by chaperone-mediated autophagy." *Science* **305**, 1292–1295.

[39] de Duve, C. and Wattiaux, R. [1966] "Functions of lysosomes." *Annu. Rev. Physiol.* **28**, 435–492.

[40] Del Roso, A., Vittorini, S., Cavallini, G., Donati, A., Gori, Z., Masini, M., Pollera, M. and Bergamini, E. [2003] "Ageing-related changes in the in vivo function of rat liver macroautophagy and proteolysis." *Exp. Gerontol.* **38**, 519–527.

[41] Deter, R. L., Baudhuin, P. and De Duve, C. [1967] "Participation of lysosomes in cellular autophagy induced in rat liver by glucagon." *J. Cell Biol.* **35**, 11–16.

[42] Devasagayam, T., Tilak, J., Boloor, K., Sane, K. S., Ghaskadbi, S. S. and Lele, R. [2004] "Free radicals and antioxidants in human health: current status and future prospects." *Japi* **52**, 794–804.

[43] Durán, R., MacKenzie, E., Boulahbel, H., Frezza, C., Heiserich, L., Tardito, S., Bussolati, O., Rocha, S., Hall, M. and Gottlieb, E. [2013] "HIF-independent role of prolyl hydroxylases in the cellular response to amino acids." *Oncogene* **32**, 4549–4556.

[44] Durán, R. V., Oppliger, W., Robitaille, A. M., Heiserich, L., Skendaj, R., Gottlieb, E. and Hall, M. N. [2012] "Glutaminolysis activates Rag-mTORC1 signaling." *Mol. Cell.* **47**, 349–358.

[45] Efeyan, A., Zoncu, R., Chang, S., Gumper, I., Snitkin, H., Wolfson, R. L., Kirak, O., Sabatini, D. D. and Sabatini, D. M. [2013] "Regulation of mTORC1 by the Rag GTPases is necessary for neonatal autophagy and survival." *Nature* **493**, 679–683.

[46] Eisenberg, T., Knauer, H., Schauer, A., Büttner, S., Ruckenstuhl, C., Carmona-Gutierrez, D., Ring, J., Schroeder, S., Magnes, C., Antonacci, L., Fussi, H., Deszcz, L., Hartl, R., Schraml, E., Criollo, A., Megalou, E., Weiskopf, D., Laun, P., Heeren, G., Breitenbach, M., Grubeck-Loebenstein, B., Herker, E., Fahrenkrog, B., Fröhlich, K.-U., Sinner, F., Tavernarakis, N., Minois, N., Kroemer, G. and Madeo, F. [2009] "Induction of autophagy by spermidine promotes longevity." *Nat. Cell. Biol.* **11**, 1305–1314.

[47] Eisenberg, T., Schroeder, S., Andryushkova, A., Pendl, T., Küttner, V., Bhukel, A., Mariño, G., Pietrocola, Eisenberg, T., Schroeder, S., Andryushkova, A., Pendl, T., K uttner, V., Bhukel, A., Mariño, G., Pietrocola, F., Harger, A., Zimmermann, A., Moustafa, T., Sprenger, A., Jany, E., B uttner, S., Carmona-Gutierrez, D., Ruckenstuhl, C., Ring, J., Reichelt, W., Schimmel, K., Leeb, T., Moser, C., Schatz, S., Kamolz, L., Magnes, C., Sinner, F., Sedej, S., Fr ohlich, K. U., Juhasz, G., Pieber, T. R., Dengjel, J., Sigrist, S. J., Kroemer, G. and Madeo, F. [2014] "Nucleocytosolic depletion of the energy metabolite acetyl-coenzyme a stimulates autophagy and prolongs lifespan" *Cell Metab.* **19**, 431–444.

[48] Eng, C. H., Yu, K., Lucas, J., White, E. and Abraham, R. T. [2010] "Ammonia derived from glutaminolysis is a diffusible regulator of autophagy." *Science Signaling* **3**, 31.

[49] Engelender, S. [2008] "Ubiquitination of α-synuclein and autophagy in Parkinson's disease." *Autophagy* **4**, 372–374.

[50] Epple, U. D., Suriapranata, I., Eskelinen, E.-L. and Thumm, M. [2001] "Aut5/Cvt17p, a putative lipase essential for disintegration of autophagic bodies inside the vacuole." *J. Bacteriol.* **183**, 5942–5955.

[51] Ericsson, J. L. E. . [1969] "Studies on induced cellular autophagy: Electron microscopy of cells with in vivo labelled lysosomes." *Exp. Cell Res.* **55**, 95–106.

[52] Eschbach, J. and Dupuis, L. [2011] "Cytoplasmic dynein in neurodegeneration." *Pharmacol. Ther.* **130**, 348–363.

[53] Eskelinen, E.-L. [2008] "To be or not to be? examples of incorrect identification of autophagic compartments in conventional transmission electron microscopy of mammalian cells." *Autophagy* **4**, 257–260.

[54] Eskelinen, E.-L., Reggiori, F., Baba, M., Kovács, A. L. and Seglen, P. O. [2011] "Seeing is believing: The impact of electron microscopy on autophagy research." *Autophagy* **7**, 935–956.

[55] Ezaki, J., Matsumoto, N., Takeda-Ezaki, M., Komatsu, M., Takahashi, K., Hiraoka, Y., Taka, H., Fujimura, T., Takehana, K., Yoshida, M., Iwata, J., Tanida, I., Furuya, N., Zheng, D. M., Tada, N., Tanaka, K., Kominami, E. and Ueno, T. [2011] "Liver autophagy contributes to the maintenance of blood glucose and amino acid levels." *Autophagy* **7**, 727–736.

[56] Galluzzi, L., Bravo-San Pedro, J. M., Vitale, I., Aaronson, S. A., Abrams, J. M., Adam, D., Alnemri, E. S., Altucci, L., Andrews, D., Annicchiarico-Petruzzelli, M. and others. [2015] "Essential versus accessory aspects of cell death: recommendations of the NCCD 2015." *Cell Death Differ.* **22**, 58–73.

[57] Galluzzi, L., Pietrocola, F., Levine, B. and Kroemer, G. [2014] "Metabolic control of autophagy." *Cell* **159**, 1263–1276.

[58] Gao, X., Zacharek, A., Salkowski, A., Grignon, D. J., Sakr, W., Porter, A. T. and Honn, K. V. [1995] "Loss of heterozygosity of the BRCA1 and other loci on chromosome 17q in human prostate cancer." *Cancer Res.* **55**, 1002–1005.

[59] Geng, J. and Klionsky, D. J. [2008] "The Atg8 and Atg12 ubiquitin-like conjugation systems in macroautophagy." *EMBO Rep.* **9**, 859–864.

[60] Giatromanolaki, A., Koukourakis, M. I., Koutsopoulos, A., Chloropoulou, P., Liberis, V. and Sivridis, E. [2011] "High Beclin 1 expression defines a poor prognosis in endometrial adenocarcinomas." *Gynecol. Oncol.* **123**, 147–151.

[61] Gibson, B. A. and Kraus, W. L. [2012] "New insights into the molecular and cellular functions of poly (ADP-ribose) and PARPs." *Nat. Rev. Mol. Cell. Biol.* **13**, 411–424.

[62] Gil, J. M. and Rego, A. C. [2008] "Mechanisms of neurodegeneration in Huntington's disease." *Eur. J. Neurosci.* **27**, 2803–2820.

[63] Gniadek, T. J. and Warren, G. [2007] "WatershedCounting3D: A new method for segmenting and counting punctate structures from confocal image data." *Traffic* **8**, 339–346.

[64] Gordon, P. B. and Seglen, P. O. [1988] "Prelysosomal convergence of autophagic and endocytic pathways." *Biochem. Biophys. Res. Commun.* **151**, 40–47.

[65] Guo, J. Y., Xia, B. and White, E. [2013] "Autophagy-mediated tumor promotion." *Cell* **155**, 1216–1219.

[66] Gwinn, D. M., Shackelford, D. B., Egan, D. F., Mihaylova, M. M., Mery, A., Vasquez, D. S., Turk, B. E. and Shaw, R. J. [2008] "AMPK phosphorylation of raptor mediates a metabolic checkpoint." *Mol. Cell.* **30**, 214–226.

[67] Hailey, D. W., Rambold, A. S., Satpute-Krishnan, P., Mitra, K., Sougrat, R., Kim, P. K. and Lippincott-Schwartz, J. [2010] "Mitochondria supply membranes for autophagosome biogenesis during starvation." *Cell* **141**, 656–667.

[68] Han, D., Williams, E. and Cadenas, E. [2001] "Mitochondrial respiratory chain-dependent generation of superoxide anion and its release into the intermembrane space." *Biochem. J.* **353**, 411–416.

[69] Han, J. M., Jeong, S. J., Park, M. C., Kim, G., Kwon, N. H., Kim, H. K., Ha, S. H., Ryu, S. H. and Kim, S. [2012] "Leucyl-tRNA synthetase is an intracellular leucine sensor for the mTORC1-signaling pathway." *Cell* **149**, 410–424.

[70] Han, K., Kim, J. and Choi, M. [2014] "Computer simulations unveil the dynamics of autophagy and its implications for the cellular quality control" *J. Biol. Syst.* **22**, 659–675.

[71] Han, K., Kim, J. and Choi, M. [2014] "Quantitative indices of autophagy activity from minimal models" *Theoretical Biology and Medical Modelling* **11**, 31.

[72] Han, K., Kim, J. and Choi, M. [2015] "Autophagy mediates phase transitions from cell death to life" *Heliyon* **1**, e00027.

[73] Han, K., Kwon, H. W., Kang, H., Kim, J., Lee, M.-S. and Choi, M. [2012] "Dynamics of macroautophagy: Modeling and oscillatory behavior" *Physica A* **391**, 686–692.

[74] Hanada, T., Noda, N. N., Satomi, Y., Ichimura, Y., Fujioka, Y., Takao, T., Inagaki, F. and Ohsumi, Y. [2007] "The Atg12-Atg5 conjugate has a novel E3-like activity for protein lipidation in autophagy." *J. Biol. Chem.* **282**, 37298–37302.

[75] Hara, T., Nakamura, K., Matsui, M., Yamamoto, A., Nakahara, Y., Suzuki-Migishima, R., Yokoyama, M., Mishima, K., Saito, I. and Okano, H. [2006] "Suppression of basal autophagy in neural cells causes neurodegenerative disease in mice." *Nature* **441**, 885–889.

[76] Hara, T., Takamura, A., Kishi, C., Iemura, S.-i., Natsume, T., Guan, J.-L. and Mizushima, N. [2008] "FIP200, a ULK-interacting protein, is required for autophagosome formation in mammalian cells." *J. Cell Biol.* **181**, 497–510.

[77] Harder, L. M., Bunkenborg, J. and Andersen, J. S. [2014] "Inducing autophagy: a comparative phosphoproteomic study of the cellular response to ammonia and rapamycin." *Autophagy* **10**, 339–355.

[78] Hardie, D. G., Ross, F. A. and Hawley, S. A. [2012] "AMPK: a nutrient and energy sensor that maintains energy homeostasis." *Nat. Rev. Mol. Cell. Biol.* **13**, 251–262.

[79] Harding, T. M., Morano, K. A., Scott, S. V. and Klionsky, D. J. [1995] "Isolation and characterization of yeast mutants in the cytoplasm to vacuole protein targeting pathway." *J. Cell Biol.* **131**, 591–602.

[80] Hawkins, A., Guttentag, S. H., Deterding, R., Funkhouser, W. K., Goralski, J. L., Chatterjee, S., Mulugeta, S. and Beers, M. F. [2014] "A non-BRICHOS SFTPC mutant (SP-CI73T) linked to interstitial lung disease promotes a late block in macroautophagy disrupting cellular proteostasis and mitophagy." *Am. J. Physiol.* **308**, 33–47.

[81] He, C., Baba, M., Cao, Y. and Klionsky, D. J. [2008] "Self-interaction is critical for Atg9 transport and function at the phagophore assembly site during autophagy." *Mol. Biol. Cell* **19**, 5506–5516.

[82] He, C. and Klionsky, D. J. [2009] "Regulation mechanisms and signaling pathways of autophagy." *Annu. Rev. Genet.* **43**, 67–93.

[83] Heilbronn, L. K. and Ravussin, E. [2003] "Calorie restriction and aging: review of the literature and implications for studies in humans." *Am. J. Clin. Nutr.* **78**, 361–369.

[84] Hofmeyr, J.-H. S. and Cornish-Bowden., A. [2000] "Regulating the cellular economy of supply and demand." *FEBS Lett.* **476**, 47–51.

[85] Hofmeyr, J.-H. S. and Rohwer, J. M. [2011] "Supply-demand analysis: A framework for exploring the regulatory design of metabolism" *Methods Enzymol.* **500**, 533–554.
URL: *http://www.ncbi.nlm.nih.gov/pubmed/21943913*

[86] Hong, S.-K., Kim, J.-H., Starenki, D. and Park, J.-I. [2013] "Autophagy sensitivity of neuroendocrine lung tumor cells." *Int. J. Oncol.* **43**, 2031–2038.

[87] Hosokawa, N., Hara, T., Kaizuka, T., Kishi, C., Takamura, A., Miura, Y., Iemura, S.-i., Natsume, T., Takehana, K., Yamada, N. and others. [2009] "Nutrient-dependent mTORC1 association with the ULK1–Atg13–FIP200 complex required for autophagy." *Mol. Biol. Cell* **20**, 1981–1991.

[88] Houtkooper, R. H., Pirinen, E. and Auwerx, J. [2012] "Sirtuins as regulators of metabolism and healthspan." *Nat. Rev. Mol. Cell. Biol.* **13**, 225–238.

[89] Hutson, N. and Mortimore, G. E. [1982] "Suppression of cytoplasmic protein uptake by lysosomes as the mechanism of protein regain in livers of starved-refed mice." *J. Biol. Chem.* **257**, 9548–9554.

[90] Inokuchi-Shimizu, S., Park, E. J., Roh, Y. S., Yang, L., Zhang, B., Song, J., Liang, S., Pimienta, M., Taniguchi, K., Wu, X., Asahina, K. and others. [2014] "TAK1-mediated autophagy and fatty acid oxidation prevent hepatosteatosis and tumorigenesis." *J. Clin. Invest.* **124**, 3566–3578.

[91] Irvine, G. and El-Agnaf, O. [2008] "Suppression of basal autophagy in neural cells causes neurodegenerative disease in mice." *Mol. Med.* **14**, 1.

[92] Itakura, E., Kishi, C., Inoue, K. and Mizushima, N. [2008] "Beclin 1 forms two distinct phosphatidylinositol 3-kinase complexes with mammalian Atg14 and UVRAG." *Mol. Biol. Cell* **19**, 5360–5372.

[93] Iwata, A., Riley, B. E., Johnston, J. A. and Kopito, R. R. [2005] "HDAC6 and microtubules are required for autophagic degradation of aggregated huntingtin." *J. Biol. Chem.* **280**, 40282–40292.

[94] Jäger, S., Bucci, C., Tanida, I., Ueno, T., Kominami, E., Saftig, P. and Eskelinen, E.-L. [2004] "Role for Rab7 in maturation of late autophagic vacuoles." *J. Cell. Sci.* **117**, 4837–4848.

[95] Jahreiss, L., Menzies, F. M. and Rubinsztein, D. C. [2008] "The itinerary of autophagosomes: from peripheral formation to kiss-and-run fusion with lysosomes." *Traffic* **9**, 574–587.

[96] Janku, F., McConkey, D. J., Hong, D. S. and Kurzrock, R. [2011] "Autophagy as a target for anticancer therapy." *Nature Reviews Clinical Oncology* **8**, 528–539.

[97] Jung, C. H., Jun, C. B., Ro, S.-H., Kim, Y.-M., Otto, N. M., Cao, J., Kundu, M. and Kim, D.-H. [2009] "ULK-Atg13-FIP200 complexes mediate mTOR signaling to the autophagy machinery." *Mol. Biol. Cell* **20**, 1992–2003.

[98] Kabeya, Y., Mizushima, N., Ueno, T., Yamamoto, A., Kirisako, T., Noda, T., Kominami, E., Ohsumi, Y. and Yoshimori, T. [2000] "LC3, a mammalian homologue of yeast Apg8p, is localized in autophagosome membranes after processing." *EMBO J.* **19**, 5720–5728.

[99] Kacser, H., Burns, J. and Fell, D. [1995] "The control of flux: 21 years on." *Biochem. Soc. Trans.* **23**, 341–366.

[100] Kadowaki, M. and Kanazawa, T. [2003] "Amino acids as regulators of proteolysis." *J. Nutr.* **133**, 2052S–2056S.

[101] Kamada, Y., Funakoshi, T., Shintani, T., Nagano, K., Ohsumi, M. and Ohsumi, Y. [2000] "Tor-mediated induction of autophagy via an Apg1 protein kinase complex." *J. Cell Biol.* **150**, 1507–1513.

[102] Kanamori, H., Takemura, G., Goto, K., Tsujimoto, A., Ogino, A., Takeyama, T., Kawaguchi, T., Watanabe, T., Morishita, K., Kawasaki, M. and others. [2013] "Resveratrol reverses remodeling in hearts with large, old myocardial infarctions through enhanced autophagy-activating AMP kinase pathway." *Am. J. Pathol.* **182**, 701–713.

[103] Kanki, T., Wang, K., Baba, M., Bartholomew, C. R., Lynch-Day, M. A., Du, Z., Geng, J., Mao, K., Yang, Z., Yen, W.-L. and others. [2009] "A genomic screen for yeast mutants defective in selective mitochondria autophagy." *Mol. Biol. Cell* **20**, 4730–4738.

[104] Kanzawa, T., Germano, I., Komata, T., Ito, H., Kondo, Y. and Kondo, S. [2004] "Role of autophagy in temozolomide-induced cytotoxicity for malignant glioma cells." *Cell Death Differ.* **11**, 448–457.

[105] Kato, H., Takahashi, S.-I., Takenaka, A., Funabiki, R., Noguchi, T. and Naito, H. [1989] "Degradation of endogenous proteins and internalized asialofetuin in primary cultured hepatocytes of rats." *Int. J. Biochem.* **21**, 483–495.

[106] Kawamata, T., Kamada, Y., Kabeya, Y., Sekito, T. and Ohsumi, Y. [2008] "Organization of the pre-autophagosomal structure responsible for autophagosome formation." *Mol. Biol. Cell* **19**, 2039–2050.

[107] Kegel, K. B., Kim, M., Sapp, E., McIntyre, C., Castaño, J. G., Aronin, N. and Di-Figlia, M. [2000] "Huntingtin expression stimulates endosomal–lysosomal activity, endosome tubulation, and autophagy." *J. Neurosci.* **20**, 7268–7278.

[108] Kihara, A., Noda, T., Ishihara, N. and Ohsumi, Y. [2001] "Two distinct VPS34 phosphatidylinositol 3–kinase complexes function in autophagy and carboxypeptidase y sorting in Saccharomyces Cerevisiae." *J. Cell Biol.* **152**, 519–530.

[109] Kim, J., Kundu, M., Viollet, B. and Guan, K.-L. [2011] "AMPK and mTOR regulate autophagy through direct phosphorylation of ULK1." *Nat. Cell. Biol.* **13**, 132–141.

[110] Kim, M. S., Song, S. Y., Lee, J. Y., Yoo, N. J. and Lee, S. H. [2011] "Expressional and mutational analyses of ATG5 gene in prostate cancers." *APMIS* **119**, 802–807.

[111] Kimura, S., Noda, T. and Yoshimori, T. [2008] "Dynein-dependent movement of autophagosome mediates effiicient encounters with lysosomes." *Cell Struct. Funct.* **33**, 109–122.

[112] Kirisako, T., Ichimura, Y., Okada, H., Kabeya, Y., Mizushima, N., Yoshimori, T., Ohsumi, M., Takao, T., Noda, T. and Ohsumi, Y. [2000] "The reversible modification regulates the membrane-binding state of Apg8/Aut7 essential for autophagy and the cytoplasm to vacuole targeting pathway." *J. Cell Biol.* **151**, 263–276.

[113] Klionsky, D. J., Abeliovich, H., Agostinis, P., Agrawal, D. K., Aliev, G., Askew, D. S., Baba, M., Baehrecke, E. H., Bahr, B. A., Ballabio, A., Bamber, B. A., Bassham, D. C. and others. [2008] "Guidelines for the use and interpretation of assays for monitoring autophagy in higher eukaryotes." *Autophagy* **4**, 151–175.

[114] Klionsky, D. J., Cueva, R. and Yaver, D. S. [1992] "Aminopeptidase I of Saccharomyces cerevisiae is localized to the vacuole independent of the secretory pathway." *J. Cell Biol.* **119**, 287–299.

[115] Köchl, R., Hu, X. W., Chan, E. Y. and Tooze, S. A. [2006] "Microtubules facilitate autophagosome formation and fusion of autophagosomes with endosomes." *Traffic* **7**, 129–145.

[116] Koga, H., Martinez-Vicente, M., Macian, F., Verkhusha, V. V. and Cuervo, A. M. [2011] "A photoconvertible fluorescent reporter to track chaperone-mediated autophagy." *Nature Communications* **2**, 386.

[117] Komatsu, M., Waguri, S., Chiba, T., Murata, S., Iwata, J.-i., Tanida, I., Ueno, T., Koike, M., Uchiyama, Y., Kominami, E. and others. [2006] "Loss of autophagy in the central nervous system causes neurodegeneration in mice." *Nature* **441**, 880–884.

[118] Komatsu, M., Waguri, S., Koike, M., Sou, Y.-s., Ueno, T., Hara, T., Mizushima, N., Iwata, J.-i., Ezaki, J., Murata, S. and others. [2007] "Homeostatic levels of p62

control cytoplasmic inclusion body formation in autophagy-deficient mice." *Cell* **131**, 1149–1163.

[119] Komatsu, M., Waguri, S., Ueno, T., Iwata, J., Murata, S., Tanida, I., Ezaki, J., Mizushima, N., Ohsumi, Y., Uchiyama, Y., Kominami, E., Tanaka, K. and Chiba, T. [2005] "Impairment of starvation-induced and constitutive autophagy in Atg7-deficient mice." *J. Cell Biol.* **169**, 425–434.

[120] Komatsu, M., Wang, Q. J., Holstein, G. R., Friedrich, V. L., Iwata, J.-i., Kominami, E., Chait, B. T., Tanaka, K. and Yue, Z. [2007] "Essential role for autophagy protein Atg7 in the maintenance of axonal homeostasis and the prevention of axonal degeneration." *Proc. Natl. Acad. Sci. U.S.A.* **104**, 14489–14494.

[121] Korolchuk, V. I., Menzies, F. M. and Rubinsztein, D. C. [2010] "Mechanisms of cross-talk between the ubiquitin-proteasome and autophagy-lysosome systems." *FEBS Lett.* **584**, 1393–1398.

[122] Kotoulas, O., Kalamidas, S. and Kondomerkos, D. [2006] "Glycogen autophagy in glucose homeostasis." *Pathology—Research and Practice* **202**, 631–638.

[123] Koukourakis, M., Giatromanolaki, A., Sivridis, E., Pitiakoudis, M., Gatter, K. and Harris, A. [2010] "Beclin 1 over-and underexpression in colorectal cancer: distinct patterns relate to prognosis and tumour hypoxia." *Br. J. Cancer* **103**, 1209–1214.

[124] Kroemer, G., Mariño, G. and Levine, B. [2010] "Autophagy and the integrated stress response." *Mol. Cell.* **40**, 280–293.

[125] Ktistakis, N. T., Andrews, S. and Long, J. [2011] "What is the advantage of a transient precursor in autophagosome biogenesis?" *Autophagy* **7**, 118–122.

[126] Kuma, A., Hatano, M., Matsui, M., Yamamoto, A., Nakaya, H., Yoshimori, T., Ohsumi, Y., Tokuhisa, T. and Mizushima, N. [2004] "The role of autophagy during the early neonatal starvation period." *Nature* **432**, 1032–1036.

[127] Kuma, A., Matsui, M. and Mizushima, N. [2007] "LC3, an autophagosome marker, can be incorporated into protein aggregates independent of autophagy: caution in the interpretation of LC3 localization." *Autophagy* **3**, 323–328.

[128] Lagouge, M., Argmann, C., Gerhart-Hines, Z., Meziane, H., Lerin, C., Daussin, F., Messadeq, N., Milne, J., Lambert, P., Elliott, P. and et al. [2006] "Resveratrol improves mitochondrial function and protects against metabolic disease by activating SIRT1 and PGC-1." *Cell* **127**, 1109–1122.

[129] Lau, A., Zheng, Y., Tao, S., Wang, H., Whitman, S. A., White, E. and Zhang, D. D. [2013] "Arsenic inhibits autophagic flux, activating the Nrf2-keap1 pathway in a p62-dependent manner." *Mol. Cell. Biol.* **33**, 2436–2446.

[130] Lee, I. H., Cao, L., Mostoslavsky, R., Lombard, D. B., Liu, J., Bruns, N. E., Tsokos, M., Alt, F. W. and Finkel, T. [2008] "A role for the NAD-dependent deacetylase sirt1 in the regulation of autophagy." *Proc. Natl. Acad. Sci. U.S.A.* **105**, 3374–3379.

[131] Lee, I. H. and Finkel, T. [2009] "Regulation of autophagy by the p300 acetyltransferase." *J. Biol. Chem.* **284**, 6322–6328.

[132] Lee, J.-A. and Gao, F.-B. [2008] "Regulation of Aβ pathology by Beclin 1: a protective role for autophagy?" *J. Clin. Invest.* .

[133] Lee, J. V., Carrer, A., Shah, S., Snyder, N. W., Wei, S., Venneti, S., Worth, A. J., Yuan, Z.-F., Lim, H.-W., Liu, S. and others. [2014] "Akt-dependent metabolic reprogramming regulates tumor cell histone acetylation." *Cell Metab.* **20**, 306–319.

[134] Lee, S. B., Kim, S., Lee, J., Park, J., Lee, G., Kim, Y., Kim, J.-M. and Chung, J. [2007] "Atg1, an autophagy regulator, inhibits cell growth by negatively regulating S6 kinase" *EMBO Rep.* **8**, 360–365.

[135] Lemasters, J. J., Nieminen, A.-L., Qian, T., Trost, L. C., Elmore, S. P., Nishimura, Y., Crowe, R. A., Cascio, W. E., Bradham, C. A., Brenner, D. A. *et al.* [1998] "The mitochondrial permeability transition in cell death: a common mechanism in necrosis, apoptosis and autophagy" *Biochim. Biophys. Acta* **1366**, 177–196.

[136] Levine, B. [2007] "Cell biology: Autophagy and cancer" *Nature* **446**, 745–747.

[137] Levine, B. and Kroemer, G. [2008] "Autophagy in the pathogenesis of disease" *Cell* **132**, 27–42.

[138] Liang, C., Feng, P., Ku, B., Dotan, I., Canaani, D., Oh, B.-H. and Jung, J. U. [2006] "Autophagic and tumour suppressor activity of a novel Beclin1-binding protein UVRAG" *Nat. Cell. Biol.* **8**, 688–698.

[139] Liang, X. H., Jackson, S., Seaman, M., Brown, K., Kempkes, B., Hibshoosh, H. and Levine, B. [1999] "Induction of autophagy and inhibition of tumorigenesis by beclin 1" *Nature* **402**, 672–676.

[140] Lipinski, M. M., Hoffman, G., Ng, A., Zhou, W., Py, B. F., Hsu, E., Liu, X., Eisenberg, J., Liu, J., Blenis, J. *et al.* [2010] "A genome-wide siRNA screen reveals multiple mTORC1 independent signaling pathways regulating autophagy under normal nutritional conditions" *Dev. Cell.* **18**, 1041–1052.

[141] Liu, H., He, Z., von Rütte, T., Yousefi, S., Hunger, R. E. and Simon, H.-U. [2013] "Down-regulation of autophagy-related protein 5 (ATG5) contributes to the pathogenesis of early-stage cutaneous melanoma" *Science Translational Medicine* **5**, 123.

[142] Loos, B., du Toit, A. and Hofmeyr, J.-H. S. [2014] "Defining and measuring autophagosome flux–concept and reality" *Autophagy* **10**, 2087–2096.

[143] Loos, B., Engelbrecht, A.-M., Lockshin, R. A., Klionsky, D. J. and Zakeri, Z. [2013] "The variability of autophagy and cell death susceptibility: Unanswered questions" *Autophagy* **9**, 1270–1285.

[144] Lopez, L. A. and Sheetz, M. P. [1993] "Steric inhibition of cytoplasmic dynein and kinesin motility by MAP2" *Cell Motil. Cytoskeleton* **24**, 1–16.

[145] Lum, J. J., Bauer, D. E., Kong, M., Harris, M. H., Li, C., Lindsten, T. and Thompson, C. B. [2005] "Growth factor regulation of autophagy and cell survival in the absence of apoptosis" *Cell* **120**, 237–248.

[146] Lussignol, M., Queval, C., Bernet-Camard, M.-F., Cotte-Laffitte, J., Beau, I., Codogno, P. and Esclatine, A. [2013] "The herpes simplex virus 1 Us11 protein inhibits autophagy through its interaction with the protein kinase PKR" *J. Virol.* **87**, 859–871.

[147] Mackeh, R., Lorin, S., Ratier, A., Mejdoubi-Charef, N., Baillet, A., Bruneel, A., Hamai, A., Codogno, P., Pous, C. and Perdiz, D. [2014] "Reactive oxygen species, AMP-activated protein kinase, and the transcription cofactor p300 regulate α-tubulin acetyltransferase-1 (αTAT-1/MEC-17)-dependent microtubule hyperacetylation during cell stress" *J. Biol. Chem.* **289**, 11816–11828.

[148] Mader, B. J., Pivtoraiko, V. N., Flippo, H. M., Klocke, B. J., Roth, K. A., Mangieri, L. R. and Shacka, J. J. [2012] "Rotenone inhibits autophagic flux prior to inducing cell death" *ACS Chem. Neurosci.* **3**, 1063–1072.

[149] Mariño, G., Pietrocola, F., Eisenberg, T., Kong, Y., Malik, S. A., Andryushkova, A., Schroeder, S., Pendl, T., Harger, A., Niso-Santano, M. *et al.* [2014] "Regulation of autophagy by cytosolic acetyl-coenzyme A" *Mol. Cell.* **53**, 710–725.

[150] Mariño, G., Salvador-Montoliu, N., Fueyo, A., Knecht, E., Mizushima, N. and López-Otín, C. [2007] "Tissue-specific autophagy alterations and increased tumorigenesis in mice deficient in Atg4C/autophagin-3" *J. Biol. Chem.* **282**, 18573–18583.

[151] Martinez-Vicente, M. and Cuervo, A. M. [2007] "Autophagy and neurodegeneration: when the cleaning crew goes on strike" *The Lancet Neurology* **6**, 352–361.

[152] Massey, A. C., Zhang, C. and Cuervo, A. M. [2006] "Chaperone-mediated autophagy in aging and disease" *Curr. Top. Dev. Biol.* **73**, 205–235.

[153] Mathew, R., Karantza-Wadsworth, V. and White, E. [2007] "Role of autophagy in cancer." *Nat. Rev. Cancer* **7**, 961–967.

[154] Matsui, Y., Takagi, H., Qu, X., Abdellatif, M., Sakoda, H., Asano, T., Levine, B. and Sadoshima, J. [2007] "Distinct roles of autophagy in the heart during ischemia and reperfusion roles of AMP-activated protein kinase and Beclin 1 in mediating autophagy" *Circ. Res.* **100**, 914–922.

[155] Matsunaga, K., Saitoh, T., Tabata, K., Omori, H., Satoh, T., Kurotori, N., Maejima, I., Shirahama-Noda, K., Ichimura, T., Isobe, T. *et al.* [2009] "Two Beclin 1-binding proteins, Atg14l and rubicon, reciprocally regulate autophagy at different stages" *Nat. Cell. Biol.* **11**, 385–396.

[156] Matsuura, A., Tsukada, M., Wada, Y. and Ohsumi, Y. [1997] "Apg1p, a novel protein kinase required for the autophagic process in Saccharomyces Cerevisiae" *Gene* **192**, 245–250.

[157] Matsuyama, S. S. and Jarvik, L. F. [1989] "Hypothesis: microtubules, a key to Alzheimer disease." *Proc. Natl. Acad. Sci. U.S.A.* **86**, 8152–8156.

[158] Mauvezin, C., Nagy, P., Juhász, G. and Neufeld, T. P. [2015] "Autophagosome-lysosome fusion is independent of V-ATPase-mediated acidification" *Nat Comms* **6**, 7007.

[159] Meijer, A. J., Lorin, S., Blommaart, E. F. and Codogno, P. [2014] "Regulation of autophagy by amino acids and mTOR-dependent signal transduction" *Amino Acids* .

[160] Mercer, C. A., Kaliappan, A. and Dennis, P. B. [2009] "A novel, human Atg13 binding protein, Atg101, interacts with ULK1 and is essential for macroautophagy" *Autophagy* **5**, 649–662.

[161] Mizushima, N. [2003] "In vivo analysis of autophagy in response to nutrient starvation using transgenic mice expressing a fluorescent autophagosome marker" *Mol. Biol. Cell* **15**, 1101–1111.

[162] Mizushima, N., Levine, B., Cuervo, A. M. and Klionsky, D. J. [2008] "Autophagy fights disease through cellular self-digestion" *Nature* **451**, 1069–1075.

[163] Mizushima, N., Noda, T. and Ohsumi, Y. [1999] "Apg16p is required for the function of the Apg12p–Apg5p conjugate in the yeast autophagy pathway" *EMBO J.* **18**, 3888–3896.

[164] Mizushima, N., Sugita, H., Yoshimori, T. and Ohsumi, Y. [1998] "A new protein conjugation system in human the counterpart of the yeast Apg12p conjugation system essential for autophagy" *J. Biol. Chem.* **273**, 33889–33892.

[165] Mizushima, N., Yamamoto, A., Hatano, M., Kobayashi, Y., Kabeya, Y., Suzuki, K., Tokuhisa, T., Ohsumi, Y. and Yoshimori, T. [2001] "Dissection of autophagosome formation using Apg5-deficient mouse embryonic stem cells" *J. Cell Biol.* **152**, 657–668.

[166] Mizushima, N. and Yoshimori, T. [2007] "How to interpret LC3 immunoblotting." *Autophagy* **3**, 542–545.

[167] Mizushima, N., Yoshimori, T. and Levine, B. [2010] "Methods in mammalian autophagy research" *Cell* **140**, 313–326.

[168] Monastyrska, I., He, C., Geng, J., Hoppe, A. D., Li, Z. and Klionsky, D. J. [2008] "Arp2 links autophagic machinery with the actin cytoskeleton" *Mol. Biol. Cell* **19**, 1962–1975.

[169] Moriya, S., Che, X.-F., Komatsu, S., Abe, A., Kawaguchi, T., Gotoh, A., Inazu, M., Tomoda, A. and Miyazawa, K. [2013] "Macrolide antibiotics block autophagy flux and sensitize to bortezomib via endoplasmic reticulum stress-mediated CHOP induction in myeloma cells" *Int. J. Oncol.* **42**, 1541–1550.

[170] Morselli, E., Mariño, G., Bennetzen, M. V., Eisenberg, T., Megalou, E., Schroeder, S., Cabrera, S., Bénit, P., Rustin, P., Criollo, A. *et al.* [2011] "Spermidine and resveratrol induce autophagy by distinct pathways converging on the acetylproteome" *J. Cell Biol.* **192**, 615–629.

[171] Morselli, E., Marino, G., Bennetzen, M. V., Eisenberg, T., Megalou, E., Schroeder, S., Cabrera, S., Benit, P., Rustin, P., Criollo, A. and et al. [2011] "Spermidine and resveratrol induce autophagy by distinct pathways converging on the acetylproteome" *J. Cell Biol.* **192**, 615–629.

[172] Mortimore, G. E., Hutson, N. J. and Surmacz, C. A. [1983] "Quantitative correlation between proteolysis and macro- and microautophagy in mouse hepatocytes during starvation and refeeding" *Proc. Natl. Acad. Sci. U.S.A.* **80**, 2179–2183.

[173] Mortimore, G. E. and Poso, A. R. [1987] "Intracellular protein catabolism and its control during nutrient deprivation and supply" *Annu. Rev. Nutr.* **7**, 539–568.

[174] Mortimore, G. E., Pösö, A. R., Kadowaki, M. and Wert, J. J. J. [1987] "Multiphasic control of hepatic protein degradation by regulatory amino acids. general features and hormonal modulation." *J. Biol. Chem.* **262**, 16322–16327.

[175] Mortimore, G. E. and Schworer, C. M. [1977] "Induction of autophagy by amino-acid deprivation in perfused rat liver" *Nature* **270**, 174–176.

[176] Muller, F. [2000] "The nature and mechanism of superoxide production by the electron transport chain: Its relevance to aging." *J Am Aging Assoc* **23**, 227–253.

[177] Nakai, A., Yamaguchi, O., Takeda, T., Higuchi, Y., Hikoso, S., Taniike, M., Omiya, S., Mizote, I., Matsumura, Y., Asahi, M., Nishida, K., Hori, M., Mizushima, N. and Otsu, K. [2007] "The role of autophagy in cardiomyocytes in the basal state and in response to hemodynamic stress." *Nat. Med.* **13**, 619–624.

[178] Nakaso, K., Yoshimoto, Y., Nakano, T., Takeshima, T., Fukuhara, Y., Yasui, K., Araga, S., Yanagawa, T., Ishii, T. and Nakashima, K. [2004] "Transcriptional activation of p62/A170/ZIP during the formation of the aggregates: possible mechanisms and the role in lewy body formation in parkinson's disease." *Brain Res.* **1012**, 42–51.

[179] Nazio, F., Strappazzon, F., Antonioli, M., Bielli, P., Cianfanelli, V., Bordi, M., Gretzmeier, C., Dengjel, J., Piacentini, M., Fimia, G. M. *et al.* [2013] "mTOR inhibits autophagy by controlling ULK1 ubiquitylation, self-association and function through AMBRA1 and TRAF6" *Nat. Cell. Biol.* **15**, 406–416.

[180] Nedelsky, N. B., Todd, P. K. and Taylor, J. P. [2008] "Autophagy and the ubiquitin-proteasome system: Collaborators in neuroprotection" *Biochim. Biophys. Acta* **1782**, 691–699.

[181] Nelson, D. L., Lehninger, A. L. and Cox, M. M. [2013] *Lehninger principles of biochemistry* New York : W.H. Freeman.

[182] Ni, H.-M., Bockus, A., Wozniak, A. L., Jones, K., Weinman, S., Yin, X.-M. and Ding, W.-X. [2011] "Dissecting the dynamic turnover of GFP-LC3 in the autolysosome" *Autophagy* **7**, 188–204.

[183] Nicklin, P., Bergman, P., Zhang, B., Triantafellow, E., Wang, H., Nyfeler, B., Yang, H., Hild, M., Kung, C., Wilson, C. and et al. [2009] "Bidirectional transport of amino acids regulates mTOR and autophagy" *Cell* **136**, 521–534.

[184] Nivikof, A. B., Essner, E. and Quintana, N. [1964] "Golgi apparatus and lysosomes." in *Federation proceedings* vol. 23 p. 1010.

[185] Nixon, R. A. [2007] "Autophagy, amyloidogenesis and Alzheimer disease" *J. Cell. Sci.* **120**, 4081–4091.

[186] Nixon, R. A., Wegiel, J., Kumar, A., Yu, W. H., Peterhoff, C., Cataldo, A. and Cuervo, A. M. [2005] "Extensive involvement of autophagy in Alzheimer disease: an immuno-electron microscopy study" *J. Neuropathol. Exp. Neurol.* **64**, 113–122.

[187] Novikoff, A. B. [1959] "The proximal tubule cell in experimental hydronephrosis" *J. Biophys. Biochem. Cytol.* **6**, 136–138.

[188] Novikoff, A. B. and Essner, E. [1962] "Cytolysomes and mitochondrial degeneration" *J. Cell Biol.* **15**, 140–146.

[189] Obara, K., Sekito, T., Niimi, K. and Ohsumi, Y. [2008] "The Atg18-Atg2 complex is recruited to autophagic membranes via phosphatidylinositol 3-phosphate and exerts an essential function" *J. Biol. Chem.* **283**, 23972–23980.

[190] Okamoto, K., Kondo-Okamoto, N. and Ohsumi, Y. [2009] "Mitochondria-anchored receptor Atg32 mediates degradation of mitochondria via selective autophagy" *Dev. Cell.* **17**, 87–97.

[191] Olivier, B. G., Rohwer, J. M. and Hofmeyr, J.-H. S. [2005] "Modelling cellular systems with PySCeS" *Bioinformatics* **21**, 560–561.

[192] Onodera, J. and Ohsumi, Y. [2005] "Autophagy is required for maintenance of amino acid levels and protein synthesis under nitrogen starvation" *J. Biol. Chem.* **280**, 31582–31586.

[193] Pan, H., Wang, Z., Jiang, L., Sui, X., You, L., Shou, J., Jing, Z., Xie, J., Ge, W., Cai, X. and et al. [2014] "Autophagy inhibition sensitizes hepatocellular carcinoma to the multikinase inhibitor linifanib" *Scientific Reports* **4**, 6683.

[194] Pandey, U. B., Nie, Z., Batlevi, Y., McCray, B. A., Ritson, G. P., Nedelsky, N. B., Schwartz, S. L., DiProspero, N. A., Knight, M. A., Schuldiner, O. *et al.* [2007] "HDAC6 rescues neurodegeneration and provides an essential link between autophagy and the UPS" *Nature* **447**, 860–864.

[195] Pankiv, S., Clausen, T. H., Lamark, T., Brech, A., Bruun, J.-A., Outzen, H., **O**vervatn, A., Bjørkøy, G. and Johansen, T. [2007] "p62/SQSTM1 binds directly to Atg8/LC3 to facilitate degradation of ubiquitinated protein aggregates by autophagy" *J. Biol. Chem.* **282**, 24131–24145.

[196] Papandreou, I., Lim, A., Laderoute, K. and Denko, N. [2008] "Hypoxia signals autophagy in tumor cells via ampk activity, independent of hif-1, bnip3, and bnip3l" *Cell Death Differ.* **15**, 1572–1581.

[197] Peng, T., Golub, T. R. and Sabatini, D. M. [2002] "The immunosuppressant rapamycin mimics a starvation-like signal distinct from amino acid and glucose deprivation" *Mol. Cell. Biol.* **22**, 5575–5584.

[198] Pfeifer, U. [1976] "Inhibition by insulin of the physiological autophagic breakdown of cell organelles." *Acta Biol. Med. Ger.* **36**, 1691–1694.

[199] Pickford, F., Masliah, E., Britschgi, M., Lucin, K., Narasimhan, R., Jaeger, P. A., Small, S., Spencer, B., Rockenstein, E., Levine, B. and et al. [2008] "The autophagy-related protein Beclin 1 shows reduced expression in early Alzheimer disease and regulates amyloid β accumulation in mice" *J. Clin. Invest.* .

[200] Pösö, A. R., Wert, Jr, J. and Mortimore, G. E. [1982] "Multifunctional control of amino acids of deprivation-induced proteolysis in liver. role of leucine." *J. Biol. Chem.* **257**, 12114–12120.

[201] Preyat, N. and Leo, O. [2013] "Sirtuin deacylases: a molecular link between metabolism and immunity" *J. Leukoc. Biol.* **93**, 669–680.

[202] Qin, Z.-H., Wang, Y., Kegel, K. B., Kazantsev, A., Apostol, B. L., Thompson, L. M., Yoder, J., Aronin, N. and DiFiglia, M. [2003] "Autophagy regulates the processing of amino terminal huntingtin fragments" *Hum. Mol. Genet.* **12**, 3231–3244.

[203] Qu, X., Yu, J., Bhagat, G., Furuya, N., Hibshoosh, H., Troxel, A., Rosen, J., Eskelinen, E.-L., Mizushima, N., Ohsumi, Y. *et al.* [2003] "Promotion of tumorigenesis by heterozygous disruption of the Beclin 1 autophagy gene" *J. Clin. Invest.* **112**, 1809.

[204] Rabinowitz, J. D. and White, E. [2010] "Autophagy and metabolism" *Science* **330**, 1344–1348.

[205] Ravikumar, B., Acevedo-Arozena, A., Imarisio, S., Berger, Z., Vacher, C., O'Kane, C. J., Brown, S. D. and Rubinsztein, D. C. [2005] "Dynein mutations impair autophagic clearance of aggregate-prone proteins" *Nat. Genet.* **37**, 771–776.

[206] Ravikumar, B., Duden, R. and Rubinsztein, D. C. [2002] "Aggregate-prone proteins with polyglutamine and polyalanine expansions are degraded by autophagy" *Hum. Mol. Genet.* **11**, 1107–1117.

[207] Ravikumar, B., Moreau, K., Jahreiss, L., Puri, C. and Rubinsztein, D. C. [2010] "Plasma membrane contributes to the formation of pre-autophagosomal structures" *Nat. Cell. Biol.* **12**, 747–757.

[208] Ravikumar, B., Vacher, C., Berger, Z., Davies, J. E., Luo, S., Oroz, L. G., Scaravilli, F., Easton, D. F., Duden, R., O'Kane, C. J. and Rubinsztein, D. C. [2004] "Inhibition of mTOR induces autophagy and reduces toxicity of polyglutamine expansions in fly and mouse models of Huntington disease." *Nat. Genet.* **36**, 585–595.

[209] Reggiori, F., Monastyrska, I., Shintani, T. and Klionsky, D. J. [2005] "The actin cytoskeleton is required for selective types of autophagy, but not nonspecific autophagy, in the yeast saccharomyces cerevisiae" *Mol. Biol. Cell* **16**, 5843–5856.

[210] Roberts, D. J., Tan-Sah, V. P., Ding, E. Y., Smith, J. M. and Miyamoto, S. [2014] "Hexokinase-ii positively regulates glucose starvation-induced autophagy through TORC1 inhibition" *Mol. Cell.* **53**, 521–533.

[211] Rodgers, K. J. and Dean, R. T. [2003] "Assessment of proteasome activity in cell lysates and tissue homogenates using peptide substrates." *Int. J. Biochem. Cell Biol.* **35**, 716–727.

[212] Rubinsztein, D. C. [2006] "The roles of intracellular protein-degradation pathways in neurodegeneration" *Nature* **443**, 780–786.

[213] Rubinsztein, D. C., Cuervo, A. M., Ravikumar, B., Sarkar, S., Korolchuk, V., Kaushik, S. and Klionsky, D. J. [2009] "In search of an "autophagomometer"." *Autophagy* **5**, 585–589.

[214] Rubinsztein, D. C., DiFiglia, M., Heintz, N., Nixon, R. A., Qin, Z.-H., Ravikumar, B., Stefanis, L. and Tolkovsky, A. [2005] "Autophagy and its possible roles in nervous system diseases, damage and repair" *Autophagy* **1**, 11–22.

[215] Rubinsztein, D. C., Mariño, G. and Kroemer, G. [2011] "Autophagy and aging" *Cell* **146**, 682–695.

[216] Sagiv, Y., Legesse-Miller, A., Porat, A. and Elazar, Z. [2000] "GATE-16, a membrane transport modulator, interacts with NSF and the Golgi v-SNARE GOS-28" *EMBO J.* **19**, 1494–1504.

[217] Saito, H., Inazawa, J., Saito, S., Kasumi, F., Koi, S., Sagae, S., Kudo, R., Saito, J., Noda, K. and Nakamura, Y. [1993] "Detailed deletion mapping of chromosome 17q in ovarian and breast cancers: 2-cM region on 17q21. 3 often and commonly deleted in tumors" *Cancer Res.* **53**, 3382–3385.

[218] Sancak, Y., Bar-Peled, L., Zoncu, R., Markhard, A. L., Nada, S. and Sabatini, D. M. [2010] "Ragulator-Rag complex targets mTORC1 to the lysosomal surface and is necessary for its activation by amino acids" *Cell* **141**, 290–303.

[219] Sarkar, S., Ravikumar, B., Floto, R. A. and Rubinsztein, D. C. [2009] "Rapamycin and mTOR-independent autophagy inducers ameliorate toxicity of polyglutamine-expanded huntingtin and related proteinopathies" *Cell Death Differ.* **16**, 46–56.

[220] Scarlatti, F., Bauvy, C., Ventruti, A., Sala, G., Cluzeaud, F., Vandewalle, A., Ghidoni, R. and Codogno, P. [2004] "Ceramide-mediated macroautophagy involves inhibition of protein kinase B and up-regulation of Beclin 1" *J. Biol. Chem.* **279**, 18384–18391.

[221] Seglen, P. O. and Gordon, P. B. [1982] "3-methyladenine: specific inhibitor of autophagic/lysosomal protein degradation in isolated rat hepatocytes" *Proc. Natl. Acad. Sci. U.S.A.* **79**, 1889–1892.

[222] Selkoe, D. J. [2001] "Clearing the brain's amyloid cobwebs" *Neuron* **32**, 177–180.

[223] Settembre, C., Fraldi, A., Medina, D. L. and Ballabio, A. [2013] "Signals from the lysosome: a control centre for cellular clearance and energy metabolism" *Nat. Rev. Mol. Cell. Biol.* **14**, 283–296.

[224] Shen, J., Xie, Y., Sun, M., Han, R., Qin, Z.-H. and He, J.-K. [2014] "Antitumor activity of cobrotoxin in human lung adenocarcinoma A549 cells and following transplantation in nude mice" *Oncol Lett* .

[225] Shi, Y.-H., Ding, Z.-B., Zhou, J., Qiu, S.-J. and Fan, J. [2009] "Prognostic significance of Beclin 1-dependent apoptotic activity in hepatocellular carcinoma" *Autophagy* **5**, 380–382.

[226] Shibata, M., Lu, T., Furuya, T., Degterev, A., Mizushima, N., Yoshimori, T., MacDonald, M., Yankner, B. and Yuan, J. [2006] "Regulation of intracellular accumulation of mutant Huntingtin by Beclin 1" *J. Biol. Chem.* **281**, 14474–14485.

[227] Shimobayashi, M. and Hall, M. N. [2014] "Making new contacts: the mTOR network in metabolism and signalling crosstalk" *Nat. Rev. Mol. Cell. Biol.* **15**, 155–162.

[228] Shvets, E., Fass, E. and Elazar, Z. [2008] "Utilizing flow cytometry to monitor autophagy in living mammalian cells." *Autophagy* **4**, 621–628.

[229] Silvera, D., Formenti, S. C. and Schneider, R. J. [2010] "Translational control in cancer" *Nat. Rev. Cancer* **10**, 254–266.

[230] Singh, R. and Cuervo, A. M. [2011] "Autophagy in the cellular energetic balance" *Cell Metab.* **13**, 495–504.

[231] Strømhaug, P. E., Reggiori, F., Guan, J., Wang, C.-W. and Klionsky, D. J. [2004] "Atg21 is a phosphoinositide binding protein required for efficient lipidation and localization of Atg8 during uptake of aminopeptidase i by selective autophagy" *Mol. Biol. Cell* **15**, 3553–3566.

[232] Sun, Q., Fan, W., Chen, K., Ding, X., Chen, S. and Zhong, Q. [2008] "Identification of Barkor as a mammalian autophagy-specific factor for Beclin 1 and class iii phosphatidylinositol 3-kinase" *Proc. Natl. Acad. Sci. U.S.A.* **105**, 19211–19216.

[233] Suzuki, K., Kirisako, T., Kamada, Y., Mizushima, N., Noda, T. and Ohsumi, Y. [2001] "The pre-autophagosomal structure organized by concerted functions of APG genes is essential for autophagosome formation" *EMBO J.* **20**, 5971–5981.

[234] Suzuki, K., Kubota, Y., Sekito, T. and Ohsumi, Y. [2007] "Hierarchy of Atg proteins in pre-autophagosomal structure organization" *Genes Cells* **12**, 209–218.

[235] Taguchi, K., Fujikawa, N., Komatsu, M., Ishii, T., Unno, M., Akaike, T., Motohashi, H. and Yamamoto, M. [2012] "Keap1 degradation by autophagy for the maintenance of redox homeostasis." *Proc. Natl. Acad. Sci. U.S.A.* **109**, 13561–13566.

[236] Takeshige, K., Baba, M., Tsuboi, S., Noda, T. and Ohsumi, Y. [1992] "Autophagy in yeast demonstrated with proteinase-deficient mutants and conditions for its induction." *J. Cell Biol.* **119**, 301–311.

[237] Tanaka, M., Kim, Y. M., Lee, G., Junn, E., Iwatsubo, T. and Mouradian, M. M. [2004] "Aggresomes formed by α-synuclein and synphilin-1 are cytoprotective" *J. Biol. Chem.* **279**, 4625–4631.

[238] Tanaka, Y., Guhde, G., Suter, A., Eskelinen, E.-L., Hartmann, D., Lüllmann-Rauch, R., Janssen, P. M. L., Blanz, J., von Figura, K. and Paul, S. [2000] "Accumulation of autophagic vacuoles and cardiomyopathy in LAMP-2-deficient mice" *Nature* **406**, 902–906.

[239] Tanida, I., Minematsu-Ikeguchi, N., Ueno, T. and Kominami, E. [2005] "Lysosomal turnover, but not a cellular level, of endogenous LC3 is a marker for autophagy" *Autophagy* **1**, 84–91.

[240] Tanida, I., Yamaji, T., Ueno, T., Ishiura, S., Kominami, E. and Hanada, K. [2008] "Consideration about negative controls for LC3 and expression vectors for four colored fluorescent protein-LC3 negative controls." *Autophagy* **4**, 131–134.

[241] Tasdemir, E., Maiuri, M. C., Galluzzi, L., Vitale, I., Djavaheri-Mergny, M., D'Amelio, M., Criollo, A., Morselli, E., Zhu, C., Harper, F. *et al.* [2008] "Regulation of autophagy by cytoplasmic p53" *Nat. Cell. Biol.* **10**, 676–687.

[242] Tellez-Nagel, I., Johnson, A. B. and Terry, R. D. [1974] "Studies on brain biopsies of patients with Huntington's chorea." *J. Neuropathol. Exp. Neurol.* **33**, 308–332.

[243] Thoresen, S. B., Pedersen, N. M., Liestøl, K. and Stenmark, H. [2010] "A phosphatidylinositol 3-kinase class iii sub-complex containing VPS15, VPS34, Beclin 1, UVRAG and BIF-1 regulates cytokinesis and degradative endocytic traffic" *Exp. Cell Res.* **316**, 3368–3378.

[244] Titorenko, V. I., Keizer, I., Harder, W. and Veenhuis, M. [1995] "Isolation and characterization of mutants impaired in the selective degradation of peroxisomes in the yeast Hansenula polymorpha." *J. Bacteriol.* **177**, 357–363.

[245] Tooze, S. A. and Yoshimori, T. [2010] "The origin of the autophagosomal membrane" *Nat. Cell. Biol.* **12**, 831–835.

[246] Tracy, K., Dibling, B. C., Spike, B. T., Knabb, J. R., Schumacker, P. and Macleod, K. F. [2007] "BNIP3 is an RB/E2F target gene required for hypoxia-induced autophagy" *Mol. Cell. Biol.* **27**, 6229–6242.

[247] Tsai, C.-Y., Chen, Y.-H., Chien, Y.-W., Huang, W.-H. and Lin, S.-H. [2010] "Effect of soy saponin on the growth of human colon cancer cells." *World J. Gastroenterol.* **16**, 3371–3376.

[248] Tsukada, M. and Ohsumi, Y. [1993] "Isolation and characterization of autophagy-defective mutants of Saccharomyces cerevisiae" *FEBS Lett.* **333**, 169–174.

[249] Tsvetkov, A. S., Arrasate, M., Barmada, S., Ando, D. M., Sharma, P., Shaby, B. A. and Finkbeiner, S. [2013] "Proteostasis of polyglutamine varies among neurons and predicts neurodegeneration" *Nat. Chem. Biol.* **9**, 586–592.

[250] Veenhuis, M., Douma, A., Harder, W. and Osumi, M. [1983] "Degradation and turnover of peroxisomes in the yeast Hansenula polymorpha induced by selective inactivation of peroxisomal enzymes" *Arch. Microbiol.* **134**, 193–203.

[251] Vilchez, D., Morantte, I., Liu, Z., Douglas, P. M., Merkwirth, C., Rodrigues, A. P. C., Manning, G. and Dillin, A. [2012] "RPN-6 determines C. elegans longevity under proteotoxic stress conditions" *Nature* **489**, 263–268.

[252] Walsh, P. J. and Wright, P. A. [1995] *Nitrogen Metabolism and Excretion* CRC Press.

[253] Wan, X.-B., Fan, X.-J., Chen, M.-Y., Xiang, J., Huang, P.-Y., Guo, L., Wu, X.-Y., Xu, J., Long, Z.-J., Zhao, Y. *et al.* [2010] "Elevated beclin 1 expression is correlated with HIF-1α in predicting poor prognosis of nasopharyngeal carcinoma" *Autophagy* **6**, 395–404.

[254] Wang, H., Bedford, F. K., Brandon, N. J., Moss, S. J. and Olsen, R. W. [1999] "GABAA-receptor-associated protein links GABAA receptors and the cytoskeleton" *Nature* **397**, 69–72.

[255] Wang, L., Chen, M., Yang, J. and Zhang, Z. [2013] "LC3 fluorescent puncta in autophagosomes or in protein aggregates can be distinguished by FRAP analysis in living cells" *Autophagy* **9**, 756–769.

[256] Wang, P., Zhang, J., Zhang, L., Zhu, Z., Fan, J., Chen, L., Zhuang, L., Luo, J., Chen, H., Liu, L. and et al. [2013] "MicroRNA 23b regulates autophagy associated with radioresistance of pancreatic cancer cells" *Gastroenterology* **145**, 1133–1143.

[257] Warr, M. R., Binnewies, M., Flach, J., Reynaud, D., Garg, T., Malhotra, R., Debnath, J. and Passegué, E. [2013] "FOXO3A directs a protective autophagy program in haematopoietic stem cells" *Nature* **494**, 323–327.

[258] Wauson, E. M., Dbouk, H. A., Ghosh, A. B. and Cobb, M. H. [2014] "G protein-coupled receptors and the regulation of autophagy" *Trends Endocrinol. Metab.* **25**, 274–282.

[259] Webb, J. L., Ravikumar, B., Atkins, J., Skepper, J. N. and Rubinsztein, D. C. [2003] "α-Synuclein is degraded by both autophagy and the proteasome" *J. Biol. Chem.* **278**, 25009–25013.

[260] White, E. [2012] "Deconvoluting the context-dependent role for autophagy in cancer" *Nat. Rev. Cancer* **12**, 401–410.

[261] White, E. [2013] "Exploiting the bad eating habits of Ras-driven cancers" *Genes Dev.* **27**, 2065–2071.

[262] Williams, A., Sarkar, S., Cuddon, P., Ttofi, E. K., Saiki, S., Siddiqi, F. H., Jahreiss, L., Fleming, A., Pask, D., Goldsmith, P., O'Kane, C. J., Floto, R. A. and Rubinsztein, D. C. [2008] "Novel targets for huntington's disease in an mTOR-independent autophagy pathway." *Nat. Chem. Biol.* **4**, 295–305.

[263] Wu, A.-G., Wong, V., Xu, S.-W., Chan, W.-K., Ng, C.-I., Liu, L. and Law, B. [2013] "Onjisaponin B derived from radix polygalae enhances autophagy and accelerates the degradation of mutant α-Synuclein and huntingtin in PC-12 Cells" *Int. J. Molec. Sci.* **14**, 22618–22641.

[264] Xia, P., Wang, J.-J., Zhao, B.-B. and Song, C.-L. [2013] "The role of Beclin-1 expression in patients with gastric cancer: a meta-analysis" *Tumor Biol.* **34**, 3303–3307.

[265] Xiao, Y., Ma, C., Yi, J., Wu, S., Luo, G., Xu, X., Lin, P.-H., Sun, J. and Zhou, J. [2015] "Suppressed autophagy flux in skeletal muscle of an amyotrophic lateral sclerosis mouse model during disease progression" *Physiol. Rep.* **3**, 12271–12271.

[266] Xie, Z., Nair, U. and Klionsky, D. J. [2008] "Atg8 controls phagophore expansion during autophagosome formation" *Mol. Biol. Cell* **19**, 3290–3298.

[267] Yamamoto, A., Cremona, M. L. and Rothman, J. E. [2006] "Autophagy-mediated clearance of huntingtin aggregates triggered by the insulin-signaling pathway" *J. Cell Biol.* **172**, 719–731.

[268] Yamamoto, A., Tagawa, Y., Yoshimori, T., Moriyama, Y., Masaki, R. and Tashiro, Y. [1998] "Bafilomycin A1 prevents maturation of autophagic vacuoles by inhibiting fusion between autophagosomes and lysosomes in rat hepatoma cell line, H-4-II-E cells." *Cell Struct. Funct.* **23**, 33–42.

[269] Yang, W., Hong, Y. H., Shen, X.-Q., Frankowski, C., Camp, H. S. and Leff, T. [2001] "Regulation of transcription by AMP-activated protein kinase" *J. Biol. Chem.* **276**, 38341–38344.

[270] Yang, Z., Huang, J., Geng, J., Nair, U. and Klionsky, D. J. [2006] "Atg22 recycles amino acids to link the degradative and recycling functions of autophagy" *Mol. Biol. Cell* **17**, 5094–5104.

[271] Ye, J., Kumanova, M., Hart, L. S., Sloane, K., Zhang, H., De Panis, D. N., Bobrovnikova-Marjon, E., Diehl, J. A., Ron, D. and Koumenis, C. [2010] "The GCN2-ATF4 pathway is critical for tumour cell survival and proliferation in response to nutrient deprivation" *EMBO J.* **29**, 2082–2096.

[272] Ylä-Anttila, P., Vihinen, H., Jokitalo, E. and Eskelinen, E.-L. [2009] "3D tomography reveals connections between the phagophore and endoplasmic reticulum" *Autophagy* **5**, 1180–1185.

[273] Ylä-Anttila, P., Vihinen, H., Jokitalo, E. and Eskelinen, E.-L. [2009] "Monitoring autophagy by electron microscopy in mammalian cells" *Methods Enzymol.* **452**, 143–164.

[274] Yoshimori, T., Yamamoto, A., Moriyama, Y., Futai, M. and Tashiro, Y. [1991] "Bafilomycin A1, a specific inhibitor of vacuolar-type H(+)-ATPase, inhibits acidification and protein degradation in lysosomes of cultured cells" *J. Biol. Chem.* **266**, 17707–17712.

[275] Young, A. R., Chan, E. Y., Hu, X. W., Köchl, R., Crawshaw, S. G., High, S., Hailey, D. W., Lippincott-Schwartz, J. and Tooze, S. A. [2006] "Starvation and ULK1-dependent cycling of mammalian atg9 between the TGN and endosomes" *J. Cell. Sci.* **119**, 3888–3900.

[276] Yu, W. H., Cuervo, A. M., Kumar, A., Peterhoff, C. M., Schmidt, S. D., Lee, J.-H., Mohan, P. S., Mercken, M., Farmery, M. R., Tjernberg, L. O. *et al.* [2005] "Macroautophagy: a novel β-amyloid peptide-generating pathway activated in Alzheimer's disease" *J. Cell Biol.* **171**, 87–98.

[277] Yuan, H.-X., Russell, R. C. and Guan, K.-L. [2013] "Regulation of PIK3C3/VPS34 complexes by m TOR in nutrient stress-induced autophagy" *Autophagy* **9**, 1983–1995.

[278] Yue, Z., Jin, S., Yang, C., Levine, A. J. and Heintz, N. [2003] "Beclin 1, an autophagy gene essential for early embryonic development, is a haploinsufficient tumor suppressor" *Proc. Natl. Acad. Sci. U.S.A.* **100**, 15077–15082.

[279] Zeng, X., Overmeyer, J. H. and Maltese, W. A. [2006] "Functional specificity of the mammalian Beclin-VPS 34 PI 3-kinase complex in macroautophagy versus endocytosis and lysosomal enzyme trafficking." *J. Cell. Sci.* **119**, 259–270.

[280] Zhang, H., Bosch-Marce, M., Shimoda, L. A., Tan, Y. S., Baek, J. H., Wesley, J. B., Gonzalez, F. J. and Semenza, G. L. [2008] "Mitochondrial autophagy is an HIF-1-dependent adaptive metabolic response to hypoxia" *J. Biol. Chem.* **283**, 10892–10903.

[281] Zoncu, R., Bar-Peled, L., Efeyan, A., Wang, S., Sancak, Y. and Sabatini, D. M. [2011] "mTORC1 senses lysosomal amino acids through an inside-out mechanism that requires the vacuolar H^+-ATPase" *Science* **334**, 678–683.